1-1-1990

The crystallization and morphology of polyethylene and its blends/

Michael M. Satkowski
University of Massachusetts Amherst

THE CRYSTALLIZATION AND MORPHOLOGY OF POLYETHYLENE AND ITS BLENDS

A Dissertation Presented

by

MICHAEL M. SATKOWSKI

Submitted to the Graduate School of the
University of Massachusetts in partial fulfillment
of the requirements for the degree of

DOCTOR OF PHILOSOPHY

February 1990

Department of Polymer Science and Engineering

THE CRYSTALLIZATION AND MORPHOLOGY OF POLYETHYLENE AND ITS BLENDS

A Dissertation Presented

by

MICHAEL M. SATKOWSKI

Approved as to style and content by:

Richard S. Stein, Chairperson of Committee

Murugappan Muthukumar, Member

David A. Hoagland, Member

William MacKnight, Acting Head
Polymer Science and Engineering

ACKNOWLEDGEMENTS

I would like to thank Drs. Muthukumar and Hoagland for serving on my committee. Their willingness to meet at nearly anytime, despite their brimming schedules, to discuss my work is greatly appreciated. My deepest thanks and gratitude go to my advisor Richard S. Stein for giving me the opportunity to work and learn under him. His unflagging energy, and the shear joy he derives from his work has been inspirational.

It gives me great pleasure to acknowledge the help and dear friendship of Dr. Saroj K. Roy who assisted in the neutron measurements of ultra high molecular weight polyethylene

Special thanks to Dr. Ben Chu and Dr. Dan Q. Wu of SUNY at Stony Brook for their help with the synchrotron measurements at Brookhaven National Laboratory. I am very grateful to. Shel McGuire and Phillipe Esnault, who accompianed me during my visits to BNL, for suffering through too little sleep and too much junk food.

I would also like to extend my thanks to "Thiyagu" Thirajagran and E. Epperson at Argonne National Laboratory for their help with the neutron measurements of LLDPE.

The only regrettable part of finishing a thesis is saying good-bye to many people who have become such good friends over the years. I would like to say thanks to the members of the extended family of the

Stein group (too many to mention here) who made the time spent at Amherst so enjoyable.

Finally and above all, I would like to thank my family, my parents, Theresa and Michael, and sister, Lynn whose never wavering support and encouragement helped me beyond measure in completing this dissertation.

ABSTRACT

THE CRYSTALLIZATION AND MORPHOLOGY OF
POLYETHYLENE AND ITS BLENDS
FEBRUARY 1990
MICHAEL M. SATKOWSKI,
B.S., WILKES COLLEGE
M.S., RENSSELEAR POLYTECHNIC INSTITUTE
Ph. D., UNIVERSITY OF MASSACHUSETTS
Directed by: Professor Richard S. Stein

The techniques of neutron and x-ray scattering have been used to study the morphology and crystallization behavior of polyethylene and blends of polyethylene.

Synchrotron radiation was used to study the crystallization behavior of blends of high density polyethylene/ low density polyethylene (HDPE/LDPE) and linear low density/ low density polyethylene (LLDPE/LDPE). Simultaneous real time small and wide angle scattering from blends slowly cooled at (0.5°C/min) seem to indicate that the lamellae are formed in bundles of primarily one component. For blends quickly cooled from the melt (quenched to 60°C) on the other hand, the lamellae are randomly mixed together. HDPE/LDPE and LLDPE/LDPE blends show qualitatively the same crystallization behavior throughout the composition range except for 10%/90% LLDPE/LDPE. At this composition, extensive cocrystallization may be occuring in even slowly cooled samples.

Small angle neutron and x-ray scattering was used to determine the location of the short chain branches in selectively deuterated LLDPE. Specially prepared LLDPE with the main chain deuterated was used in these experiments to provide contrast for neutron scattering. Despite density contributions to the neutron scattering from crystalline and amorphous regions, differences between the x-ray and neutron scattering suggest that the concentration of branches may be enhanced at the crystal- amorphous boundary. The extent of this branch-rich region was estimated to be about 30Å.

Lastly, the chain orientation of ultra high molecular weight PE (UHMWPE) was examined by small angle neutron scattering. A circularly averaging technique was applied in order to avoid sample alignment problems. Between extension ratios of 12 and 60, hot drawn (125°C) gel crystallized UHMWPE does not show appreciable change in the perpendicular radius of gyration. However, changes in the asymptotic behavior of the scattering intensity from $I \sim q^{-1.56}$ at 12x to $I \sim q^{-1.2}$ at 60x indicate a change in geometry toward more rod like segments in the higher drawn material.

TABLE OF CONTENTS

LIST OF TABLES

LIST OF FIGURES

CHAPTER I

GENERAL INTRODUCTION

Although polyethylene has been studied for the past fifty years, there still remains a great deal about it that is a mystery. The simplicity of its composition belies the complexity of structure and morphology this polymer can obtain. Different methods of synthesizing this material produce varying chain structure that result in dramatic changes in physical properties. A wide array of processing techniques can be used to obtain different morphologies which consequently result in distinctly different physical properties. Polyethylene can be produced in such wildly varying forms as cheap grocery bags for local supermarkets or high modulus fibers used in state-of the-art sails for 12 meter racing yachts.

There are three commercially available types of polyethylene: low density, high density, and linear low density (see figure 1). High density (or linear) polyethylene or (HDPE) has a density of about 0.96, and melts at typically 135° C. It is primarily linear in structure with few side branches (less than one side chain per 200 CH_2 units). HDPE is highly crystalline, with crystallinities as much as 90% by volume. HDPE has good tensile strength and hardness, enabling its use in bottles and containers for example. Linear polyethylene can be made with molecular weights of up to 6 million. Known as ultrahigh molecular weight polyethylenes (UHMWPE), these polymers have exceptional abrasion and impact resistance compared to its lower molecular weight relatives[1].

The second type of polyethylene, low density polyethylene (LDPE) has a density range of 0.91-0.94. and melts at roughly 115° C. LDPE differs from HDPE by the presence of many branches. These branches lower the crystallinity of LDPE (generally 50% or lower) as compared to HDPE. This generally increases flexibility making LDPE good for use in films. The branches are of two types. The first kind is caused by intermolecular chain transfer, which produces branches as long as the main chain. The second type results from intramolecular chain transfer and produces short branches of about four CH_2 units. LDPE is synthesized by free radical polymerization under high pressure.

The third and last type of polyethylene, linear low density polyethylene (LLDPE) consists of linear polyethylene with branches of short length (2-8 CH_2 units). It is produced by copolymerization of ethylene with butene, hexene, or octene. By varying the number of branches, crystallinity can be controlled. This allows LLDPE to be produced in flexible films like LDPE or more rigid structures like HDPE. Because LLDPE is not produced under high pressure, like LDPE, it is cheaper to make than LDPE.

This thesis will describe three areas of research concerning polyethylene's morphology and crystallization. The first topic is the crystallization of blends of high, low, and linear low density polyethylene. While recent neutron scattering studies show that these polymers are miscible in the melt, DSC measurements indicate that

these polymer form separate crystals[2]. In this work, the blends are studied on the lamellar and crystallite size scale using high flux X-ray synchrotron radiation. This parallels light scattering studies undertaken in this laboratory, which demonstrate that the kinetics of the blend are dramatically changed upon the addition of small amounts of one component. The objective of the work will be to study how the crystallization conditions affect the morphology of the blend, and to study the degree of segregation that takes place as crystallization occurs

The second topic will concern the morphology of LLDPE alone. The distinguishing feature of LLDPE is its short chain branches. While these branches limit the crystallinity of LLDPE, it is not the only through this effect that they alter physical properties. Variations in the length of the branch can affect impact resistance and tensile strength. A combination of neutron and X-ray scattering is used to attempt to determine the role of the branches play in defining the morphology of the system.

Lastly, the structure of highly drawn ultrahigh molecular weight polyethylene is investigated by neutron scattering. In this case, the interest is focused on the nearly extended polyethylene chain and its conformation. The modulus of drawn polyethylene fibers continue to increase as the draw ratios exceed 100x[3], yet most measures of orientation in the polymer , such as the alignment of the crystal c-axis, reach a saturating value after extensions as little as 10 times. Neutron scattering is used in this study to examine the transverse width of the

extended molecule, in order to determine what conformational changes are occurring in the nearly extended chain molecule.

REFERENCES

1. T.P. Snell in *Modern Plastics Encyclopedia*, J. Agranoff, ed., Vol. 59, McGraw Hill, New York, 1982.

2. M. Ree, Ph.D. Thesis, University of Massachusetts, Amherst 1987.

3. P. Smith, P. Lemstra, *J. Colloid Polym. Sci.*, 258, &, (1980).

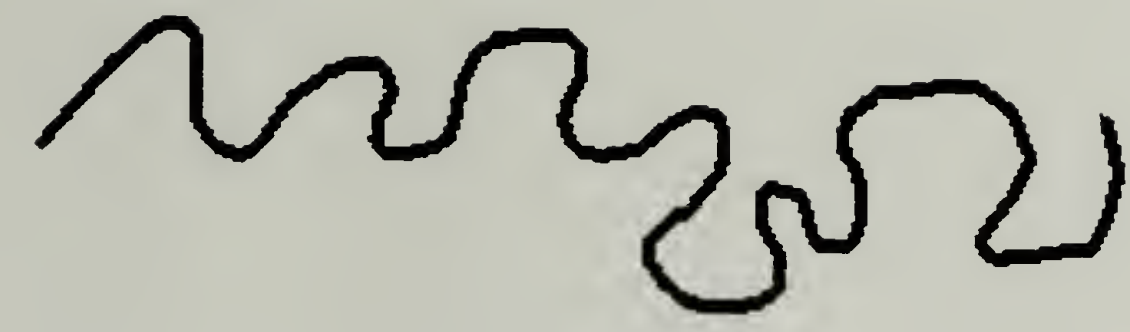

HDPE

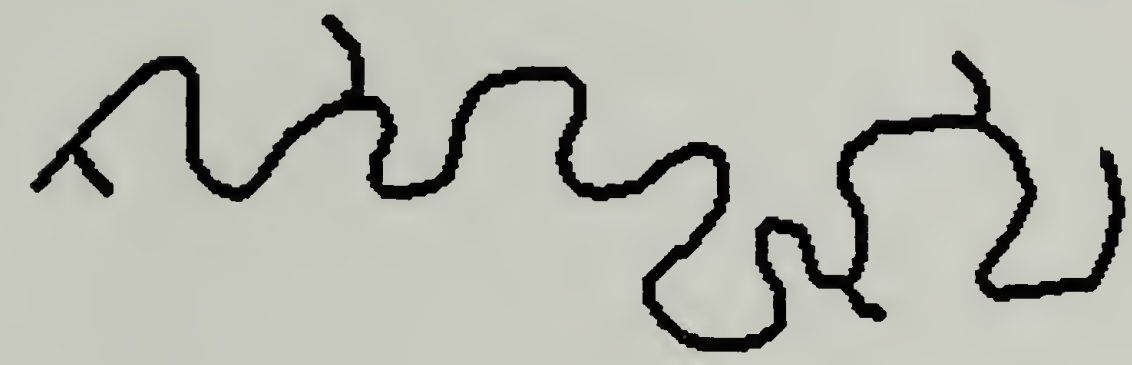

LLDPE

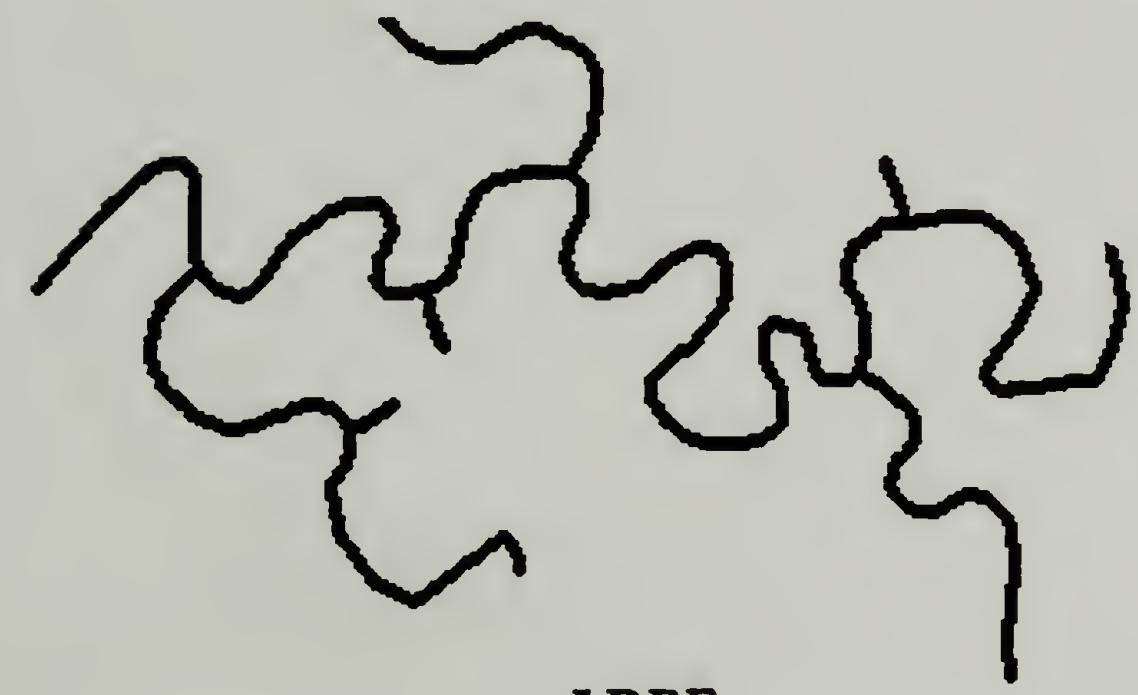

LDPE

Figure 1.1 A schematic illustration of various polyethylenes

CHAPTER 2
SYNCHROTRON STUDIES OF HDPE/LDPE AND LLDPE/LDPE BLENDS

2.1 Introduction

The crystallization of polyethylene has been extensively studied since the 1930s[1,2]. Most of the work done has focused on HDPE and LDPE alone. Recently, the crystallization behavior of polyethylene blends has been of considerable interest in this and other laboratories.[3-5] Blends of linear low, low density, and high density polyethylene are important for many commercial uses. The blend systems possess physical properties that cannot be attained by the homopolymers alone.[6-8] The recognition of the need to recycle plastics has also highlighted the importance of polyethylene blends. Polyethylene accounts for nearly 40% of the plastic waste in the U.S.[9] Since it is impractical to distinguish between the various types of PE, some type of blending will inevitably become necessary in order to recycle these polymers economically. Knowledge of the crystallization behavior of these blends will be indispensable in determining their structure property relationships.

Upon crystallization from the melt, segregation or co-crystallization of the blended polyethylene specie can occur, depending on the composition and crystallization conditions. For example, blends of LLDPE/HDPE, LLDPE/UHMWPE , and

HDPE/UHMWPE can co-crystallize under rapid or slow cooling.[10-12] On the other hand, for LLDPE/LDPE, HDPE/LDPE, and UHMWPE/LDPE blends, the components crystallize separately under most crystallization conditions. [5, 10] This is shown primarily by DSC, where two distinct peaks are present in the endotherms, corresponding to the two different types of PE crystals present. Clearly there is segregation on the crystallite scale, the question is to what scale does this segregation extend,.and how is it affected by crystallization conditions.

Light scattering and optical microscopy can give information about crystallization on the micron size scale by following the growth of the spherulite radius. Ree, and more recently McGuire and Esnault[13,14] have studied the light scattering of blends of HDPE/LDPE and LLDPE/HDPE. For the crystallization conditions studied, isothermal crystallizations from 80°- 110°C and for constant cooling rates between 20 and 2 °C/min. , both components crystallized within the same spherulite. Furthermore, in both HDPE/LDPE and LLDPE/LDPE blends at crystallization temperatures greater than 104° C, the spherulite radii of the blends were roughly the same as that of the higher temperature crystallizing component (HDPE and LLDPE). At greater supercoolings, the tendency of the LLDPE in the LLDPE/LDPE blend to control the radius diminished. Not only the morphology, but also the kinetics of crystallization were found to be greatly influenced by the blend component with the higher T_m. The spherulitic growth rate and crystallization rate of the LLDPE/LDPE blends crystallized above 102°C were dramatically increased by the

addition of as little as 5% of LLDPE. The growth rates of 50/50 blends were nearly the same as that of the homopolymer with the higher T_m .

On the basis of these results, it was speculated that two crystallization processes, depending on the undercooling, were taking place. In the first process, for moderate to low undercoolings, the high T_m component crystallizes to form open, coarse spherulites which span the entire sample volume. The lower T_m component crystallizes within or perhaps on the framework provided by the faster crystallizing component. The second process occurs when the supercooling is large. Here both components crystallize rapidly, more or less at once.

To investigate this hypothesis further it is necessary to examine the crystallization of these blends on a smaller spatial scale and on a similar time scale as that of the light scattering. The focus of the present study will be the morphology and the crystallization of HDPE/LDPE and LLDPE/LDPE blends on a crystallite and lamellar size scale. This will be undertaken using real time wide angle (WAXS) and small angle x-ray scattering (SAXS) using a high flux x-ray synchrotron source. These super high intensity sources have fluxes that are thousands of times higher than conventional x-ray generators. WAXS can be used to follow the degree of crystallinity with time, while SAXS can reveal information on the formation of lamellae.

Shultz et. al has studied the crystallization of linear polyethylene[15-17] and poly(TMPS) fractions[18] by real time SAXS using conventional x-ray sources. Because of limited x-ray intensities, only crystallization temperatures above 110° C for either polymer could be studied by real time methods. For isothermal crystallizations of poly(TMPS) in this temperature range, the long period remained virtually constant with time once the lamellae had formed. Upon additional cooling of these isothermally crystallized samples, the long period spacing decreased drastically. This decrease was interperted as consequence of crystallization between previously formed lamellae. Static SAXS at lower crystallization temperatures of PE showed that the long periods remained relatively constant at crystallization temperatures lower than 110° C . For higher crystallization temperatures of HDPE the long period increased with increasing temperature. Samples isothermally crystallized at high temperature and subsequently cooled to room temperature showed long periods that increased with increasing time at T_c. The authors concluded that there exists a competition between the processes of lamellar thickening and the formation of new crystallites between the earlier formed lamellae. The amorphous density at various crystallization temperatures was reported to be approximately the same as an extrapolation from the melt density, taking into account thermal expansion.

Reckinger et. al.[19] have studied a 50/50 blend of high and low density PE by static SAXS. Their conclusion was that for slowly cooled samples the stacking of the lamellae occured in a statistical (random)

fashion. They described the scattering in terms of a paracrystalline model with a bimodal distribution of crystalline widths. Static SAXS did not permit real time measurements at fast cooling.

2.2 Theory and Data Analysis

The theory of x-ray scattering is well established[20-22]. Scattering arises due to fluctuations in electron density, ρ, within the irradiated volume . The angles at which the scattering occurs roughly determines the size scale in the sample which is probed. For wide angle x-ray diffraction, this size scale is that of the crystal lattice itself. Consequently, WAXS can be used to measure the degree of crystallinity of the polymer. The intensity coherently scattered over all angles by an assembly of atoms is constant regardless of the state of order.[23,24] Therefore, if one can separate the contribution of the scattering due to the crystalline regions, one can write the degree of crystallinity, x_c, as

$$x_c = \frac{\int_0^\infty s^2 I_c(s)\, ds}{\int_0^\infty s^2 I(s)\, ds} \qquad (2.1)$$

where $s=2\_\sin\theta / \lambda$, θ is one half the scattering angle, λ is the wavelength of the x-ray used, I (s) is the scattered intensity, and I_c (s) is the intensity concentrated in the crystalline peaks. Equation (2.1) tends to be less than the true amount of crystallinity. This is because some of the crystalline intensity is lost to the diffuse scattering as a

result of atomic thermal vibrations and lattice imperfections. Ruland[25,26] has developed the most rigorous method of determining x_c by WAXS, taking into account these lattice imperfections. According to Ruland:

$$x_c = \frac{\int_0^\infty s^2 I_c(s)\, ds \int_0^\infty s^2 f^2\, ds}{\int_0^\infty s^2 I(s)\, ds \int_0^\infty s^2 f^2 D\, ds} \qquad (2.2)$$

Here f^2 is the mean square atomic scattering factor of the polymer repeat unit and D is the imperfection factor which accounts for lattice imperfections and thermal motion. In general (2.2) is difficult to apply in practice because the determination of D involves measuring I over a wide range of s.

Small Angle X-ray Scattering (SAXS) is sensitive to larger scale electron density fluctuations than WAXS[27]. These size scales are typically 50-1000 Å. At these spatial scales, the scattering is generally produced from the alternating crystalline and amorphous layers within the polymers. Typically, scattering patterns that occur for bulk crystallized polymers feature one or possibly two broad peaks. The position of the first peak is inversely related to the long period, Lp, the repeat distance of the lamellae. A quantity Q called the invariant can be defined as the integrated intensity of the small angle scattering[28].

$$Q = \int_0^\infty s^2 I(s)\, ds \qquad (2.3)$$

The angular range here excludes that of the WAXS where crystal periodicities occur. For a two phase system of average electron densities ρ_a and ρ_b with sharp boundaries between the phases[29]:

$$Q = K\, 4\pi\, \phi_b\, \phi_a\, (\rho_b - \rho_a)^2 \qquad (2.4)$$

where K is a constant and ϕ_a and ϕ_b are the volume fractions of phases a and b. Thus Q can be used to follow the evolution of a two phase structure with time.

2.3 Experimental

2.3.1 Materials

Samples of LLDPE, a poly(ethylene-co-butene-1) (LPX-2, lot number 50225) , LDPE (LD 122.0P, lot number 16291) and HDPE (lot number)were supplied by EXXON Chemical Americas (Baton Rouge, LA). The LLDPE has $\overline{Mw}$ = 114,000, $\overline{Mw}/\overline{Mn}$ = 4.5, 18 short chain branches / 1000 C, and a density of 0.918 g/cm^3. The LDPE has $\overline{Mw}$ = 286,000, $\overline{Mw}/\overline{Mn}$ = 16, 26 short chain branches / 1000 C, 34 long chain branches per weight average molecule, and a density of 0.920 g/cm^3. The HDPE has Mw=160,000, Mw/Mn= 7.1 , short chain branching of 1 branch every 1000 carbons, and a density of 0.957 gm/cm. These are the same materials used for previous light scattering studies in this laboratory[5,11-14] .

Purification and blending of the homopolymers is accomplished by dissolving the desired weight ratio of polymers in p-xylene (2 g PE per 100 mL p-xylene) and heating to 130 °C for 1 hour. To inhibit oxidation, 2,6-di-tert-butyl-4-methylphenol (1% by weight of PE) was added. The polymers were precipitated in cold methanol, filtered on a glass filter and washed with methanol. The samples were dried in a vacuum oven at 50 °C for two days, or until free of the solvent odor.

2.3.2 X-ray Measurements

Experiments were conducted at the SUNY beam line of the National Synchrotron Light Source, Brookhaven national Laboratory. A schematic of the experimental apparatus is shown in figure (2.1) . The x-rays were collimated by use of a modified Kratky system described elsewhere[30]. The wavelength of the radiation was 1.54 Å and the beam size at the sample surface was 1x2 mm. The small angle scattered intensity was collected by a linear position sensitive photo diode array coupled to an Optical Multichannel Analyzer system (Princeton Applied Research). The wide angle scattering was collected by a Braun linear position sensitive detector. In this manner, both WAXS and SAXS could be measured simultaneously. Data collection times ranged from as little as 5 seconds for the quick cool to 60° C, to 120 seconds for the slow cool. Raw data runs were saved at National Synchrotron Light Source on magnetic media and transfered to the University of Massachusetts for subsequent analysis. Data were corrected for detector dark current, background and sample absorption.

A specially designed thermal sample holder was used to achieve a rapid temperature jump. As seen in figure (2.2) ,the device consists of two large thermal chambers kept at the desired temperatures T_1 and T_2 . The copper sample cell is rapidly transferred from one chamber (T_1) to the other (T_2) by means of a metal rod connected to a pneumatic pressure device. After the sample reaches the temperature of the second chamber, the x-ray measurement is started. The time for a sample to reach an equilibrium temperature (T_2) is thus dependent on the magnitude of the temperature difference between the chambers ($dT= T_2-T_1$) . For example, when dT = 25° C, the sample can reach an equilibrium state in 20 seconds. For slow cooled runs the temperature was controlled by a Valley Forge temperature controller model . The absolute temperature was accurate to 1° C, while fluctuations in temperature are less than 0.1°C.

2.4 Results and Discussion

Blends of LLDPE/LDPE and HDPE/LDPE were studied under various types of thermal treatments. In the first type of treatment the samples were quickly cooled to 60° C by the temperature jump cell described above. The second type of treatment was cooling the sample at a constant slow cooling rate (0.3 or 0.5 °C/min) and following the crystallization as a function of the temperature. The motivation behind these two treatments was to study the effect of cooling rate on the segregation of the crystal species. Along these same lines , samples were studied under a two step cooling process. Here the blend was cooled rapidly to a temperature T_1, below T_c for one of the

homopolymers, but still above T_c for the LDPE, held for a predetermined amount of time , then cooled to temperature T_2 which is below T_c for both blend components. Finally, some preliminary studies concerning LLDPE with different branch content are presented.

2.4.1 HDPE/LDPE Quench vs. Slow Cooling

Preliminary synchrotron work was done on a 50/50 HDPE/LDPE blend in collaboration with Dr. Ben Chu, SUNY at Stony Brook[31]. In these first series experiments, LDPE, HDPE and the blend was cooled at a constant rate (0.3 C° /min). For these initial experiments, only SAXS were observed. Some of the Lorentz corrected scattering patterns are shown in figure 2.3 . Each scattering curve in these figures took 10 seconds to accumulate. It is interesting to note that both the HDPE and the 50/50 blend show two distinct maxima even early in the crystallization process. The second order SAXS peak in crystalline polymers is generally seen in systems with a narrow distribution of crystalline and amorphous widths and in systems with a high degree of crystallinity[32, 33].

In figure 2.4 the integrated intensities, Q, normalized by the maximum, Qmax, are plotted as a function of the temperature. As can be seen in figure 2.4, both homopolymers exhibit S - shaped curves. For the case of the blend, however, the integrated intensity shows a two step increase. This behavior is due to the separate crystallization of each species. The curve can be separated into three sections. In the first region, from temperatures 120° C to 110° C, Q rises rapidly to a

plateau at 116° C. At these temperatures, HDPE is the only species crystallizing. In the second region, from 110° C to 100° C, both LDPE and HDPE are crystallizing. Finally in the third region, from 100° C to 90° C, LDPE dominates the crystallization.

These initial experiments demonstrated the feasibility of real time SAXS and the possibility of obtaining quantitative data on the crystallization of PE blends. Improvements in the experimental design were undertaken. Computer control over the data collection was made more efficient. This eliminated the gaps in the plots of invariants as a function of temperature shown in figure 2.4. Another improvement was the addition of a second detector for WAXS. Now both the crystallinity and the lamellae formation could be measured at the same time.

In the first series of experiments with simultaneous SAXS and WAXS, HDPE/LDPE blends were rapidly cooled to 60°C from the melt. Blends 10/90, 30/70, 50/50, 70/30 by weight HDPE/LDPE and the homopolymers were studied. Figure 2.5 shows a representative SAXS profiles of a 30/70 HD/LD blend cooled under these conditions. The Intensity is plotted as a function of q ; each curve was accumulated for 5 seconds. Profiles are corrected for background scattering and absorption of the sample. Soon after the temperature jump., the scattering increases in intensity at the smallest angles and results in a monotonically decreasing profile. This type of scattering is indicative of single particle scattering. At this stage, the lamellae are widely separated; no interference effects are seen. After about 30 seconds

this forward scattering begins to decrease and first a shoulder then a distinct peak forms. At this time the are enough lamellae close enough to produce correlations in the arrangement of crystal layers, and consequently interferences in the scattered amplitudes. This peak sharpens and moves out to larger angles with time, indicating that the long period (lp= $1/ s_{max}$) decreases with time.

The long periods for all the HDPE/LDPE blends are plotted as a function of time in figure (2.6). Clearly, the lp 's decrease drastically in the first 20 seconds of the crystallization, then decrease much more slowly after 30 seconds, remaining virtually constant after 75 seconds. The drastic drop in the long period at early times is due to lamellae forming between already present crystal layers. The final Lps of the blends are nearly a weighted average of the homopolymer long periods.

The normalized invariants Q are shown in Figure 2.7 . The vertical axis is shifted by 0.5 for each plot for clarity. For all blends the invariant rises smoothly with time to a plateau value . For HDPE, and blend concentrations above 50% HDPE a slight maximum is observed just before the plateau value is reached. This is explained by equation (2.4) . Q passes through a maximum when ϕ_c , the degree of crystallinity by volume reaches 50%. For HDPE, the degree of crystallinity generally exceeds 50%.

The representative wide angle diffraction patterns are shown in figure (2.8). Like the SAXS, each pattern were collected for 5 seconds.

The scattering was corrected for background and air scatter. The patterns in the melt exhibit a broad maximum characteristic of the amorphous phase. As crystallization occurs, crystalline peaks become evident. For PE, the visible peaks in the angular region observed are the (110) and (200). Because of the collimation conditions of these first series of experiments with simultaneous WAXS and SAXS were adjusted for optimum small angle scattering, the crystal peaks are not sharp as they should be. Some of the scattering in the crystal peaks were lost to the diffuse background. Consequently, it was impossible to obtain precise enough WAXS data to obtain true crystallinity via the Ruland method (equation 2.2). The relative crystallinity can be obtained through equation (2.1), however, and it is in this parameter that we are primarily interested. For each scattering curve an amorphous halo was determined by fitting the melt scattering modified by scaling factors to the experimental profile. Crystallinity index is plotted as a function of time for the homopolymers in figure (2.9). Because of the uncertainty in the data as a result of the short accumulation time, it was extremely difficult to determine a reproducible amorphous halo from which to subtract the total scattering. This problem of reproducibility in the amorphous curves accounts for the large error bars displayed in figure (2.9). Little more can be said except that for all blends the crystallinity shows a monotonic increase to a near constant value, and in all cases it appears that the crystallinity reaches its plateau value about 30 sec. after the quench begins. For these quenched samples, the uncertainty is so large it is difficult to determine in differences in crystallinity between the different blends.

The trends in crystallinity, invariant and long period spacings for slowly cooled samples are markedly different from the quenched samples. These samples, 10/90, 30/70, 50/50 HDPE/LDPE and the homopolymers, were cooled from the melt at a constant rate (0.5°C/min). Data was collected for 60 seconds every two minutes. Shown in figure (2.10) is the normalized SAXS invariant as a function of temperature. The homopolymers show much the same behavior as when quenched, rising to a near constant value. The HDPE shows a slight decrease in Q once 50% crystallinity is exceeded. The blends, however, show a two step behavior. The step is most clearly seen in the 10/90 HDPE/LDPE blend, but is also quite distinguishable in the 50/50 case. The invariant for the blends begin to increase at roughly 120°C, about 5°C less than that of the HDPE. The second step generally occurs at about 108°C, appearing to begin at a slightly higher temperature than that of LDPE alone.

The crystallinity determined by WAXS also follows this two step behavior. Figure (2.11) shows the crystallinity index (a relative measure of crystallinity) of the blends. Again, the 10/90 HDPE/LDPE blend shows the effect most clearly, while smaller second step increases can be seen in the 30/70 and 50/50 HDPE/LDPE blends. The observations regarding the initial crystallization temperatures for the SAXS Invariants seem to hold true for the crystallinity index of the blends as well. A 5° C depression in the initial crystallization temperature for the blends with respect to pure HDPE is seen.

The long periods of the slowly cooled HDPE/LDPE blends (figure 2.12) as a function of temperature also indicate a two step process. The Lp of the HDPE homopolymer decreases gradually from temperatures 120°C to 90°C. The long period of the pure LDPE deceases at a faster rate starting at about 100°C. The lamellae periodicities take some time to form, so the starting temperatures of the long periods do not correspond to the initial crystallization temperatures given by the invariant or WAXS. For the 50/50 and the 30/70 HDPE/LDPE blend, the long periods appear to be identical to that of the homopolymer until about 102°C . After this temperature, the long period decreases in a manner very similar to that of the LDPE. The 10/90 HDPE/LDPE blend also shows this two step behavior, except that the Long period in the initial stages of crystallization is not the same as the pure HDPE. The blend long periods in this case tend to be in between the homopolymer long periods.

The differences in behavior between the invariants, crystallinity and long periods, with time suggest different patterns of segregation for the quenched and slowly cooled samples. As mentioned earlier, Ree's results show that HDPE and LDPE do not co-crystallize to any appreciable extent near the conditions explored here. With HDPE and LDPE forming in different crystallites, three basic types of morphologies are then conceivable. (see figure 2.13) In the first type, each component can crystallize into separate spherulites of purely HDPE or LDPE. In the second type of morphology, HDPE and LDPE can form in separate lamellae within the same spherulite. The

segregation scale is inter-lamellar and the lamellae of LDPE and HDPE are mixed together. Thirdly, HDPE and LDPE could form separate lamellae within the same spherulite, but in this case the lamellae form stacks of primarily LDPE or HDPE. This gives rise to a morphology that consists of bundles of lamellae of one component.

Among the three types of cases examined here the first has already been rejected by the recent study of HDPE/LDPE blends by Ree and Stein[34]. Differential Scanning Calorimetry and Small Angle Light Scattering showed that in the slowly cooled (2° C/ min) blends, the entire sample volume was first filled with open spherulites of HDPE and then LDPE crystallized within the previously formed spherulites. We turn our attention then, to differentiating between cases two and three, and the question of whether the lamellae of HDPE and LDPE are intermixed or segregated into stacks of primarily of one component.

The shapes of the scattering patterns from these two cases is expected to be quite different. If the lamellae are in bundles of a single component, and these bundles are relatively large in spatial extent, there should little interference between the large stacks and the pattern should be a superposition of scattering from LDPE and HDPE homopolymers. This interfibrillar segregation should also contribute to the forward scattering, depending on the size scale of the segregation. If the size scale of the interfribrillar regions are small , the forward scattering could become quite intense and could even appear superimposed on lamellar scattering.

For the case of inter lamellar segregation, a number of different profiles could result depending on the exact type of separation of components. If the lamellae are intermixed and alternating in a random fashion , the scattering observed would arise from an average of the lamellar widths of LDPE and HDPE. In this instance, no superposition of the scattering from the homopolymers occurs. This type of scattering can be modeled using the paracrystalline statistics of Reckinger et al. However, the LDPE still might crystallize between the HDPE lamellae, but not in lamellar form. This could happen because of spatial restraints between the previously formed lamellae. These small crystallites might act to raise the electron density in the area between the lamellae. This effect could manifest itself in changes in the Invariant depending on the size scale of these inter lamellae crystallites. If the these crystallites are small compared to the width of the lamellae, their presence would tend to increase the average electron density of the amorphous region. This would, in turn, decrease the invariant.

The SAXS and WAXS data from quenched samples. seem to point toward a morphology where the lamellae are randomly intermixed (case two above). The invariants for the blends rise in a manner similar to that of the homopolymers. This indicates that lamellae formation of both the LDPE and HDPE is occuring at similar time scales. The WAXS crystallinity also seem to support this. It is unlikely that given such short time (< 10 seconds) the HDPE and LDPE could segregate to any appreciable extent. The long periods of the quenched blend samples

are to, within experimental error, an average of the weighted homopolymer long periods. This supports an intermixed morphology.

For the case of slowly cooled samples, the results indicate segregation of the blend into form bundles of lamellae of primarily LDPE or HDPE. For the first sample of 50/50 HDPE cooled at 0.3°C/min, one sees evidence for the segregation of lamellae into stacks in the apparent increase in scattered intensity between the two maxima after cooling to temperatures below 110° C. Note from figure that in the first phase of cooling (125° C-110° C) of the blend, where the HDPE crystallizes, the heights of the two maxima grow monotonically. In the next stage of cooling when the LDPE begins crystallizing, the intensity at angles between the two maxima seems to increase. In order to study this increase further, the net intensity changes at different temperature regions are calculated and plotted in figure (2.14). The temperature regions chosen were the three regions in the integrated Intensity : 1) 125° C> T< 110° C, where HDPE crystallizes ,2) 110° C> T< 100° C, where LDPE and HDPE both crystallize and 3) T< 100° C where mostly LDPE crystallizes. Each curve in figure represents the amount the intensity changes with a difference of 5° C within each of the respective Temperature regions. Curves one and three in figure 2.14 resemble the SAXS patterns of HDPE and LDPE homopolymers, respectively, in that the maxima occur at the same positions. Curve two shows a mixed pattern of each homopolymer. Such decomposition of SAXS intensities of the blend into the profiles of the two homopolymers strongly suggest that this

system crystallizes to form bundles of lamellae comprised of mostly HDPE or LDPE.

This same pattern of segregation is also present in the subsequent work at 0.5°C/min. Once again the invariant shows a step-like increase (figure 2.10). However in this work the regions are more clearly seen. As in case above, the differential scattering at temperatures lower than 105°C is mainly from LDPE crystallizing, while scattering at higher temperatures is primarily due to HDPE. This domination of the scattering by HDPE is seen in the long periods as well, with the 50/50 and 30/70 HDPE/LDPE blends maintaining the same long period as the pure HDPE until the LDPE begins to crystallize. After this point the decrease in long period is a manifestation of the fact that the peaks of HDPE and LDPE overlap to some extent, and the "shift" seen is primarily a consequence of the addition of scattering from the LDPE. If the molten LDPE were in between lamellae of HDPE, one would expect to see at temperatures ,T, where Tm (HDPE)> T > Tm (LDPE), the long period of the blend to be larger than that of the homopolymers. The presence of LDPE between the HDPE lamellae would be necessary for an intermixed lamellae morphology to form. For the 50/50 and 30/70 blends this is not the case. For the 10/90 HDPE/LDPE blend the long period is actually smaller than that of pure HDPE. This seems to indicate there is at least some interaction of the LDPE and HDPE during crystallization. A possible explanation for this decrease in the long period might be that the small amount of crystalline HDPE acts as a nucleus for some of the more crystallizable elements in the LDPE to

grow on. These elements would be the more linear components in the LDPE. This in turn could produce lamellae smaller in size than the pure HDPE, yet slightly larger than the pure LDPE.

2.4.2 HDPE/LDPE Isothermal Crystallization at Two Successive Temperatures

In a previous set of experiments mentioned earlier, the crystallization of a 50/50 blend of HDPE/LDPE was studied under rapid cooling. For this case results suggested that the lamellae of different PE were not separated in bundles, but rather were mixed together. This is in contrast to slow cooling which did show lamellar segregation. To further study the behavior of the blend under fast coolings , the sample was subjected to two rapid drops in temperature. The blend, initially kept at 150° C , was quickly cooled to 110° C. At this temperature only the HDPE component of the blend was expected to crystallize. After 45 minutes, the time it takes most of HDPE to crystallize, the sample was then cooled to 100° C. At this temperature the LDPE crystallizes. In this way the contributions to the scattering of HDPE and LDPE can be separated.

Figure (2.15) shows some of the Lorentz corrected SAXS intensities measured during the first step of the crystallization at 110° C. The curves show only a single peak which grows in the usual manner. After the second temperature decrease to 100° C, the LDPE begins to crystallize. The resulting scattering profiles can be seen in the in figure (2.16). Note the shift in peak position from small to wider angles. This is evidence for the LDPE crystalizing in between

previously formed HDPE lamellae, resulting in a smaller long period. This behavior is quite similar to that of rapidly cooled samples directly quenched below T for LDPE. The same conclusion is drawn for the rapid two step crystallization as for the rapid one step crystallization, that is lamellae of HDPE and LDPE are mixed together. There is no evidence for the segregation of lamellae seen in the slow cooled sample.

2.4.3 LLDPE/LDPE Quench vs. Slow cooling

Blends of LLDPE and LDPE studied under a quick cool to 60°C show similar behavior to that of the HDPE/LDPE blends. Figure (2.17) shows the SAXS invariant as a function of time for LLDPE, LDPE and their blends. The samples were cooled to 60°C in the same manner as the HDPE/LDPE systems. Again, a smooth increase in Q to a plateau value is seen. This time, however their is no small peak in the Q- t plots because the crystallinity for pure LLDPE is below 50%. The corresponding plots of long periods (figure 2.18) show much the same behavior as those for the long periods of quenched HDPE/LDPE blends. The lp's are once again, roughly an average of the homopolymer's long periods.

Differences between HDPE/LDPE and LLDPE/LDPE systems are seen in the scattering from slow cooling runs, however. This is most clearly seen in the SAXS Invariant. The samples were cooled identically as the HDPE/LDPE samples (0.5°C/min). The invariant of the pure LLDPE , rather than showing a sigmoidal rise as LDPE and

HDPE, displays two regions which increase at different rates. The first region ,which begins at 120°C and ends at 112°C, exhibits behavior much like HDPE or LDPE homopolymers. After 112°C, instead of leveling off, the invariant continues to rise at a different rate than the previous region.

The non-monotonic increase in the invariant of pure LLDPE is a reflection of the fact that LLDPE is heterogeneous in branch distribution from chain to chain. Recently, using temperature rising elution fractionation[35, 36](TREF) it has been suggested that LLDPE is actually bimodal in chain distribution, consisting of two components, with one component having fewer branches than the other. The component with fewer branches crystallizes at a higher temperature than the other, more highly branched part. This lightly branched component accounts for the initial rise in the LLDPE invariant. As the temperature is lowered further, the rest of the LLDPE begins to crystallize and causes the second region of increases Q.

For temperatures greater than the crystallization temperature of LDPE (about 107°C), the invariants of the blends also show these two regions of different increase rates of the invariant. As the temperature is lowered below 107°C, the 50/50 and 30/70 blend invariants increase as the LDPE crystallizes. This increase is difficult to distinguish as it is superimposed on the still increasing invariant of the LLDPE component.

The crystallinity by WAXS of the slowly cooled 50/50 and 30/70 LLDPE/LDPE blends also exhibit this step-wise increase. As shown in figure (2.20) , the pure LLDPE crystallinity rises quickly from 118°C to 114°C . After 114°C the crystallinity continues to rise, but at a reduced rate. The blends mimic this behavior, although the crystallization starts at a slightly lower temperature (116°C). At 110°C, the LDPE begins to contribute to the crystallization.

The long period change of 30/70 and 50/50 LLDPE/LDPE blends under slow cooling are shown in figure (2.21) It is not as easy here to distinguish between two regions of crystallization as it was for the HDPE/LDPE blends. This is because the LDPE and LLDPE long periods decrease at about the same rate . Once again the blends if anything, show initial long periods the same as or less than the LLDPE homopolymer long period. Interestingly, the 30/70 LLDPE/LDPE blend becomes identical to the LDPE homopolymer long period at higher temperatures.

The most striking difference between the HDPE/LDPE and LLDPE/LDPE blends occur in the lowest composition studied (10/90). Shown in figure (2.19) is the invariant of the 10/90 LL/LD blend under slow cooling. The multi-step behavior of the higher composition LLDPE/LDPE blends is completely absent. Instead one sees a smooth increase in Q, in a manner similar to LDPE, except that the Q increase starts at a higher temperature than just pure LDPE. In contrast, the HDPE/LDPE 10/90 blend exhibits a dramatic two-step rise in Q. The fact that the temperature at which the lamellae

formation begins in the 10/90 blend is above that of the pure LDPE indicates some interaction between blend components occurs. The LLDPE may serve as nuclei for the LDPE. This would indicate that to some degree less than 10%, co-crystallization does occur in LLDPE/LDPE blends.

2.4.4 Inhomogeneity in LLDPE.

The heterogeneity of LLDPE in comonomer composition has complicated the results the studies of LLDPE/LDPE blends. Depending on the LLDPE crystallization temperature, comomer type, content, and distribution, multiple peaks can be observed in DSC melting endotherms of these materials. These multiple peaks are due to a wide distribution in crystal size and perfection. Recently Reynaers and co-workers[37] have studied the melting behavior of octene-LLDPEs by synchrotron radiation. Although the molecular weights and branch contents studied were different from those examined in this work, the Invariants showed qualitatively the same type of behavior, indicative of a wide distribution of crystal sizes.

Recently, we have obtained LLDPEs which show no multiple melting endotherms in DSC. The characteristics of these samples are listed in table 2.1. They will be refered to by the codes RB22 and RB48. Synthesized by Dr. Ferd Stehling of Exxon, these LLDPEs are produced by Zeigler-Natta polymerization with different catalysts than conventional LLDPE. Multiple polymerization sites on the catalylst are thought to be responsible for the mutiple nature of branch distribution along the chain. These RB LLDPEs are thought be more homogeneous

in branch distribution. The heterogeneity in branch content usually produces two endotherm peaks during melting. The high temperature peak is associated with a so-called 'linear' component, which contains few side chains. The lower temperature peak is caused by more highly branched components. The SC branches will lower Tm by restricting crystal size (if excluded from the crystal) or crystal perfection (if included in the crystal).

Shown in figure (2.22) is the invariants of these new LLDPEs under slow cooling from the melt at 0.5°C/min along with the conventional commercial LLDPE used in the blend work. RB48 is the most highly branched sample (35 branches/ 1000 backbone C) and has low crystallinity and a lower melting point than LDPE, about 90°C (see table 2.1) RB22 has less branching (15 branches/ 1000 backbone C) than RB48 and approximately the same amount of branching on average as conventional LLDPE (18 branches /1000 backbone C). RB22 still has a lower Tm than LLDPE. This may be a reflection of the fact that LLDPE is heterogenous in branch distribution among chains. The T_m of LLDPE is probably weighted more toward the higher crystalline, linear-like component which would dominate the contribution to DSC measuremnets. Both the invariants of the RB LLDPEs show a small increase in Q before the major increase in Q near the respective melting temperatures. This 'foot' in the Q curves is caused by a slight increase in scattering at small angles with no discernable peak. It does not seem to be associated with any lamellae- like structure. Possibly it could be very small amounts (less than a few percent) of a linear component which

might be crystallizing first, producing isolated crystallites, which would produce no scattering peak.

A 50/50 blend of RB48/LDPE was prepared by the same procedure as described for the previous blends, and also subjected to slow cooling from the melt. In this case it is the LDPE which is the high melting temperature component. The Invariants are shown in figure (2.23). There is no sudden jump in the blend invariant after 90°C, only a continuous rise in Q as the RB48 crystallizes. The blend long period is larger than the pure LDPE. This means at least some of the RB48 must be trapped between the crystallizing LDPE lamellae. This is in contrast with the previous cases studied in slow cooling.

2.5 Conclusions

Small and wide angle x-ray scattering intensity observed during the crystallization of a blends of HDPE/LDPE and LLDPE/LDPE have shown the segregation scale to be at the lamellar level. The extent of the segregation observed depends on the thermal treatment and the composition of the blend.

For rapid cooling, the lamellae tend to be intermixed in a more or less random fashion. For the case of slow cooling, the behavior of the SAXS invariant and WAXS have suggested that segregation occurs on a lamellar level. At slow coolings of 0.3°C patterns taken at 120° C-110 resemble HDPE homopolymer scattering , while those taken at 100° C- 90° C resemble the LDPE homopolymer. Between 110° C-100° C the scattering appears to be a superposition of both HDPE and LDPE.

Such decomposition of the SAXS intensities into patterns of the homopolymers would be typical of the formation of bundles of lamellae of primarily one component.

At slightly faster coolings (0.5°C/min), this trend continues for blends composed of 30% or more of the faster crystallizing component. In blends consisting of 10% LLDPE or HDPE, with LDPE, the long period spacings along with the WAXS, suggest at least some interaction between the components. In the case of 10/90 LLDPE/LDPE, co-crystallization may occur. For 10/90 HDPE/LDPE, the invariant and crystallinity clearly shows two distinct steps as the crystallization occurs. Yet the long period, is smaller than that of the pure HDPE for temperatures above which LDPE should not be crystallizing.

The LLDPE itself was found to exhibit crystallization behavior indicating the formation of crystals heterogeneous in either perfection or size. This might be caused by the presence of a 'linear'-like component possessing less short chain branching than the rest of the material. Attempts at producing LLDPE's with more uniform short chain branch distribution seem to be at least partially successful. However there may still exist small amounts of linear-like molecules in these newer LLDPE's.

TABLE 2.1

Types of LLDPE Used in

SAXS/WAXS

Sample	Branch Content mole % Hexene	Tm (DSC) °C	Mw	Mw/Mn
RB48	7.1	91	50,600	1.86
RB22	3.0	109	65,500	2.10

REFERENCES

1. T. O. J. Kessler, *Polyethylene*, Reinhold Publishing Corporation, New York, 1958.

2. L. Mandelkern, *Crystallization of Polymers*, McGraw Hill, New York, 1964.

3. J. M. Rego Lopez and U. W. Gedde, *Polymer* , **30**, 22 (1989).

4. M. Ree, T. Kyu, and R. S. Stein, *J. Polym Sci. Polym. : Phys. Ed.*, **25**, 105 (1987).

5. T. Kyu, S-R. Hu and R. S. Stein, *J. Polym Sci. Polym. : Phys. Ed.*, **25**, 89 (1987).

6. M. R. Shishesaz and A. A. Donatelli, *Polym Eng. Sci.*, **21**, 869 (1981).

7. F. P. LaMantia and D. Acierno, *Eur. Polym. J.*, **21**, 811 (1985).

8. D. Acierno, D. Curto, F. P. LaMantia and A. Valenza, *Polym. Eng. Sci.*, **26**, 28 (1986).

9. A. M. Thayer, *Chem. Eng. News*, **67**, 7 (January 30, 1989).

10. M. Ree, Ph.D. Thesis, University of Massacusetts, Amherst 1986.

11. S. Hu, T. Kyu, R. Stein, *J. Polym Sci Polym* **25**, 7 (1987).

12. L. Minkova, M. Mihailov, *Colloid & Polymer Sci.*, **265**, 1 (1987).

13. S. McGuire, Masters Thesis, University of Massachusetts, Amherst 1989.

14. S. McGuire, P. Esnault, M. Satkowski, R.S. Stein (Manuscript Submitted *Macromolecules*)

15. J. M. Shultz, .*J. Polym. Sci.*, **14**, 2291 (1976).

16. J.S. Lin, R.W. Hendricks, J. Shultz, andM.J. McCready *J. Polym. Sci. Polym. : Phys. Ed.*, **20**, 1365 (1982).

17. J.M. Shultz, J.S. Lin, and R.W. Hendricks, *J. Appl. Crystallogr.* **11**, 551 (1978).

18. J. H. Magill, J. M. Schultz, and J. S. Lin, *Colloid &Polymer Sci.* **265**, 193 (1987).

19. C. Reckinger, F. C. Larbi, J. Rault, *J. Macrol. Sci.*, **B23,** 511 (1985).

20. L. E. Alexander, *X-Ray Diffraction Methods in Polymer Science*, Robert E. Kreiger Publishing Company, New York, 1979.

21. M. Kakudo and N. Kasai,*X-Ray Diffraction by Polymers* ,Elsevier Publishing Company, New York, 1972.

22. G.D. Wignal, B. Crist, T.P. Russel, and E.L. Thomas, ed. , *Scattering, Deformation and Fracture in Polymers*, Materials Research Society Symposia Proceedings, Pittsburgh, 1987

23. A.W. Coven, *Phys Rev.*, **41**,422 (1932).

24. G.E.M. Jauncey and F. Pennell, *Phys. Rev.*, **43**, 585 (1932).

25. W.Ruland, *Acta Cryst.* **14**, 1180 (1961).

26. W.Ruland, *Polymer*, **5**, 89 (1964).

27. A. Guinier and A. Fournet, *Small Angle X-ray Scattering*, Wiley, New York 1955.

28. G. Porod, *Kolloid-Z.*, **124**, 83 (1951).

29 G. Porod, *Kolloid-Z.*, **125**, 51 (1952).

30. Chu, B. ; Wu, D. Q.; Wu, C., *Rev. Sci. Instrum.*, **58**, 1158 (1987).

31. H.H. Song, D.Q. Wu, B. Chu, M. Satkowski, M. Ree, R.S. Stein, and J.C. Phillips, *Macromolecules* (in press).

32. Hoseman , Bachhi , *Direct Analysis of Diffraction by Matter*, Interscience Publishers, New York, 1962.

33. Vonk, C., in *Small Angle Scattering*, H. Brumberger, ed., John Wiley, 1977.

34. M. Ree and R.S. Stein , *Macromolecules* (Submitted)

35. F. Mirabella, and E. Ford *J. Polym Sci: Part B: Polymer Physics*, **25**, 777 (1987)

36. F. Mirabella, S. Westphal, P. Fernando, E. Ford, and J. Williams *J. Polym Sci: Part B: Polymer Physics*, **26**, 1995 (1988).

37. P. Schouterdern,M. Vandermarliere, C. Rickel, M.H. Koch, G. Groeninckx, and H. Reynaers *Macromolecules* **22**, 237 (1989).

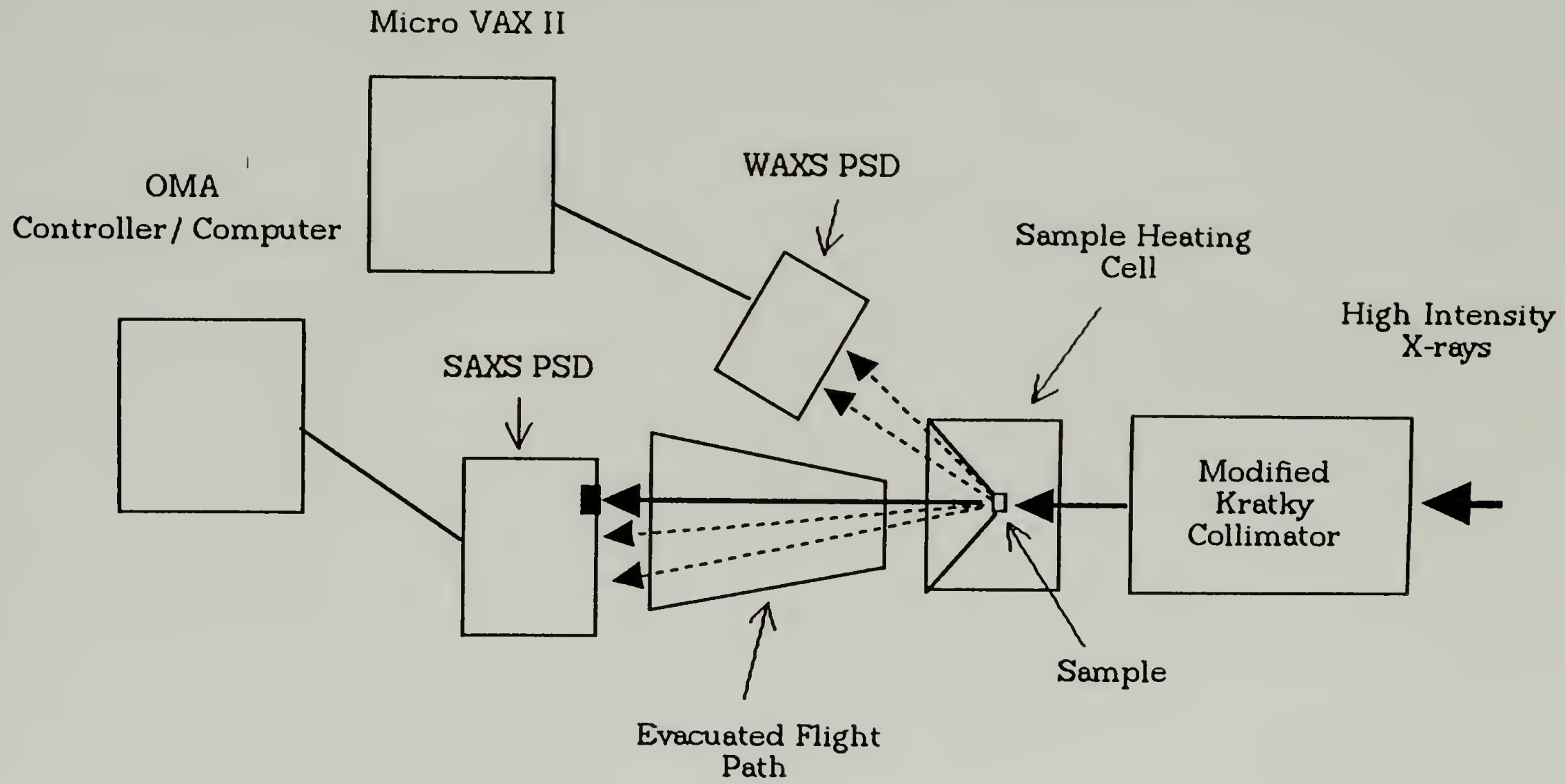

Figure 2.1 Brookhaven synchrotron x-ray apparatus.

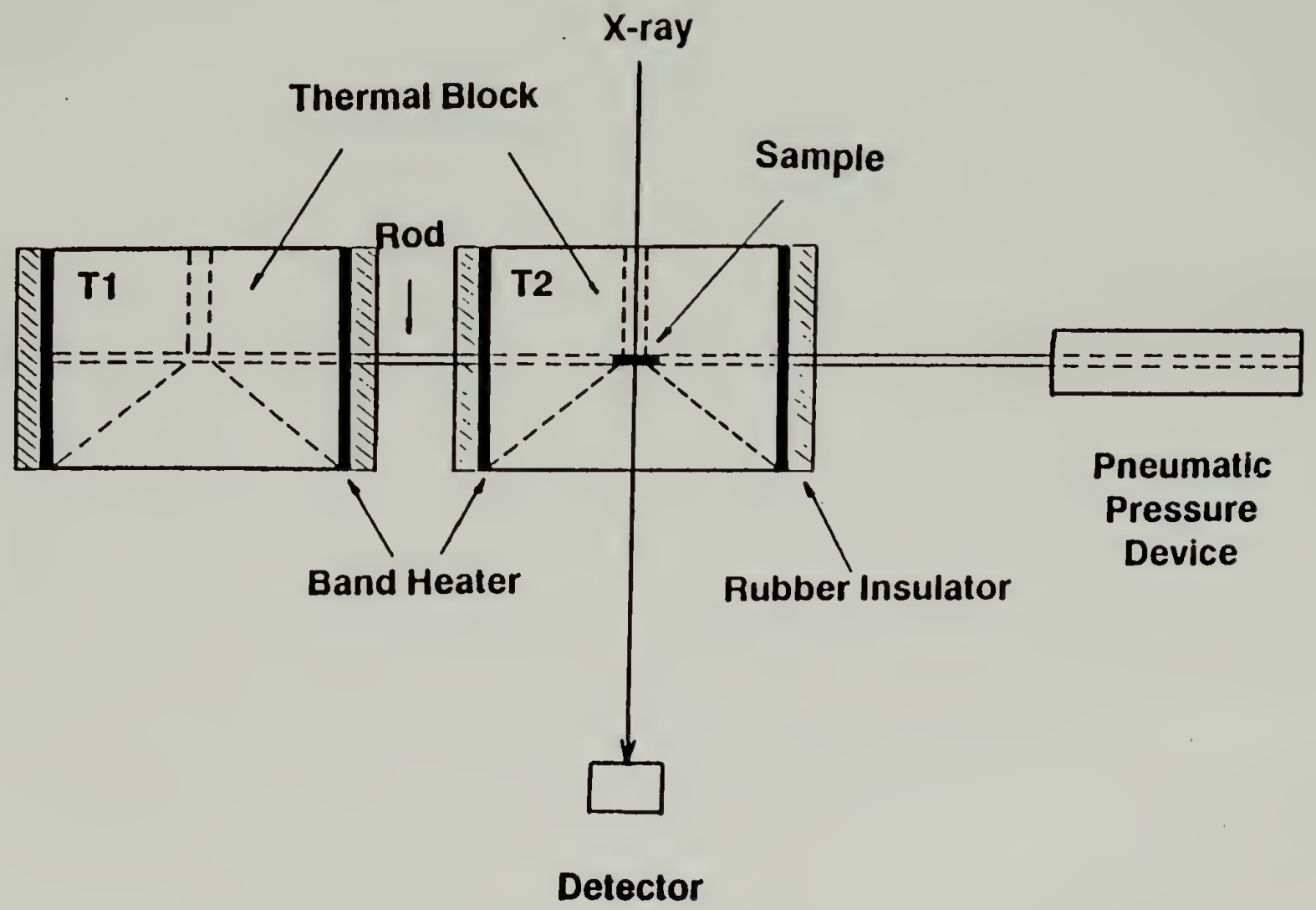

Figure 2.2 Temperature jump cell.

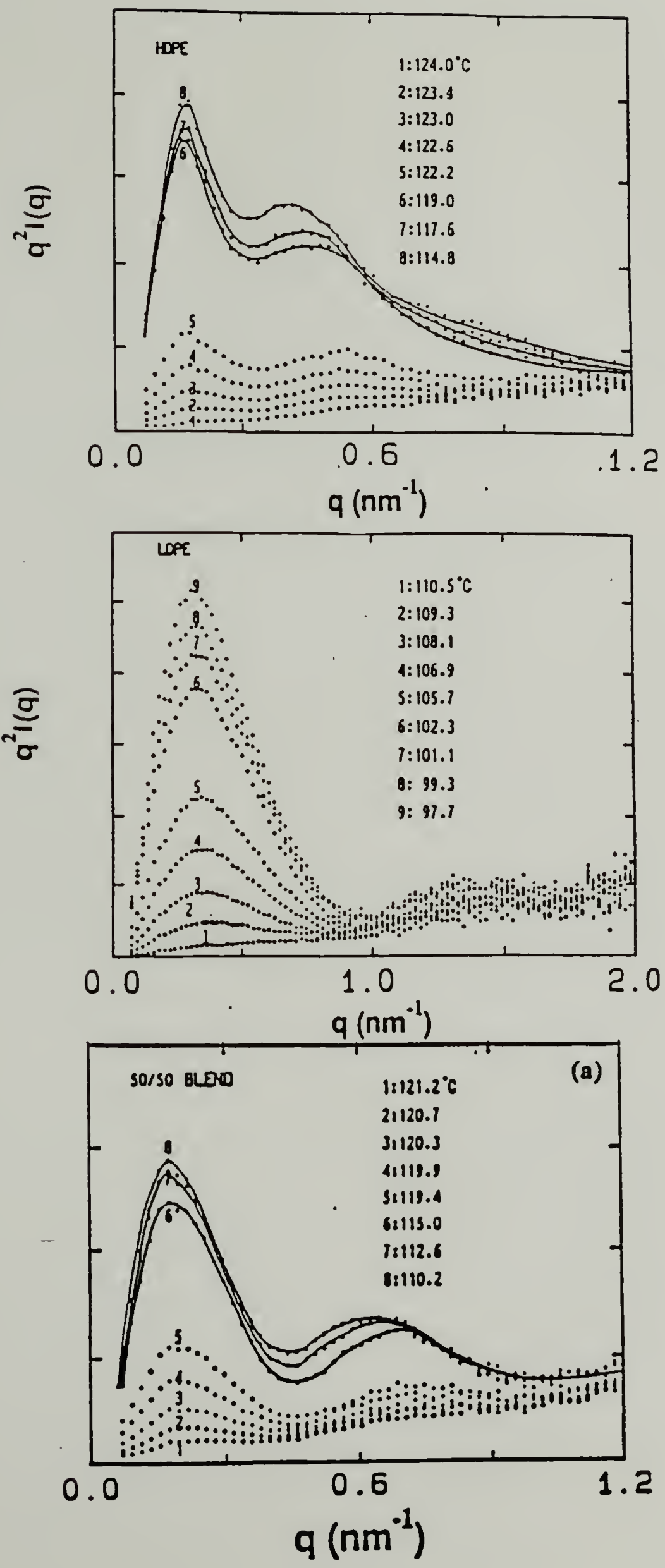

Figure 2.3 Lorentz corrected scattering of HD, LD, and 50/50 HD/LD blend cooled at 0.3°C/min.

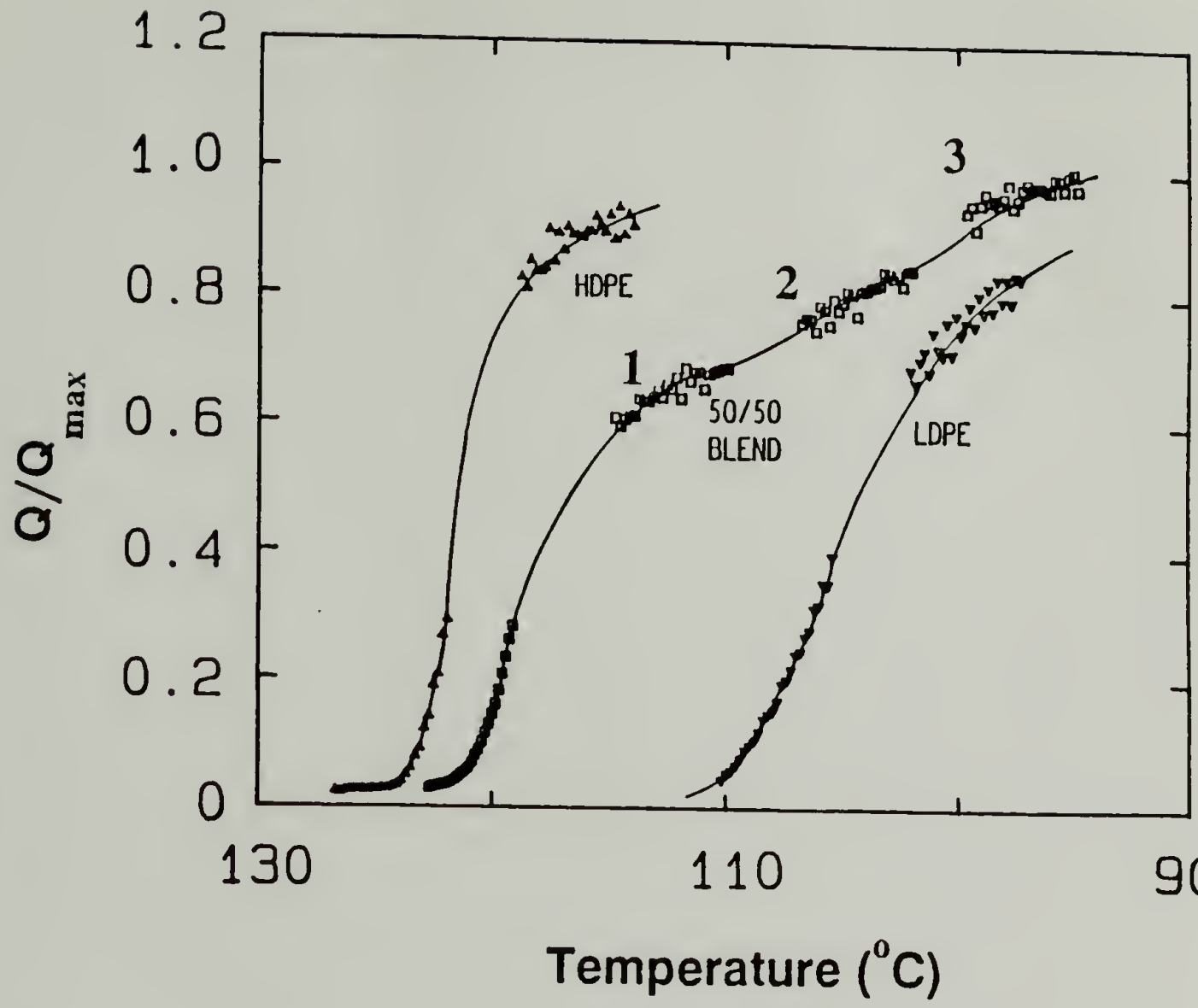

Figure 2.4 Normalized invariant of slow-cooled HD/LD Blend. Cooling rate was 0.3°C /min. Numbered regions correspond to temperatures where the homopolymers contribute to the scattering. See figure 2.14.

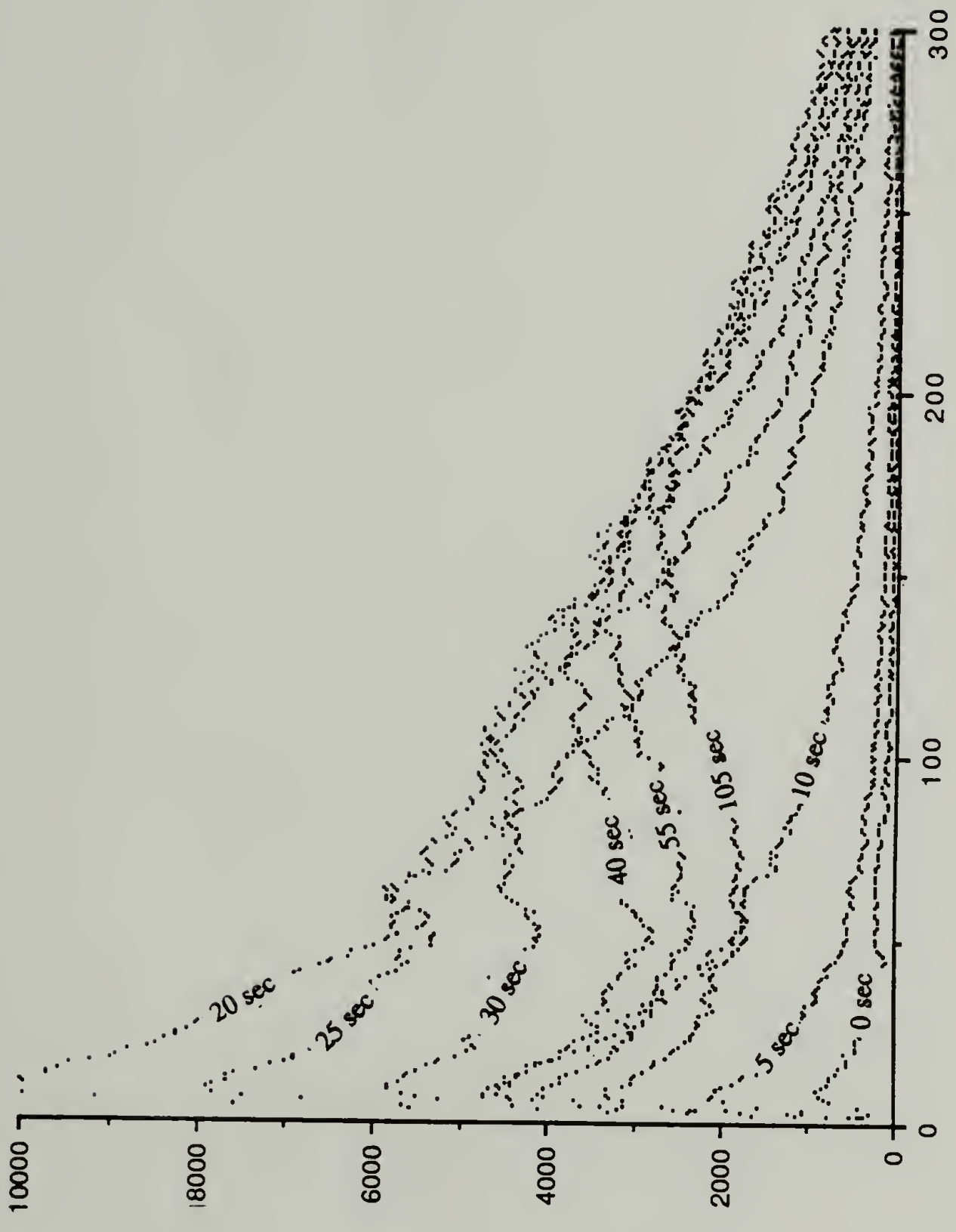

Figure 2.5 SAXS from 30/70 HD/LD under quench to 60°C from the melt. The collection time per curve was 5 sec. Time after quench for each curve is given in the figure.

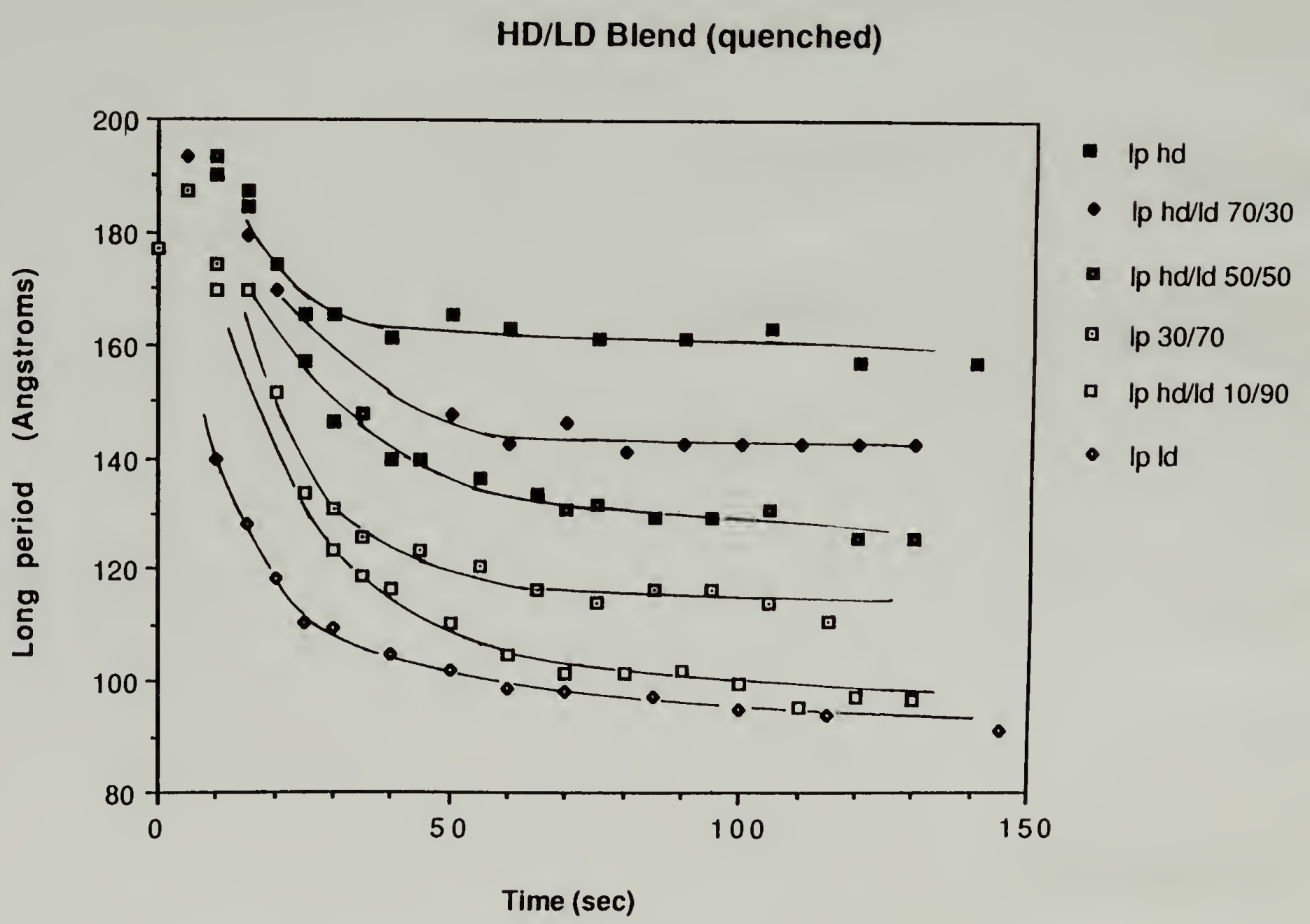

Figure 2.6 HD/LD long periods as a function of time. Quenched to 60°C from the melt.

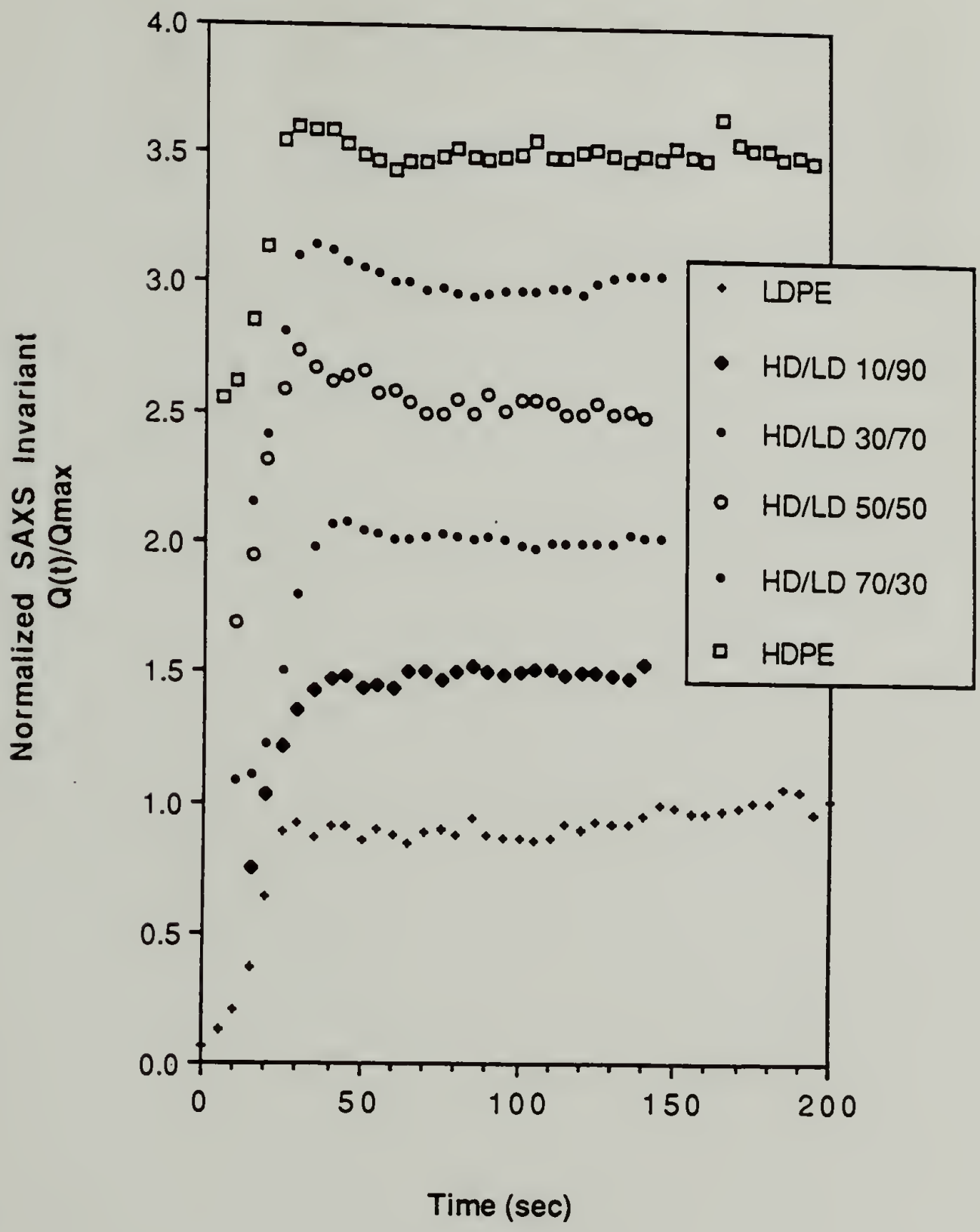

Figure 2.7 HD/LD invariants vs. time. Quenched to 60°C from the melt. The abscissa has been displaced +0.5 for each blend for clarity.

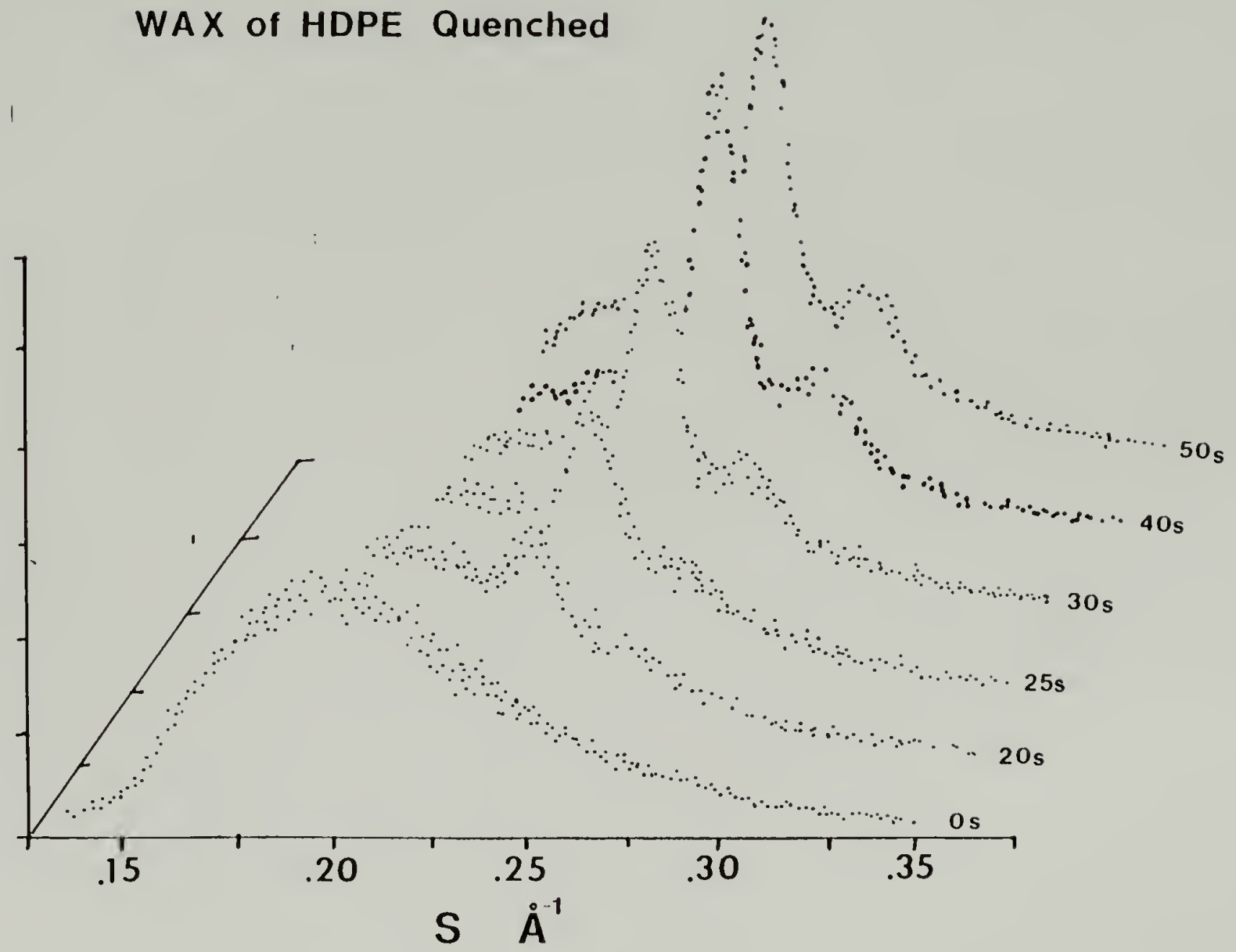

Figure 2.8 Uncorrected WAXS of quenched HDPE. Each curve is collected for 5 sec. Time after quench is given in the figure.

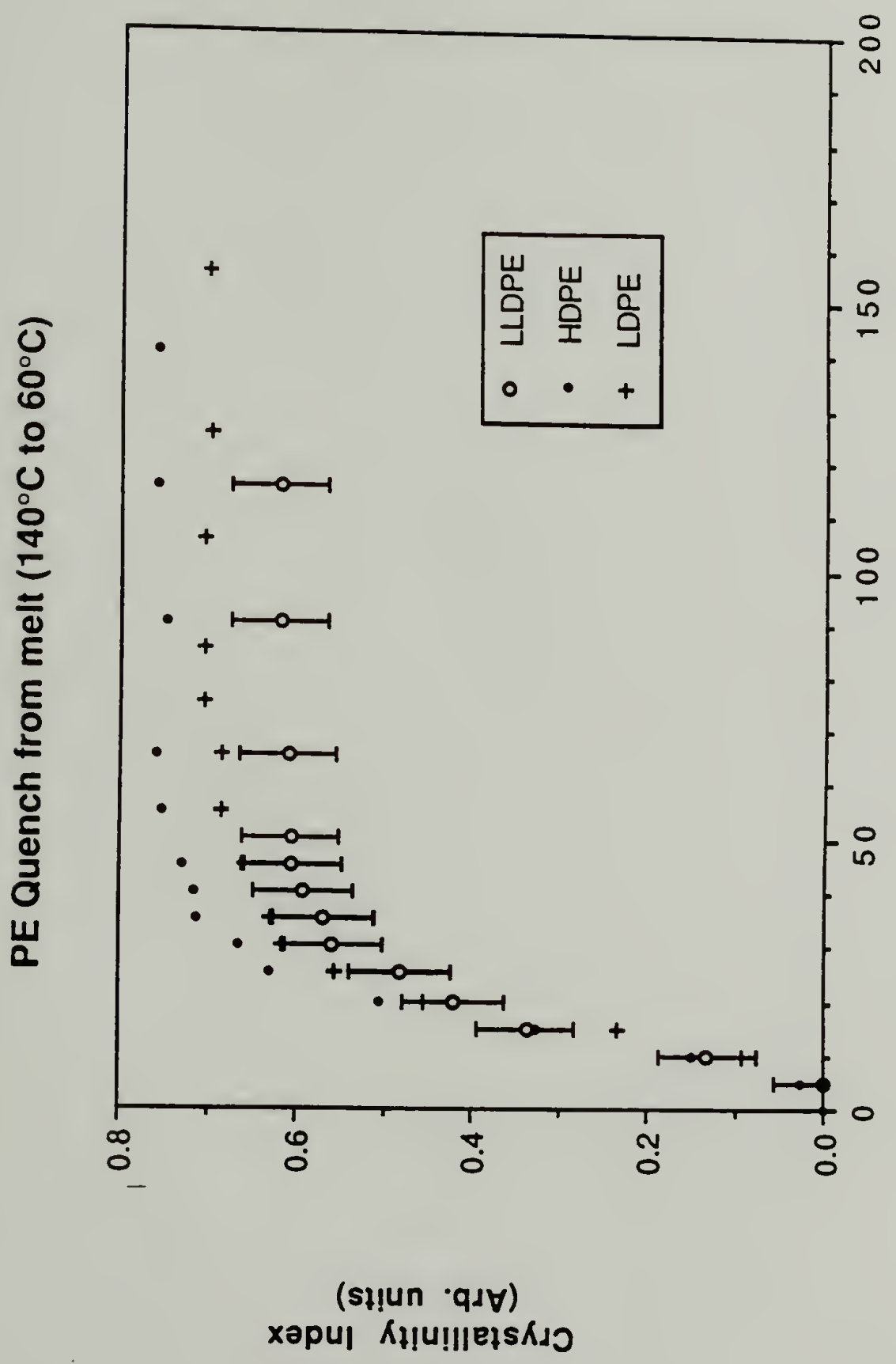

Figure 2.9 Crystallinity index of quenched PE's. Quenched to 60°C from the melt.

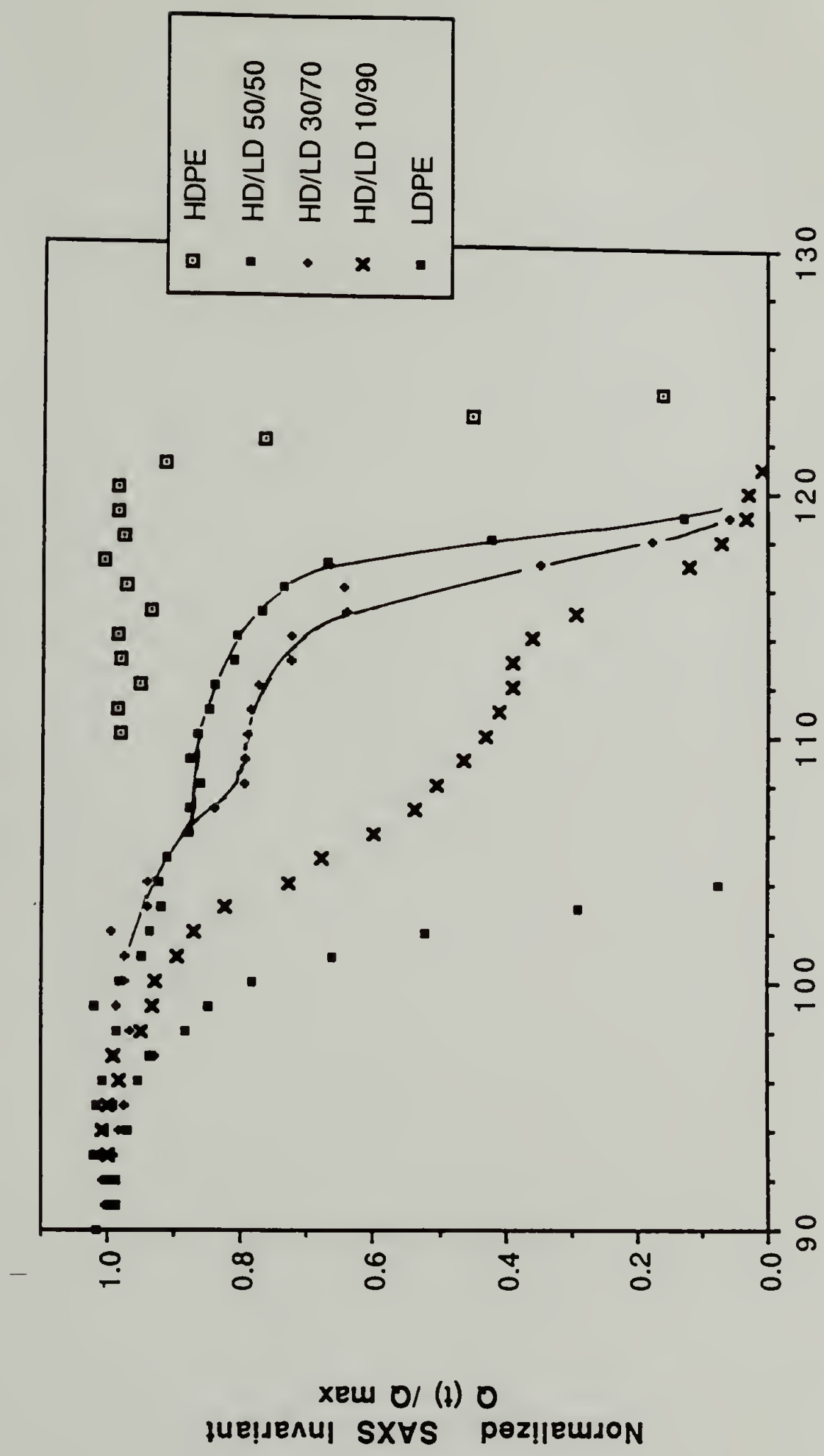

Figure 2.10 Normalized invariants of slow cooled HD/LD blends.as a function of temperature. The cooling rate was 0.5°C/min.

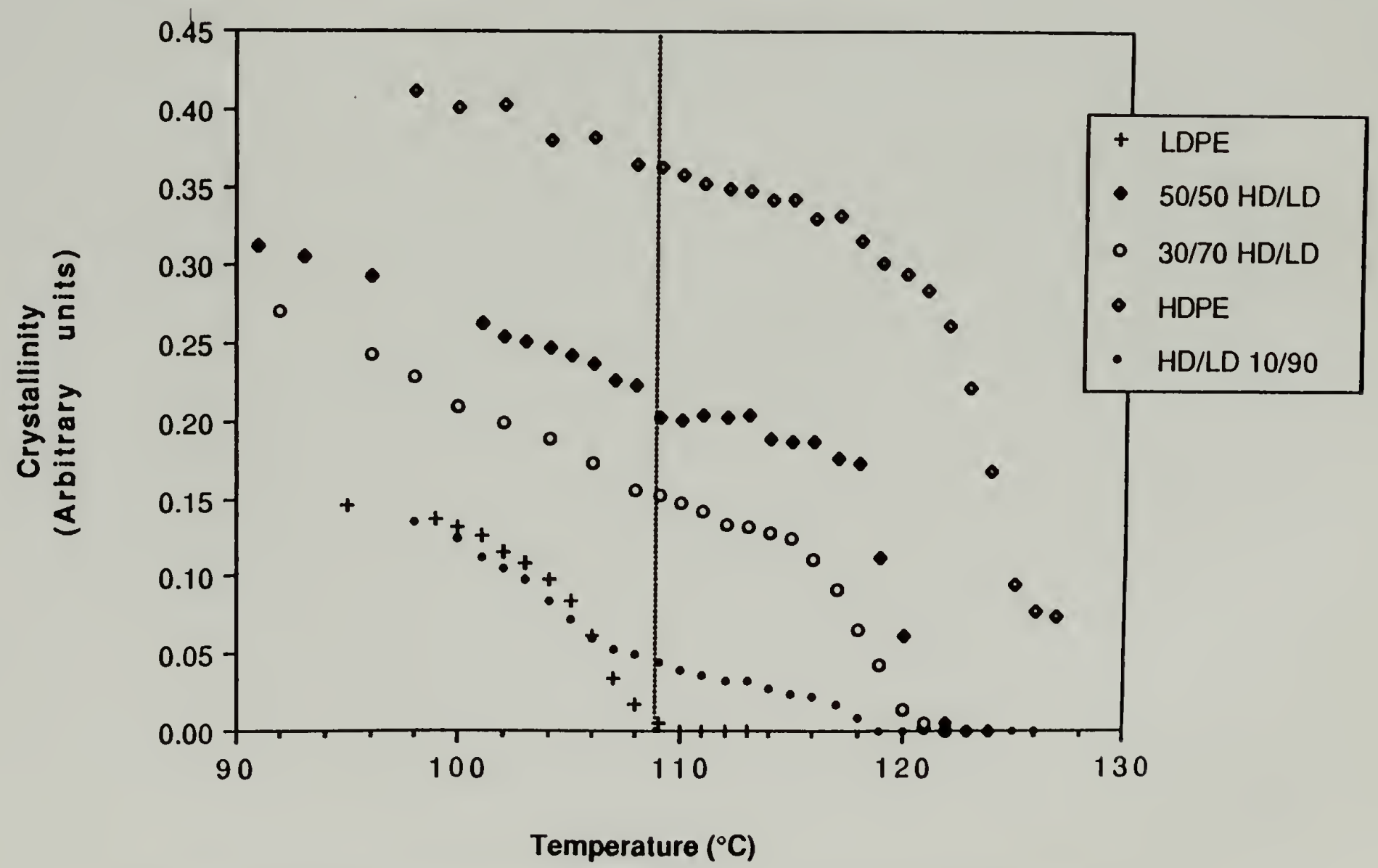

Figure 2.11 Crystallinity index of slow cooled HD/LD blends as a function of temperature. The cooling rate was 0.5°C/min.

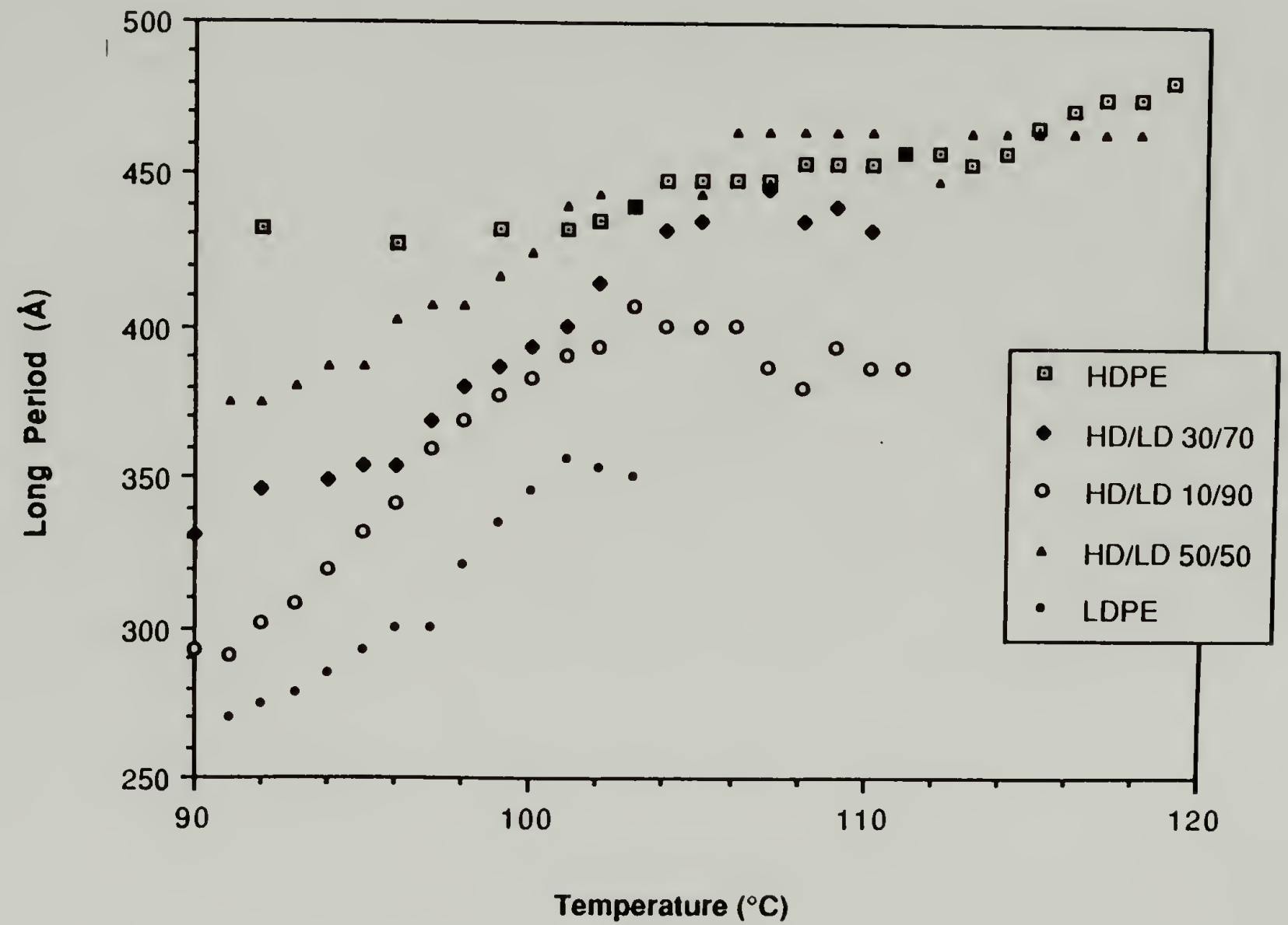

Figure 2.12 Long periods of slow cooled HD/LD blends as a function of temperature. The cooling rate was 0.5°C/min.

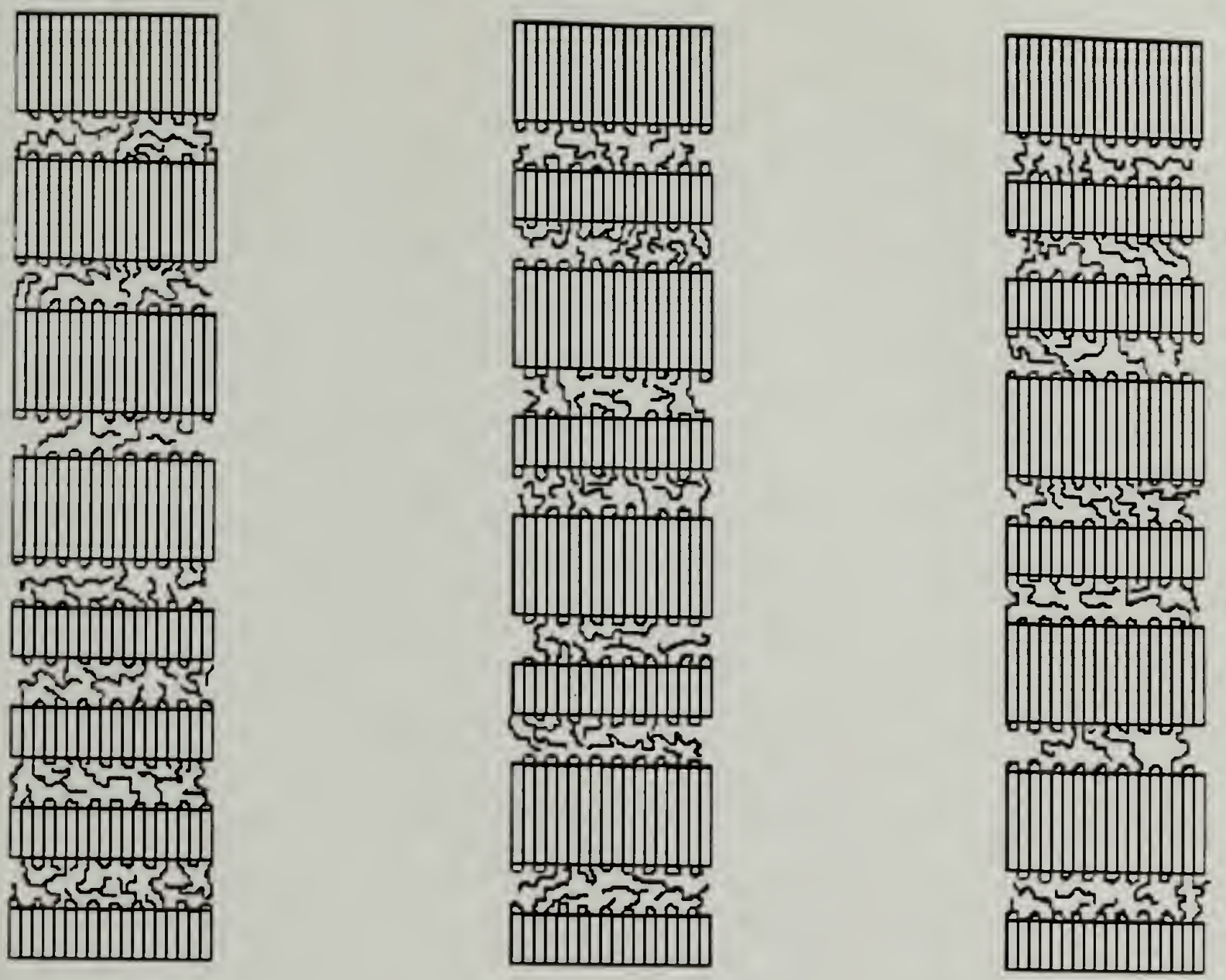

Figure 2.13 Schematic of possible lamellar morphologies in PE blends. A) Segregated into bundles. B) Alternating . C) Randomly mixed.

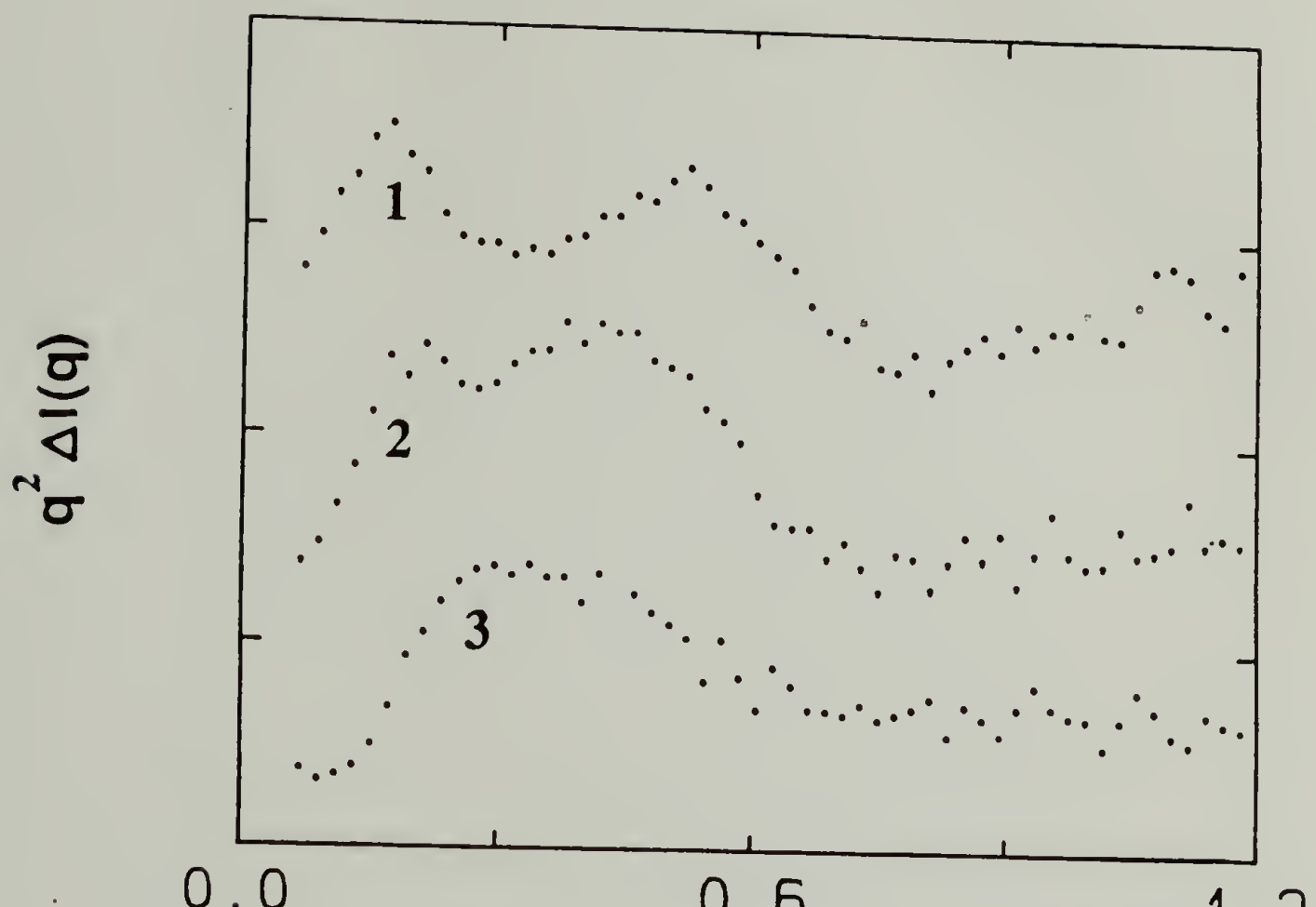

Figure 2.14 Differential intensity vs. temp for 50/50 HD/LD blend cooled at 0.3°C/min. 1). Between 115°C and 110°C. 2) Between 108°C and 103°C 3) Between 100°C and 95°C

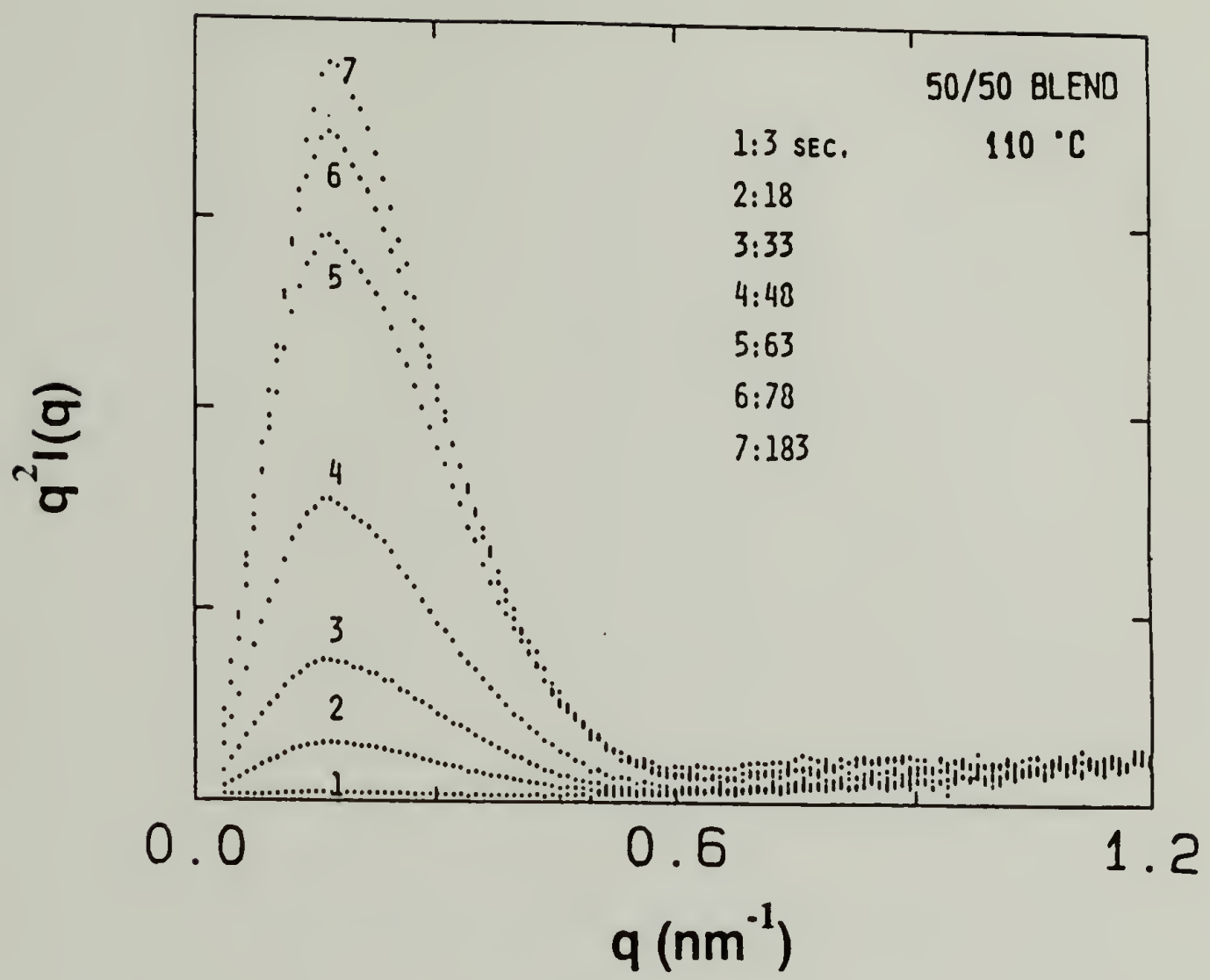

Figure 2.15 SAXS intensity of 50/50 HD/LD blend crystallized at 110°C.

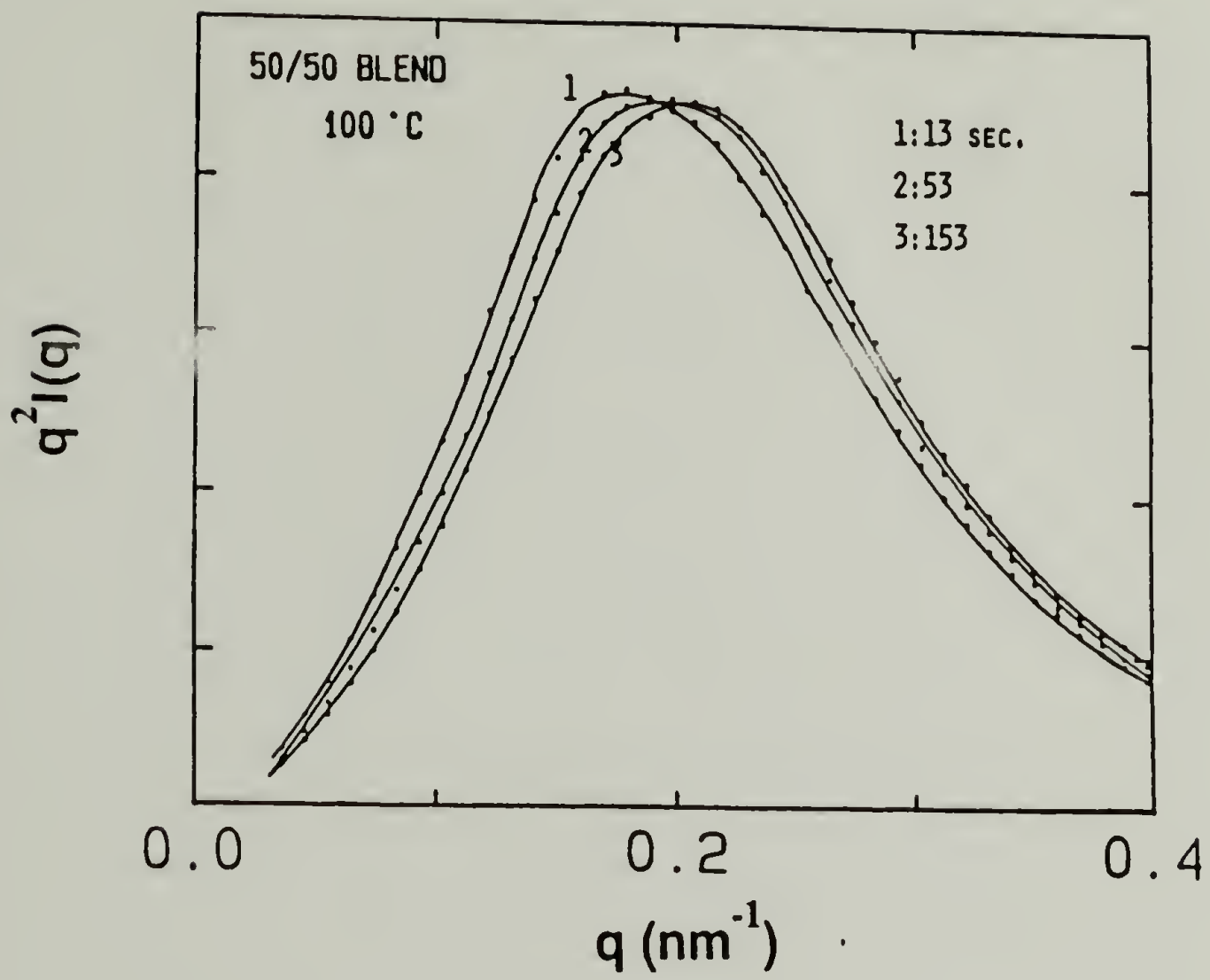

Figure 2.16 SAXS intensity of HD/LD blend crystallized at 110°C for 45 minutes, then crystallized at 100°C

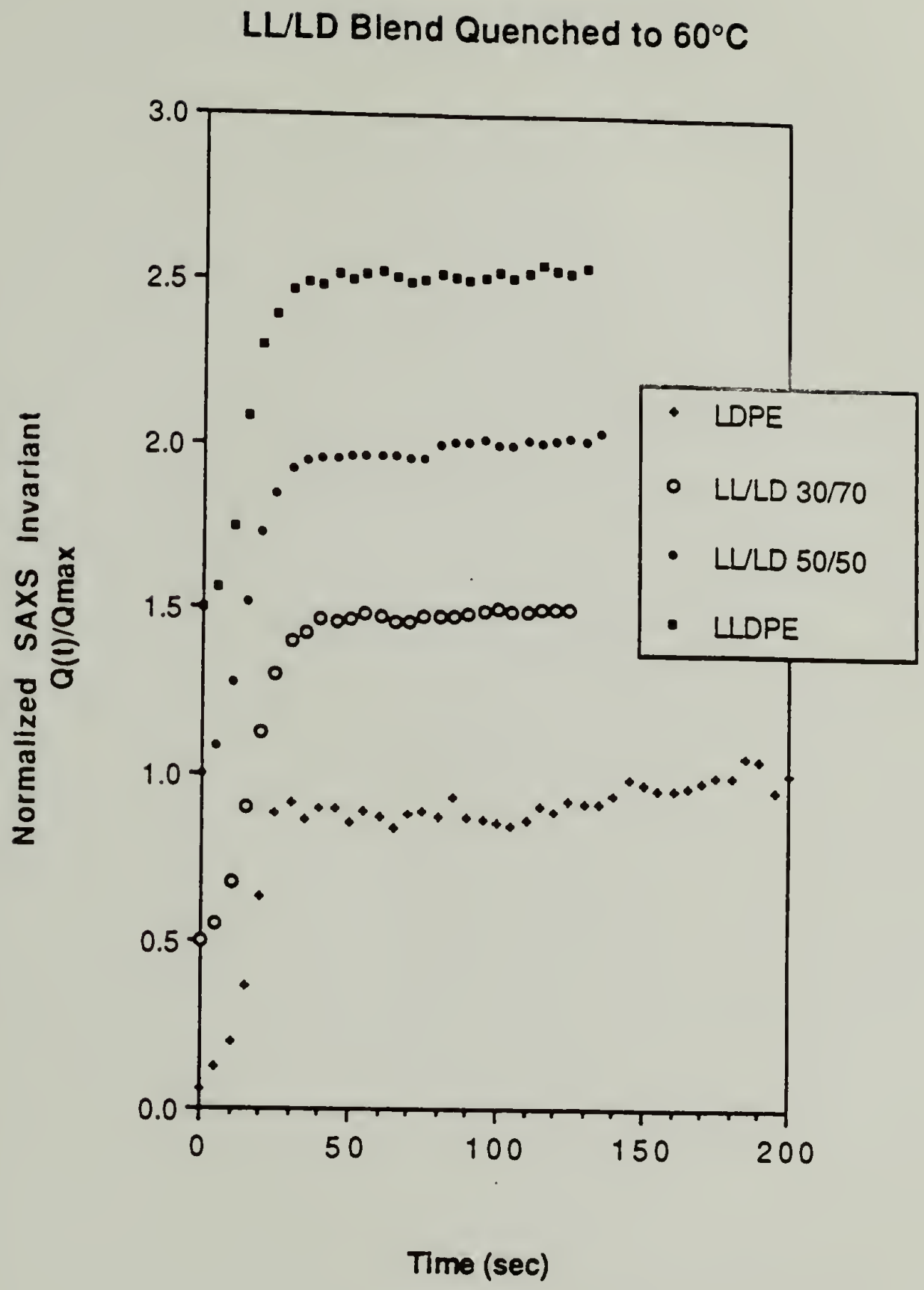

Figure 2.17 Invariants of LLD/LD blends vs. time Quenched to 60°C. The abscissa has been displaced +0.5 for each blend for clarity.

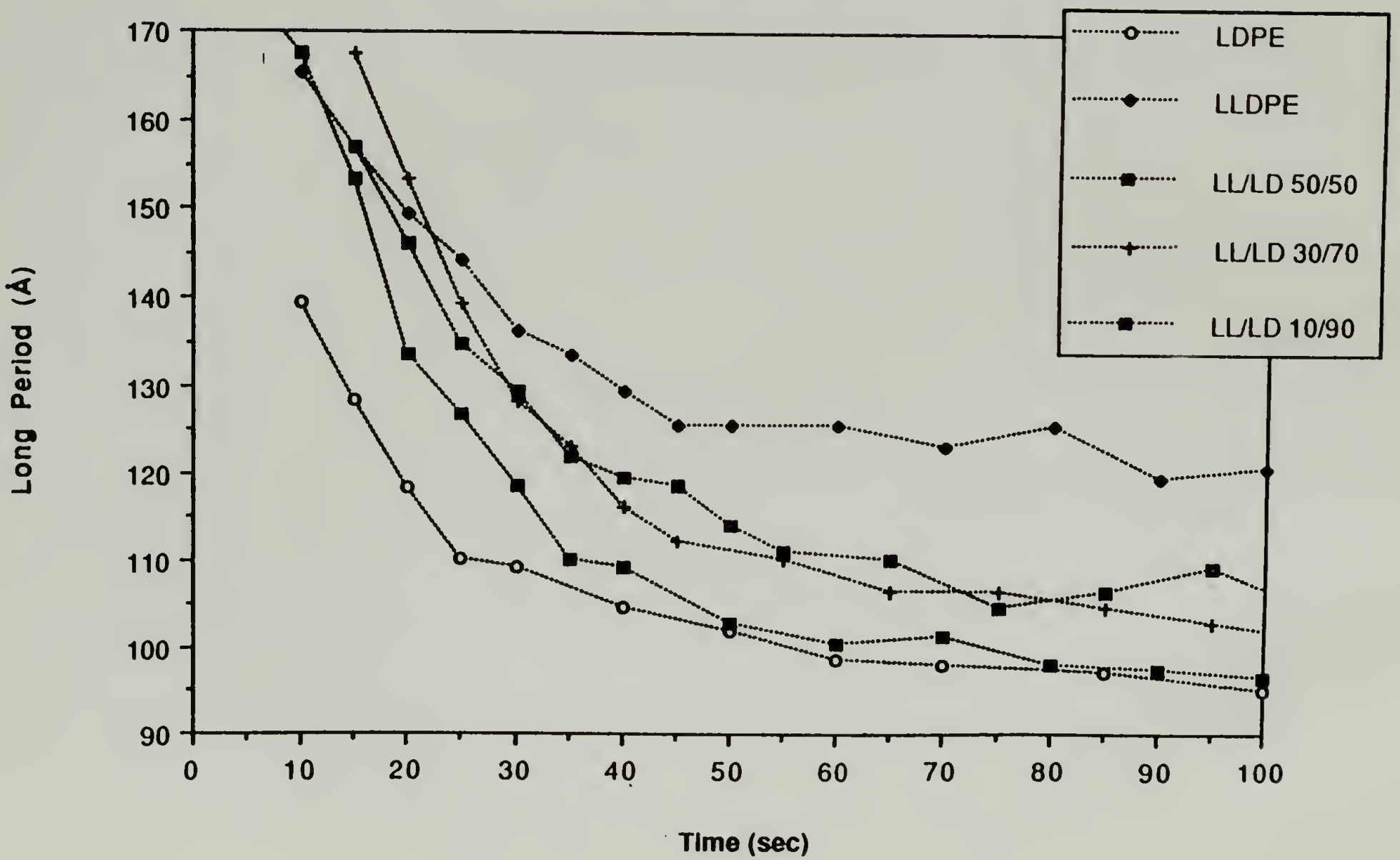

Figure 2.18 Long periods of LLD/LD blends vs. time Quenched to 60°C.

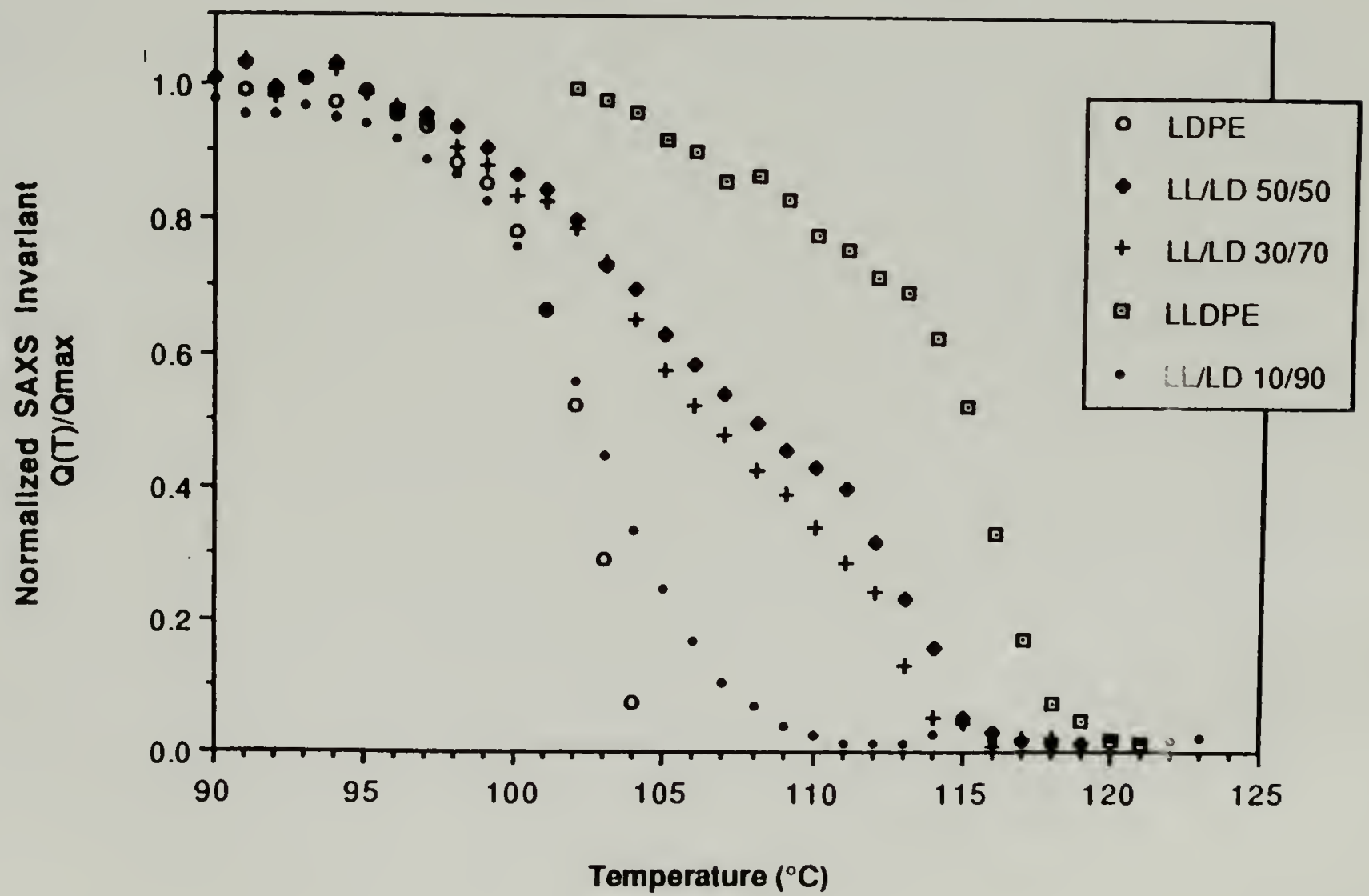

Figure 2.19 Normalized invariants of slow cooled (0.5°C/min) LLD/LD blends as a function of temperature

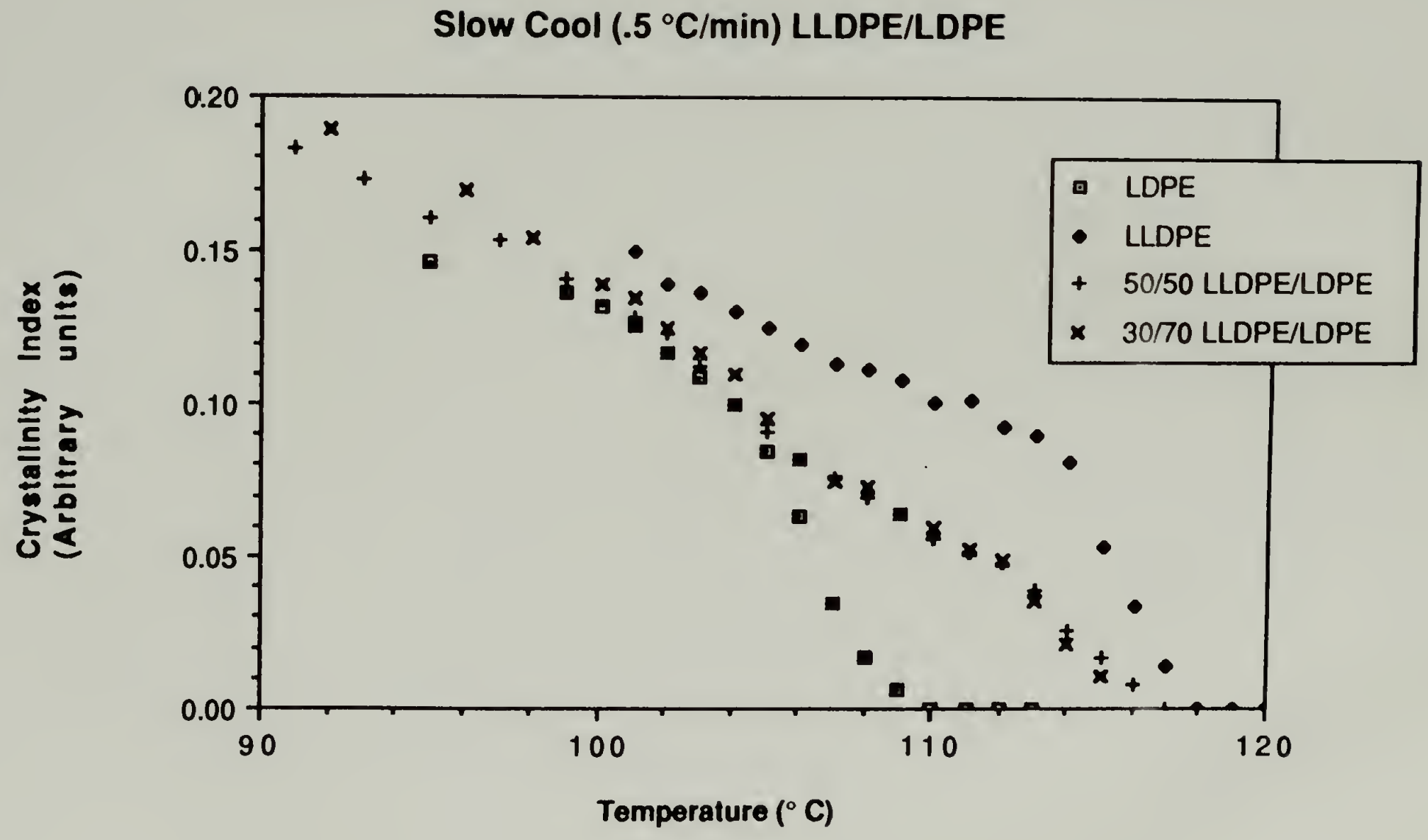

Figure 2.20 Crystallinity Index of slow cooled LLD/LD blends a function of temperature. The cooling rate was 0.5°C/min.

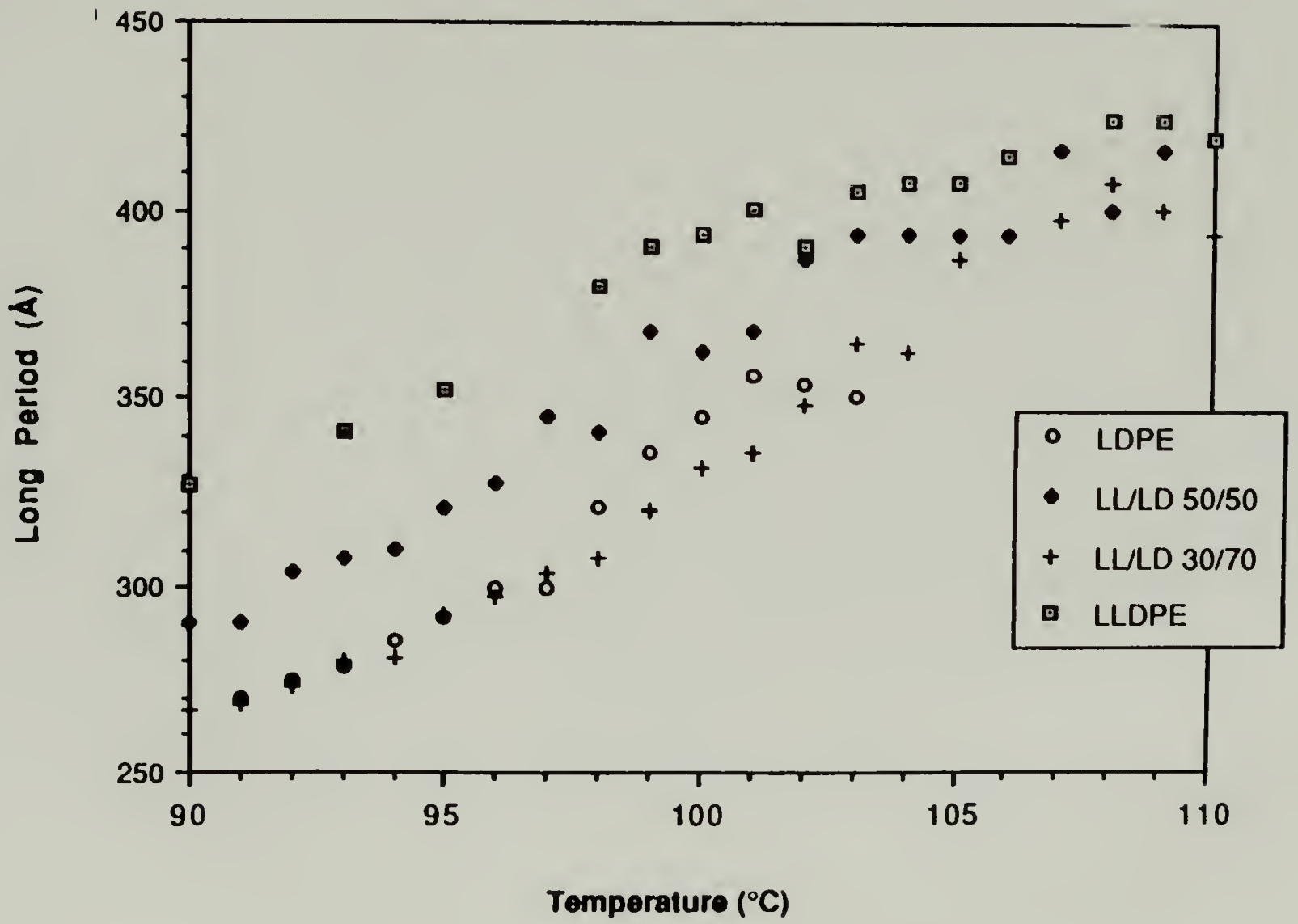

Figure 2.21 Long periods of slow cooled (0.5°C/min) LLD/LD blends as a function of temperature.

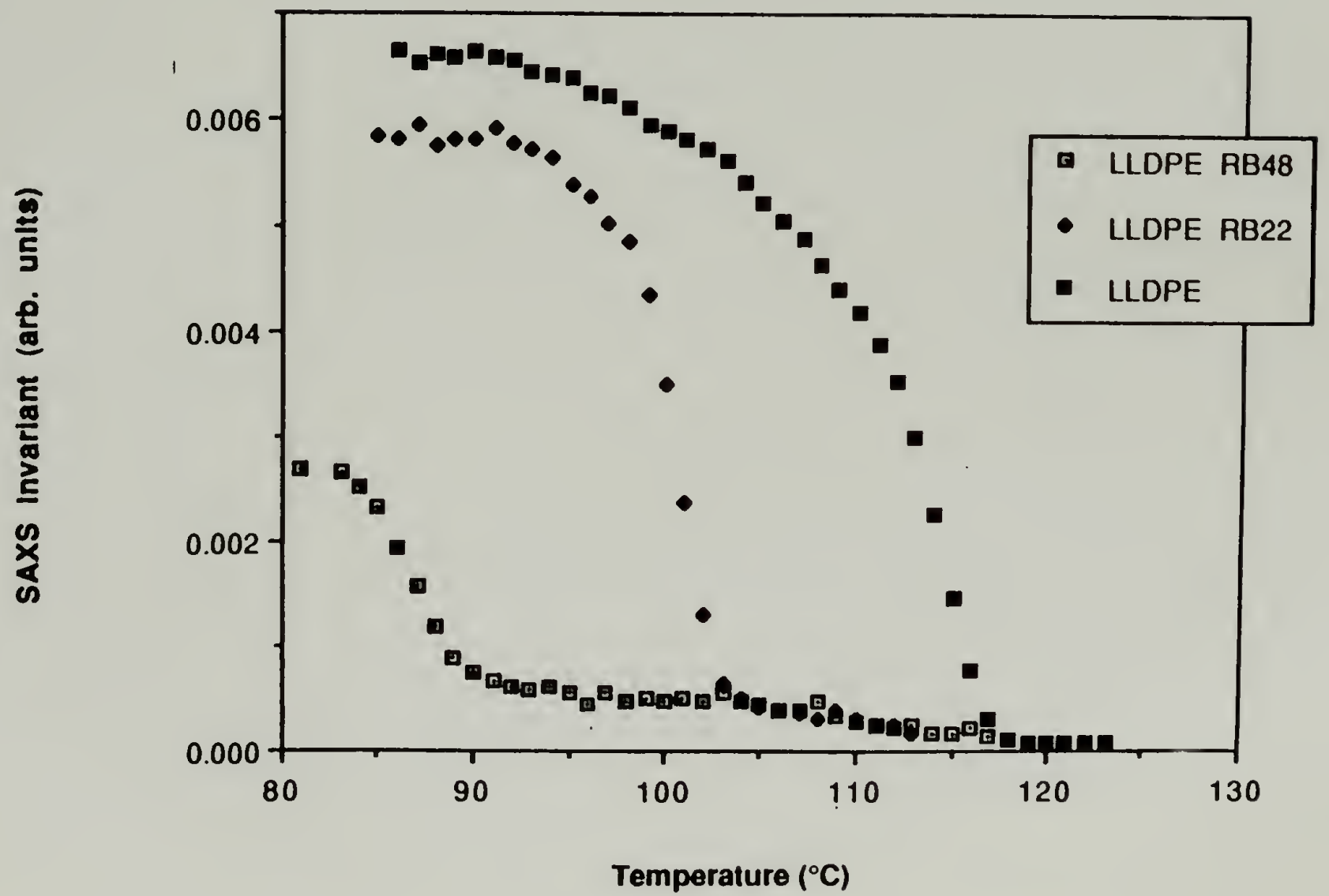

Figure 2.22 Invariants of different LLDPEs under slow cooling (0.5°C/min).

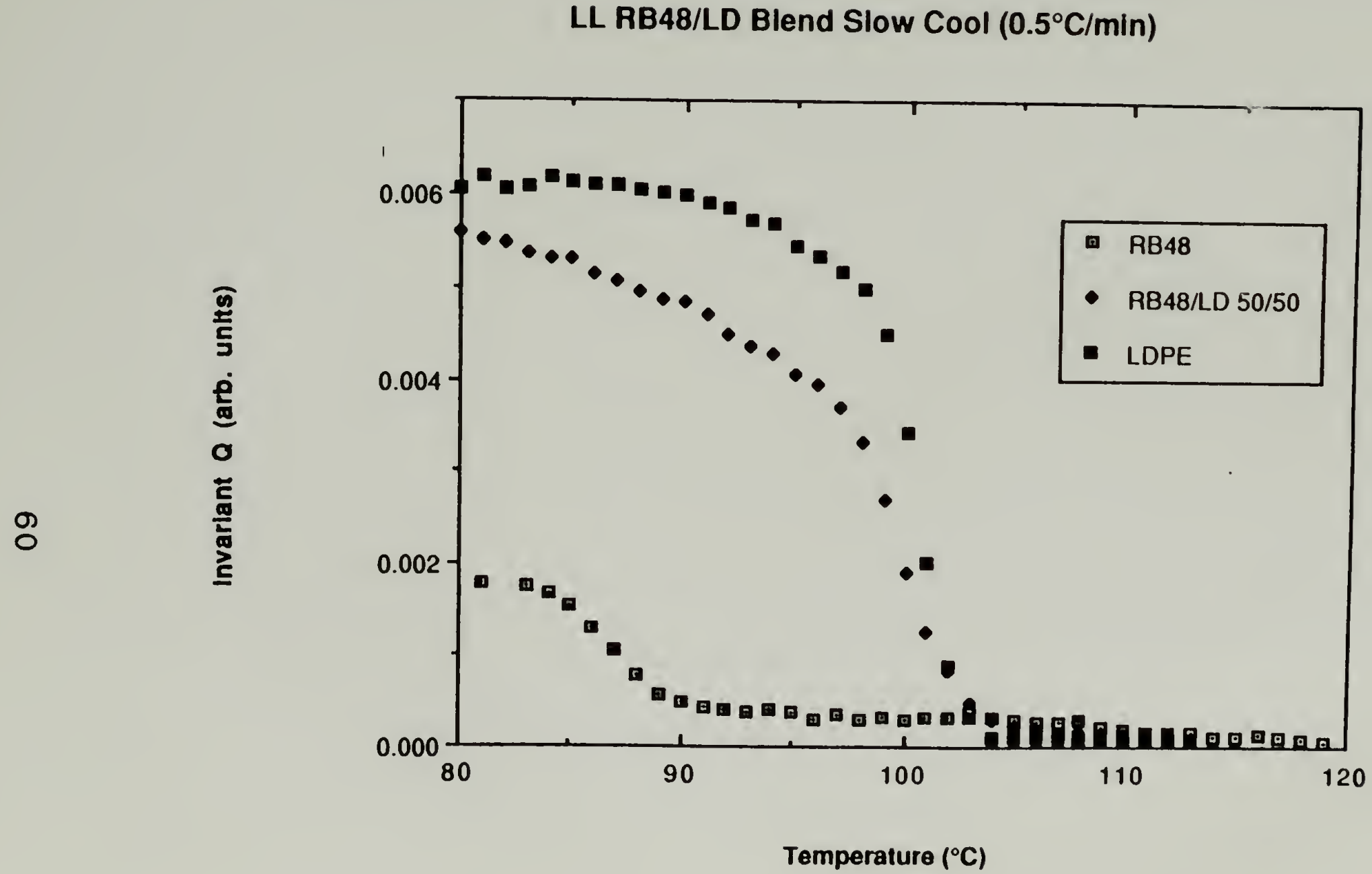

Figure 2.23 Invariants of RB48/LLDPE under slow cooling. (0.5°C/min).

CHAPTER 3

SMALL ANGLE SCATTERING OF SELECTIVELY DEUTERATED LINEAR LOW DENSITY POLYETHYLENE

3.1 Introduction

Linear low density polyethylene (LLDPE) is distinguished from high density (linear) and low density (highly branched) polyethylene by the presence of exclusively short chain branching (SCB). LLDPE is a copolymer of ethylene and some n-alkene, synthesized by Zeigler-Natta processes. The length of these branches can vary, depending on the comonomers used in the synthesis. Monomers such as hexene, octene, or butene are used commercially[1,2] The number of branches per chain varies depending on the application. In LLDPE films, for example the number branches per 1000 backbone carbon atoms is about 30 . For applications where stiffness is more important such as in pipes and conduits, the SCB/1000 C can be fewer than 10.

The most obvious way the branching affects the properties is through the crystallinity. Varying the density of the short chain branches on the main chain allows one to control the crystallinity fairly easily. However, crystallinity is not the only factor in determining the properties. The length of the branches can also influence the properties, as well. For example, hexene-LLDPE generally has higher tensile and impact strength than comparably crystalline butene-LLDPE[3].

The role of these branches in the morphology of the polymer are intimately connected with the mechanical properties of the material. While it is known that methyl branches can include themselves in the crystalline regions in PE,[4-6] the location of larger branch segments and their relationship to the mechanical properties are unsettled questions. It appears that branches larger than an ethyl group are for the most part excluded from crystallites. The work of Cole and Holmes[7], Baker and Mandelkern[5] and Preedy[8] have shown that the crystal perfection is markedly decreased when the short chain branches are methyl groups. Larger side groups (C_2H_4 and larger) do not seem to affect crystal perfection as much as the small side groups. On the other hand, the small side groups do not limit the crystallinity as much as an equal number of larger groups. This is strong evidence for exclusion of the branches from the crystalline zones. Yet, there is some reason to believe that under some conditions at least some of the larger branches might be included in the crystallites. Evidence of the presence of larger branches inside the crystal cores have been found by nitric etching techniques by Holdsworth and Keller[9], and by Vile et al.[10] The amount of incorporation that is found varies with the type of comonomer used as well as the thermal history. The highest estimates indicate that as much as 20% of the branches can be included in the crystal. For slow coolings and the larger branches (larger than C_2H_4) the amount of branches included is small (of the order of a few percent). Because of the experimental uncertainties in this work, these numbers are rough estimates at best. Clearly however, the majority of branches longer

than methyl are not incorporated in the crystallites and are present mostly in the amorphous regions

How these branches may be organized inside the amorphous regions is unclear. They could be present throughout the amorphous region or they could be segregated near the crystalline-amorphous interface. The latter possibility is suggested by computer simulations by Mattice et. al.[11,12] Essentially a thermodynamic argument, his results point toward a clustering of branches at the surface in order to maximize entropy of the chains in the amorphous region. Clearly, however, not only thermodynamics, but also steric arguments suggest that branches might be concentrated at the surface. Vonk[13] has described a scheme where both inclusion of the branches inside the crystal and segregation of branches to the crystal surface occur. Chains offered at the growth face of a lamellae are accepted regardless of whether the nucleating stem possesses a branch point or not. Crystallization proceeds by chain folding in either direction until a branch point is met. Although it is difficult to justify why initial stems with branches are accepted, while during chain folding, subsequent stems with branches are not, this description does give us a qualitative picture of how the branches may be concentrated preferentially at the crystal - amorphous boundary. If this branch rich region exists at the crystalline amorphous boundary, its spatial extent, and density of branch segments within it would be interesting parameters to relate to the type of LLDPE comonomer used. Knowledge of these relationships could give insight into why different comonomers in LLDPE result in different properties.

In view of these questions of short chain branch position, a combination of neutron and X-ray scattering experiments were conducted to study the position of these branches. Specially synthesized LLDPEs were obtained having deuterated backbones with normal hydrogenous chain branches. The resulting neutron scattering length contrast between the branches and the main chain can be used to determine if segregation of the branches occur upon crystallization. While neutrons are sensitive to the presence of scattering length density fluctuations, X-ray scattering is dependant on electron density fluctuations. Therefore, X-ray scattering can give information on the crystalline and amorphous regions of the LLDPE.

This approach using neutron and X-ray scattering to compliment each other has been used by this laboratory in the past.[14,15] The blends of polyvinylidiene fluoride and poly methy methaculate were studied with both techniques. For PVF_2/ PMMA, the favorable interactions of PMMA with PVF_2 coupled with the inherently low diffusion rate of PMMA force a morphology where the PMMA is in the amorphous region between crystalline PVF_2 The nature of interfacial region between the crystalline and amorphous components were studied by deuterating one component. In this work we will examine the nature of this region in regards to branch content in a homopolymer, namely LLDPE.

3.2 Data Analysis / Theory

X-ray scattering as described in section 2.11. is dependant on the electron density differences in the material. For crystalline polymers, the X-ray scattering in the small angle region generally arises from the alternating crystalline- amorphous lamellae. The theory of small angle neutron scattering is nearly completely analogous to SAXS,. In the case of SANS, scattering arises from fluctuations in scattering length density difference. The scattering length of a atom is a nuclear quantity, depending on the atomic mass and spin state of a given nucleus. Scattering lengths for some atoms of interest in this work are given in table 3.1.

In this work, the backbone of the LLDPE is deuterated. This causes a scattering length density difference between the CH_2 and CD_2 groups in the branch and chain, respectively. Thus the neutron scattering will depend on the arrangement of these branch segments with respect to the backbone segments. The SAXS, on the other hand, merely depends on the electron density difference between the crystalline and amorphous regions. Given this, there exists three possibilities for the X-ray and neutron scattering of these tagged LLDPEs.

Case one: The branches are present in the crystalline and amorphous regions in equal amounts. Here, the sizes of the branches are small compared to the length scales being investigated with

neutrons (on the order of 100Å). Consequently, the system should appear as homogeneous and little neutron scattering should be detected. SAXS on the other hand would yield intensity profiles typical of crystalline polymers.

Case two: The branches are distributed uniformly through the amorphous regions. The branches in the amorphous region would serve to lower the average scattering length density in the amorphous zone compared to the crystalline zone. This would give rise to a scattering length density difference between the crystal and amorphous layers. The SANS should appear as a standard two phase lamellar system scattering. In this case X-ray scattering on the same system should give identical results as the neutron scattering.

Case three: The branches segregate near the amorphous-crystalline boundary. The system in this case is still two phase. However the widths of the two phases determined by neutron scattering will be different from that of X-ray scattering. The neutron scattering depends on the scattering length density differences between the branch-rich and branch depleted areas. This is controlled by branch segregation. The X-ray scattering is obvious to the segregation of the branches and depends only on the electron density differences produced by the crystalline and amorphous areas.

Up to this point, only scattering from pure selectively deuterated LLDPE's with deuterated backbones and hydrogenous short chain branches have been discussed. Blends of these tagged LLDPE's

with matching non-deuterated LLDPE's make possible an interesting class of neutron scattering experiments that study the effect of SCBs on chain folding. The most general expression of scattered Intensity is given by[16]

$$I(q) = \sum_{i=1}^{N} \sum_{j=1}^{N} f_i f_j \frac{\sin 2\pi r_{ij}}{2\pi r_{ij}} \qquad (3.1)$$

where f_i is the scattering power for the i th scattering segment and r_{ij} is the distance between segments i and j. When a mixture of protanated and deuterated chains is dilute in one component the scattering is essentially from a single chain, free from interchain interferences. Flory and Yoon[17,18,19] among others[20,21,22], have noted that the scattering at intermediate q (0.1 $Å^{-1}$ > q >.01 $Å^{-1}$) is strongly related to the relative positions of the linear polymer segments or 'stems' forming the crystal. Using computer simulations of chains in lamellae scattering, various scattering patterns can be calculated for different extents of stem adjacency (i.e. chain folding).

Chain folding in crystalline polymers can be envisioned as falling between two extremes . The first, adjacent reentry, is characterized by the polymer chain folding in a regular manner along some specific crystallographic direction. For this type of reentry, crystal stems of the same molecule will be tightly packed next to one another. The second extreme, random or switchboard re-entry, features segments of different chains entering the crystal next to each other. Thus, the

crystal stems of one molecule tend to more widely dispersed within the same crystal than if the reentry pattern was adjacent. The effect of the degree of adjacent chain reentry on neutron scattering has been calculated by a number of researchers using a variety of models for the behavior or chains within the amorphous zone. An example of Flory's work is given in figure 3.1. Generally, adjacency of the crystal stems tend to increase the scattering at intermediate angles.

The presence of short branches in LLDPE may disrupt the folding mechanism enough to induce more tie chains between crystalline and amorphous regions. This in turn would reduce the adjacency of the crystalline stems and lower the scattering at intermediate angles..

3.2.1 Thickness of Lamellae: The Correlation Function

The interpretation of scattering from lamellar systems has been pioneered by Vonk [23,24]. He originally described the scattering from alternating layers of crystalline and amorphous materials. However, with the substitution of scattering length for electron density, it can apply equally well for neutron scattering. In this case it would describe the scattering for layered regions of alternating scattering length density. The intensity of scattered radiation can be written as

$$I(s) = \int_0^\infty x^2 \gamma(x) \frac{\sin(2\pi xs)}{2\pi xs} dx \qquad (3.2)$$

where x is the coordinate perpendicular to the lamellae stacks , and γ is a one dimensional correlation function. A Fourier inversion of equation 3.2 gives

$$\gamma(x) = \frac{\int_0^\infty I(s)\, s^2 \cos(2\pi xs)\, ds}{\int_0^\infty I(s)\, s^2\, ds} \qquad (3.3)$$

The correlation function describes the probability that a rod of length x, positioned perpendicular to the lamellae, will have both its ends in the same phase. γ is unity at x=0, and has a maximum corresponding to the repeat period of the lamellae structure. For lamellae with a distribution of widths, the correlation function decreases to 0 as x increases. An important result of the correlation function is that the first minimum has a depth of $(1-\phi)/\phi$ where ϕ is the volume fraction of one of the phases.

3.2.2 The Effect of Transition Zones

The intensity of scattering from lamellar systems as derived by Vonk assume that the transition between crystal and amorphous layer is sharp. For any two phase system where the boundary between the

phases is distinct, the small angle scattered intensity will drop off as the inverse fourth power of q. as q approaches infinity, Hence ,

$$\lim_{q\to\infty} (I(q)\, q^4) = \text{constant} \qquad (3.4)$$

This relationship is known as Porod's law[25].

In theory, a plot of $I\, q^4$ vs q should yield a flat line at large angles. In practice, this is not always true. Some systems show a gradually increasing $I\, q^4$, while others show a nearly linear decrease in $I\, q^4$. These discrepancies are referred to, respectively, as positive or negative deviations from Porod's law. Positive deviations arise from thermal density fluctuations or from mixing within the phases. Negative deviations are caused by the presence of diffuse phase boundaries in the system.

The depletion of scattering at large angles, caused by a diffuse transition zone, has been derived by Ruland[26]. The actual scattering power density can be considered as a convolution of the ideal two phase distribution with a smoothing function. The smoothing function is chosen depending on the type of transition zone. The scattering in the simplest case, that of a linear transition zone of width E is given to a good approximation as

$$I(q) = (K/s^4)\,(1 - E^2\, q^2 / 12) \qquad (3.5)$$

where K is a constant.

The invariant as given by equation 2.4 is derived for the case of a sharp two phase boundary. Deviations from porod's law from diffuse boundaries will decrease the invariant. If the transition layer varies linearly, Q is given by

$$Q = \left[\phi(1-\phi) \cdot \frac{E\,S}{6\,V}\right](\rho_c - \rho_a)^2 \qquad (3.6)$$

where S/V is the specific surface of the phase boundary. S/V can be related to the slope of the correlation function γ at the origin by

$$\left(\frac{d\gamma(x)}{dx}\right)_{x=0} = \frac{S/V}{2\,\phi(1-\phi)} \qquad (3.7)$$

3.2.3 The Effect of Density Contributions to the Scattering

As stated earlier, the intensity of scattered neutrons is a consequence of fluctuations of scattering length density in the material. We have assumed that these fluctuations arise solely from the difference in the scattering length between the hydrogenous short chain branches and the deuterated main chain. This is not completely true. The density difference between the crystalline and amorphous parts of the main chain will also create an difference in scattering length density. This density difference will contribute to the neutron scattering.

The neutron scattering invariants can be calculated to determine how much this density difference contributes to the scattering. Shown in figure 3.2 is a schematic of the lamellar system with the corresponding electron density and scattering length density profiles. In the ideal case the electron density varies as a step function between the electron density of the crystalline, ρ_c, and amorphous , ρ_a, layers. Assuming the branches are segregated near the amorphous -crystalline boundary in a branch- rich layer of length t_b, the scattering length density varies between three values, a_a,, a_b ,and a_c . a_a is the scattering length density of the amorphous layer; a_c is that of the crystalline; and a_b is the scattering length density of the branch rich layer. For this type of a three phase system with sharp boundaries, the invariant Q is given by

$$Q = \phi_a \phi_c (a_a - a_c)^2 + \phi_c \phi_b (a_c - a_b)^2 + \phi_a \phi_b (a_a - a_b)^2 \quad (3.8)$$

here, ϕ_i is the volume fraction of the ith phase. Each term in equation 3.8 represents the total integrated scattering from fluctuations between two types of phases. The scattering we are interested in in the neutron case is the scattering which arises because of the differences in b between branches and the main chain. This scattering is accounted for in the last two terms. The first term represents contributions to the scattering from the crystal-amorphous density difference. To determine the extent of this contribution, one must calculate the scattering length density differences. These can be written as

$$(a_a - a_c) = b_{ch} (n_c - n_a) \quad (3.9a)$$

$$(a_c - a_b) = b_{ch} (n_c - n_b(1 - f)) - b_b n_b f \quad (3.9b)$$

$$(a_a - a_b) = b_{ch} (n_a - n_b(1 - f)) - b_b n_b f \quad (3.9c)$$

Here, b_b is the scattering length of the repeat unit of the branch, b_{ch} is the scattering length of the repeat unit of the main chain. The term n_i is the number density of repeat units in phase i (branch-rich zone, amorphous, or crystal), and f represents the fraction of the branch-rich zone units that are branches. The calculation depends primarily on the degree of crystallinity, and the degree of branch segregation. For the crystallinities of the samples dealt with here (25-30%) and a segregation (f = 0.5) , 20% of the neutron Q value is due to crystal-amorphous density contributions. This is a significant number, but it still should be possible to detect branch segregation if it exists.

3.3. Experimental

Samples of LLDPE of varying comonomer content have been obtained from Dr. Ferd Stehling of Exxon Baytown Laboratory. Two types of LLDPE were used, one with a branch length of two carbons long and another with a branch length of six carbons These samples were synthesized with comonomers C_4H_8/C_2D_4 and C_8H_{16}/C_2D_4, respectively. Corresponding hydrogenous samples were also obtained in order to blend for intermediate angle scattering and also to use to subtract incoherent background. The molecular weights and polydispersities of the samples are given in table 3.2. For the neutron and X-ray studies on pure d-comomomer LLDPE, samples were prepared under two different crystallization conditions, a quench from

the melt, and an isothermal crystallization at 105°C for 8hrs. For the chain reentry experiments, where blends were needed, the desired proportions by weight of each polymer were solution blended as in the previous chapter with the exception that the solvent used was ortho - dichlorobenzene.This solvent was used in order to attain higher blending temperature (185° C). This procedure has been shown to inhibit segregation of the deuterated polymer.[27,28]

Neutron scattering was conducted at the Intense Pulsed Neutron Source, Argonne National Laboratory, Argonne, Illinios. The small angle diffractomer-1 (SAD-1) beamline was used. (see figure 3.3) Pulsed neutron sources uses pulses of neutrons at a range of wavelengths The scattering is recorded as a function of angular position at the detector and time of arrival. The wavelength is dependent on the time of arrival Analysis programs at IPNS sort out the contributions of each wavelength of scattered neutrons to the appropriate wave vector q. In this manner a larger q range can be measured than with a monochromatic source using the same geometry.

The Small angle X-ray scattering was measured at the University of Massachusetts. A standard Phillips generator was used, operating at 40 kV and 20 mA. The SAXS instrument featured a Kratky collimator and a Braun Linear Position Sensitive detector. Some additional scattering measurements were conducted at the National Synchrotron light source, using the experiments set up described in the previous chapter.

The degree of crystallinity in the LLDPE samples was determined by differential scanning calorimetery (DSC). A Perkin-Elmer DSC was used, scanning at a heating rate of 20°C/min. The crystallinity was calculated from the area under the endotherms.

3.4 Results

3.4.1 Scattering from Deuterated LLDPE

Neutron scattering profiles of the selectively deuterated butene-LLDPE and hexene-LLDPE are shown in figure 3.4. The profiles have been corrected for background, absorption, and incoherent scattering. The latter correction was accomplished by subtracting the appropriate fraction of the scattering from a completely hydrogenated sample of LLDPE. The corrected intensity has been multiplied by q^2 ($q=4\pi/\lambda \sin(\theta/2)$), the so-called Lorentz correction, to account for the lamellar character of the system. All samples show a prominent peak. For both the C_4H_8/C_2D_4 and the C_8H_{16}/C_2D_4 samples, the peak position occurs at larger angles for the quenched samples than for the crystallized samples. The scattering from the octene-LLDPE is much greater than the scattering from the butene-LLDPE in both the quenched and crystallized samples.

The periodicity spacings and neutron invariants from the neutron scattering curves are given in table 3.3. Q nearly doubles from the C_4H_8 sample to the C_8H_{16} sample. Since the crystallinities of these two samples are not radically different (between 30% and 22%), this doubling reflects the fact that the scattering is primarily from the

branch-main chain contrast rather than from contrast from the density difference between the crystalline and amorphous phases. If the scattering were due to the crystalline-amorphous density difference, then this would imply a doubling of $\delta^2=(\delta_a-\delta_b)^2$ from a quenched system to a isothermally crystallized system. This is too large a change in the scattering length density difference to caused by crystalline-amorphous density differences alone.

Representative small-angle X-ray scattering on the same samples is shown in figure 3.5. The curves were corrected for background, and absorption. The SAXS long period spacing are given in table 3.3 Comparing the periodicities of the SAXS and the SANS, the SAXS periodicities are nearly double of the corresponding SANS. Clearly the SANS and SAXS yield different scattering curves. This is accordance with case 3 discussed above, that of the case of the branches segregated on some scale smaller than that of the lamellae.

That the periodicity of the neutron scattering is roughly half that of the X-ray scattering suggests a model shown in figure 3.6. The crystal thickness is given by t_c , the amorphous thickness by t_a . A high concentration of branches are segregated in a layer near the crystal-amorphous boundary, whose thickness is denoted by t_b. In this scheme, the periodicity from the SANS is arises from the spacings of the branch-rich layers (lp_{SANS}), while the SAXS yields the conventional lamellae crystal spacings (lp_{SAXS}). This type of model has been suggested by computer simulations of Mattice, where a square lattice was used to determine the position of branches of one and two

lattice points in length, which were excluded from the crystalline regions. The model, while not allowing quantitative comparisons, agrees with the data in a number of qualitative observations.

If the neutron scattering is indeed from the segregation of the branches, then the tails of the neutron profiles should be indicative of the sharpness of the boundary between the branches and the crystalline/ amorphous phases. Figure 3.7 shows Porod plots from the neutron scattering Although scatter in the data is quite large, all figures show a roughly flat region after the initial rise. This is indicative of a sharp boundary between the two phases. For both the isothermally crystallized and quenched samples, the boundary is extremely sharp. The isothermally crystallized LLDPE of both branch length have no measurable interfacial region. This is in agreement with the simulations of Mattice which conclude that the density of branches drops off radically as one moves away from the crystal surface. This drop off is might be faster than the resolution of the neutron scattering in this region (5Å). Of course, the situation is complicated by the fact that the branch-rich layer have two types of surfaces, a crystal facing side, and an amorphous facing side. Normally, one would expect the crystal facing side to be sharp if there was segregation at the boundary. The Porod plots from the X-ray scattering contrast the neutron porod plots. Shown in figure 3.8, a negative deviation in Porod law is observed for both the butene and hexene LLDPEs,. This is clearly indicative of a transition zone in the electron density. The transition zone has been determined from equation 3.5 to be ca. 30 Å in thickness.

For the model of branch segregation as outline here one would expect the SANS lp to half the SAXS lp. Although the SANS lp spans crystalline and amorphous zones, the average SANS lp still. should be half the SAXS. Table 3.3 shows that this is obviously not true. The discrepancy is doubtless due to the crystalline-amorphous density contributions to the neutron scattering discussed in section 3.2.3. This scattering can, in principle be subtracted from the total scattering to yield the branch layer scattering. The problem here is that how much of a contribution of the Branch layer scattering makes is controlled by the branch segregation at the layer (see equations 3.9). Therefore, there is no way of knowing how much crystalline-amorphous scattering to subtract. Samples prepared with reverse deuteration deuterated branches on a normal hydrogenous backbone would remedy this problem. This will be discussed further in Chapter 5.

Despite this problem of crystalline amorphous density scattering, we would like to at least estimate how thick is the branch-rich layer. This has been done using the correlation function approach outlined in section 3.2 . Correlation functions calculated from the neutron scattering are shown in figure 3.9. As discussed in section 3.2.1 . the value of the minimum in the correlation function is related to the volume fraction of the smaller phase. With uncertainties arising from crystalline scattering it must be remembered that this calculation is an estimate only, but it does provide an order of

magnitude estimate as well as an example of the method to be used in future work with reverse deuteration.

DSC was used to determine the degree of crystallinity in the samples With the information on the long period by SAXS and the estimation of the branch rich layer thickness t_b. by the correlation functions, all the parameters of the segregated branch model can be calculated. The results are summarized in Table [illegible] The thickness of the branch rich layer is found to be about 30Å. The error in the assumptions in the two phase system used here makes this value an estimation at best. Although there is a slight increase in t_c between the octene LLDPE and the butene LLDPE, the difference is within experimental errors and no real trend can be said to be seen.

3.4.2 Chain Reentry

As mentioned earlier, short chain branches may affect the physical properties of LLDPE by inducing more tie chains between neighboring crystalline regions. While the number of tie chains cannot be directly measured by neutron scattering, information on the of crystal stem distribution can be deduced from intermediate neutron scattering. This information is the degree of adjacency of the stems in a crystal. The theory of the scattering at these angles is at this point controversial. Different forms of models give varying results for the intermediate scattering. Yet, a number of trends in these models are universal. The purpose of this work will not be to determine quantitatively the degree of adjacency, but rather compare the

intermediate scattering from different LLDPEs and HDPE to determine any relative differences in adjacency.

Figure (3.10) shows the neutron scattering of a 10/90 blend of C_2D_4 C_4H_8 LLDPE / C_2H_4 C_4H_8 LLDPE as well as a 10/90 blend of dHDPE/ C_2H_4 C_4H_8 LLDPE. At these blend concentrations, the sample scattering should be indicative of relatively isolated deuterated chains in a matrix of normal hydrogenous chains. Because of the selective deuteration LLDPE, the neutrons only "see" the LLDPE backbone. Hence scattering at q> .02 $Å^{-1}$ is related to the arrangement of molecular stems in the crystal. The butene-d-ethylene LLDPE blend scattering profile is much like that of the theoretical curves shown in figure 3.1. The dHDPE/ butene- ethylene LLDPE exhibits a markedly different scattering pattern, showing a prominent peak at a q value corresponding to 318 Å. The appearance of such a peak is probably due to segregation of the dHDPE. It has been observed before from DSC in earlier work that LLDPE and HDPE can co-crystallize. Apparently, at these concentrations, branch content, and crystallization conditions (quench to 0°C), LLDPE and dHDPE a significant amount of segregation still takes place

Neutron scattering profiles for the corresponding Octene-LLDPE are shown in figure 3.11. The polymers here are 10/90 blends of C_2D_4 C_8H_{16} LLDPE / C_2H_4 C_8H_{16}LLDPE and dHDPE / C_2H_4 C_8H_{16} LLDPE. The profiles are nearly identical to the butene series. In the case of the dHDPE/ octene-d ethylene LLDPE the peak occurs at the same position and has the same intensity. The same pattern of segregation

is at work here. The profiles for the 10/90 C_2D_4 C_4H_8 LLDPE / C_2H_4 C_4H_8 LLDPE and 10/90 C_2D_4 C_8H_{16} LLDPE / C_2H_4 C_8H_{16} LLDPE are identical except for some scatter in the octene data below q= 0.02 $Å^{-1}$. The similarity of the octene-d-ethylene scattering to the butene-d-ethylene scattering indicate that there is no difference in the reentry patterns in these blends measurable by neutron scattering. The segregation of the dHDPE in both the octene and butene LLDPEs renders comparison to the LLDPE blends dubious at best.

3.4.3 The Problem of Segregation

The preceding study on chain re entry in the dHDPE/LLDPE system were marred by segregation of the dHDPE upon crystallization. This produced disappointing results from a perspective of examining chain stem adjacency of HDPE in LDPE. However, it can yield some interesting information on the segregation phenomenon in PE itself, confirming some of the findings of the previous chapter, while extending some of the observations to LLDPE/HDPE systems.

Pictured in figure (3.12) is the scattering from 10/90 octene-d-ethylene LLDPE/ octene-ethylene LLDPE with that of a 50/50 mixture of the same blend. the 50/50 blend features two maxima at q=0.0152 $Å^{-1}$ and q=0.057 $Å^{-1}$, corresponding to distances of 411 Å and 109 Å. The single chain scattering character of the 10/90 blend is completely gone from the 50% mixture. The presence of peaks at these positions indicate some form of segregation is taking place in 50/50 blend. The cause of this segregation upon crystallization is the 6° C temperature difference between the crystallization temperatures of pure $-(C_2H_4)_n-$

and $-(C_2 D_4)_n-$. This is a very similar case to the HDPE/LDPE and LDPE/LLDPE blends. In those polymer systems a difference in melting points in the components were brought about by the introduction of non-crystallizable entities (branch points).

The size scale of d-LLDPE/ h-LLDPE segregation is made clear by examining the corresponding small angle X-ray scattering in the same q region. This is given in figure (3.13). In this case, one peak is seen for each blend at the position q=0.046 $Å^{-1}$. This SAXS periodicity corresponds closely with the second peak in the 50/50 neutron scattering. Clearly then, this second neutron peak arises from scattering length density differences in the deuterated polymer alone. The larger periodicity seen in the SANS but not the SAXS must arise from differences in scattering length of between the deuterated and hydrogenous components of the blend. This size scale is related to the segregation scale of the deuterated component in the hydrogenous component. The 411 Å size scale indicates a segregation size over three times the spatial scale of the crystalline long periods.

If we assume that d-LLDPE and h-LLDPE crystallize in separate lamellae (or nearly so), a system of alternating stacks of lamellae would yield a neutron long period double the SAXS long period (see figure 3.14). If the lamellae were grouped into stacks of two , the neutron long period would be four times the SAXS long period. The results from above indicate a randomly intermixed, nearly alternating lamellae structure. This was the case for rapidly cooled PE blends of LLDPE/LDPE and HDPE/LDPE studied in the previous chapter.

In the neutron scattering profiles of dHDPE / LLDPE signs of segregation are seen even at the low concentration of 10% HDPE. Figure 3.15 shows the neutron scattering profiles of 10/90 dHDPE/ octene-LLDPE and 10/90 dHDPE/ butene-LLDPE along with the scattering of pure dHDPE. The pure dHDPE scattering arises solely from the periodicity of crystalline lamellae. The long period is 281 Å. The periodicities of both blends are slightly larger than the pure dHDPE. This would indicate that the segregation is of the same order of the lamellae long period . The SAXS from the 10/90 dHDPE/ LLDPE blends show a long period of roughly 160 Å. (see figure 3.16). This is again due to the crystalline lamellae repeat period and is much shorter than the neutron periodicity as expected when segregation of the deuterated species.occurs.

3.5 Conclusions

Clearly ,SANS and SAXS results point toward a complicated morphology for LLDPE where the short chain branches are segregated at scale smaller than that of the crystalline lamellae. Observations of the long periods of SAXS and SANS suggest that the concentration of branches may be enhanced at the crystalline-amorphous boundary. Preliminary calculation of the the thickness of this branch rich region using correlation functions indicates that the layer is roughly 30Å thick. It is acknowledged that this is only a estimate of the thickness because contributions to the neutron scattering from density differences between the crystal and amorphous parts of the molecule.

account for perhaps 20% of the scattering, depending on the concentration of the branches in the interfacial zone.

Intermediate angle scattering of blends of 10/90 d LLDPE/LLDPE and dHDPE/LLDPE was attempted in order to study chain trajectory in the bulk. The octene / d-ethylene LLDPE and the butene / d-ethylene LLDPE showed no significant differences in intermediate angle neutron scattering. Obvious segregation of the dHDPE in LLDPE spoiled comparisons for an unbranched chain in matrix of short chain branched LLDPE.

This segregation of the deuterated components, although ruining some of the chain re-entry work, did confirm a number of observations made in the previous chapter. For 50/50 blends of octene/ d-ethylene LLDPE and octene /ethylene LLDPE, the segregation scale was larger the lamellar spacing. In fact it indicated on average that the lamellae were intermixed in a fashion that saw bundles of lamellae not more than perhaps 400 Å in extent. This corresponds to about three or so crystal repeat periods. This is consistent with the findings of the quenched blends described in chapter 2.

Table 3.1

Selected Neutron Scattering Lengths, Cross Sections and X-ray Atomic Form Factors

Nucleus	Scattering length x 10^{12}cm	Incoherent Scattering Cross Section x 10^{24} cm^2	Cross Section of Absorption x 10^{24} cm^2	Atomic form factor at q=0 x 10^{12} cm
^{1}H	-0.374	79.9	0.19	0.28
^{2}H	0.667	2.0	0.00	0.28
^{12}C	0.665	0.0	0.00	1.69

Table 3.2

Molecular Weights, Melting Points and Branch Content of Selectively Deuterated LLDPE's and Corresponding h-LLDPE's

Sample Monomer/ Comonomer	M_n x 10^4	M_w x 10^4	T_m °C	Mole % Comonomer
C_2H_4 / C_4H_8	62.5	108.0	106.0	4.4
C_2H_4 /C_8H_{16}	57.1	96.0	108.0	3.0
C_2D_4 / C_4H_8	42.9	70.0	101.5	4.5
C_2D_4 /C_8H_{16}	53.0	95.0	99.8	3.0
C_2D_4	38.4	60.7	125.0	---

TABLE 3.3

Data from Neutron and X-Ray Scattering Measurements

Sample	Neutron Long Period Å	Neutron Scattering Invariant (10^{5} Å^{-3} cm^{-1})	X-ray Long Period Å	X-ray Invarant (relative units)
C_4H_8/C_2D_4 (quench)	119 ±5	4.30 ± 0.5	198 ±10	7.0
C_4H_8/C_2D_4 (isothermal)	147	5.13	220	7.5
C_8H_{16}/C_2D_4 (quench)	119	7.55	195	6.8
C_8H_{16}/C_2D_4 (isotherm)	134	9.36	208	7.2

Table 3.4

Calculated Model Parameters from LLDPE Scattering

Sample	Crystal Volume Fraction	Volume fraction Branch layer	Crystal width t_c Å	Amorphous width t_a Å	Branch width t_b Å
C_4H_8/C_2D_4 (quench)	0.28	0.26	56±5	142±15	30±10
C_4H_8/C_2D_4 (isothermal)	0.30	0.23	66	154	33
C_8H_{16}/C_2D_4 (quench)	0.22	0.28	43	152	33
C_8H_{16}/C_2D_4 (isotherm)	0.25	0.24	52	156	34

References

1. C.S. Speed, *Plastic Eng.*, July, **29** (1982).
2. N. Datta, A. Birley, *Plas. Rub. Pro. Appl.*, **2**, 237 (1982).
3. G. Foster, from *Polymer Reaction Engineering, an Intensive Short Course on Production Technology of Polyolefins*, McMaster Univesity, 1989.
4. P.R. Swan *J.Polym. Sci.* **56**, 409 (1962).
5. C.H. Baker, L. Mandelkern, *Polymer*, **7**, 71 (1966).
6. I.G. Voight-Martin, R. Alamo, L. Mandelkern, *J. Polym. Sci. Phys. Ed.*, **24**, 1283 (1986).
7. E.A. Holmes, *J. Polym. Sci.*, **46**, 245 (1960).
8. J.E. Preedy, *Br. Polym. J.* **5**, 13 (1973).
9. P.J. Holdsworth, A. Keller, *Makromol. Chem.*, **125**, 82 (1969).
10. J. Vile, J. Hendra, H.A. Willis, M.E.A. Cudby, and A. Bunn, Polymer, 25, 1173 (1984).
11. S. Mathur, W. Mattice, *Macromolecules*, **21**, 1354 (1988).
12. S. Mathur, W. Mattice, personal communication.
13. C.G. Vonk and A.P. Pijpers, *J. Polym. Sci.* **23**, 2517 (1985).
14. W. Herman, Ph.D Dissertation, Univ. Massachusetts, Amherst, 1987.
15. T.P. Russel, R.S. Stein , *J. Polym. Sci. Phys.*, **20**, 1593 (1982).
16. P. Debye, *Ann. Physik*, **46**, 809 (1915).
17. D.Yoon, P.J. Flory *J. Appl. Cryst.*, **11**, 531 (1978).
18. D.Yoon, P.J. Flory, *Macromolecules*, **9**, 294 (1976).
19. D.Yoon, P.J. Flory *Polymer*, **16**, 645 (1975).
20. C.Guttman, J.D. Hoffman, E. Dimarzio *Diss. Faraday Soc.* (1979).
21. C.Guttman, J.D. Hoffman, E. Dimarzio, *Polymer*, **22**, 1466 (1981).

22. R.J. Roe, *J. Chem Phys.*, **53**, 3026 (1973).

23. G. Kortleve, C. Vonk, *Kollid. Z.* , **225**, 124 (1968).

24. G. Kortleve, C. Vonk, *Kollid. Z.* , **220**, 19 (1967).

25. G. Porod *Kolloid-Z.* **124**, 83 (1951).

26. W. Ruland *J. Appl. Cryst.* **4**,70 (1971).

27. J.Schelten,G.H. Ballard, G.D. Wignall, G.W. Longman, and W.Schmatz, *Polymer*,**17**,751 (1976).

28. R. Lo , Ph. D Thesis, University of Massachusetts, Amherst 1987.

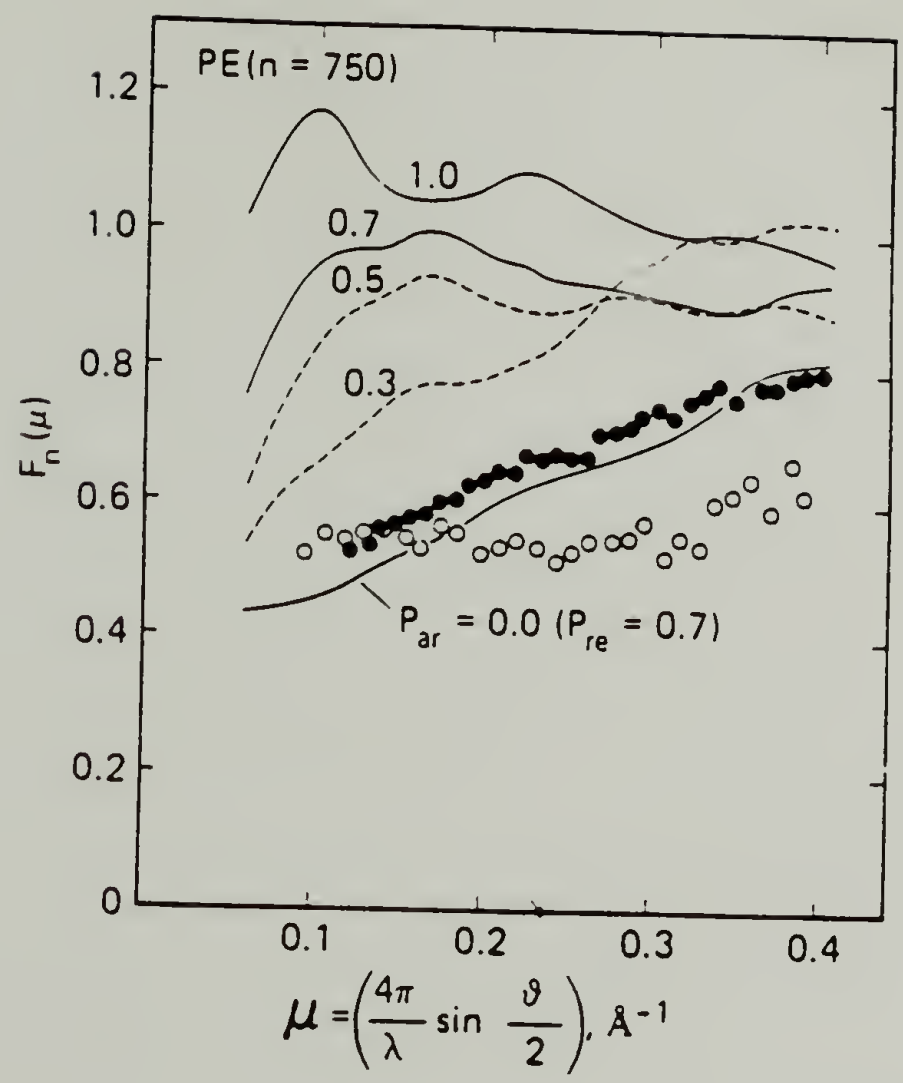

Figure 3.1 Theoretical intermediate angle scattering of PE for various probabilities of adjacent reentry (P ar). The number of bonds is given as n=750. Circles are experimental data for HDPE. From reference 19.

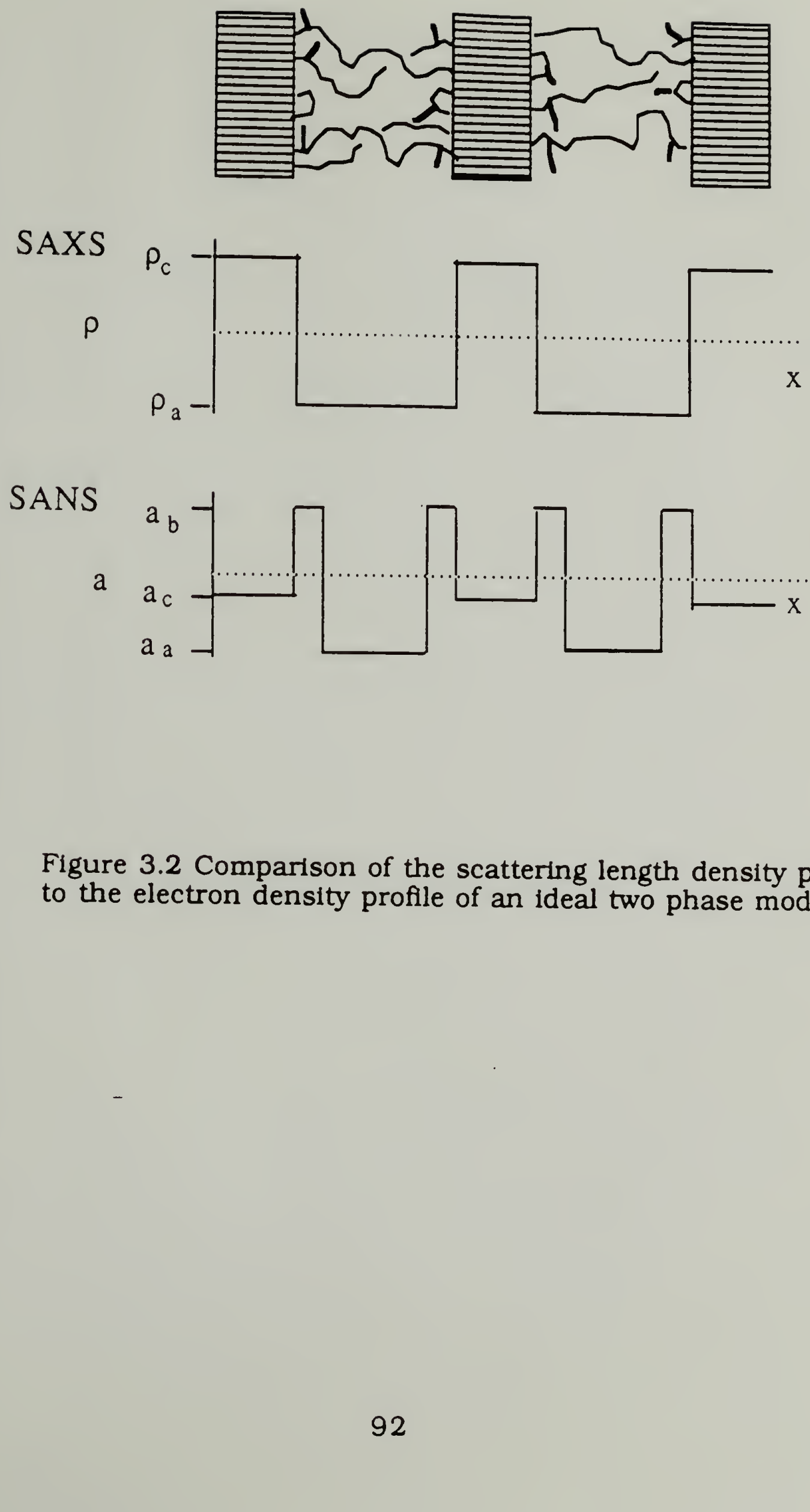

Figure 3.2 Comparison of the scattering length density profile to the electron density profile of an ideal two phase model.

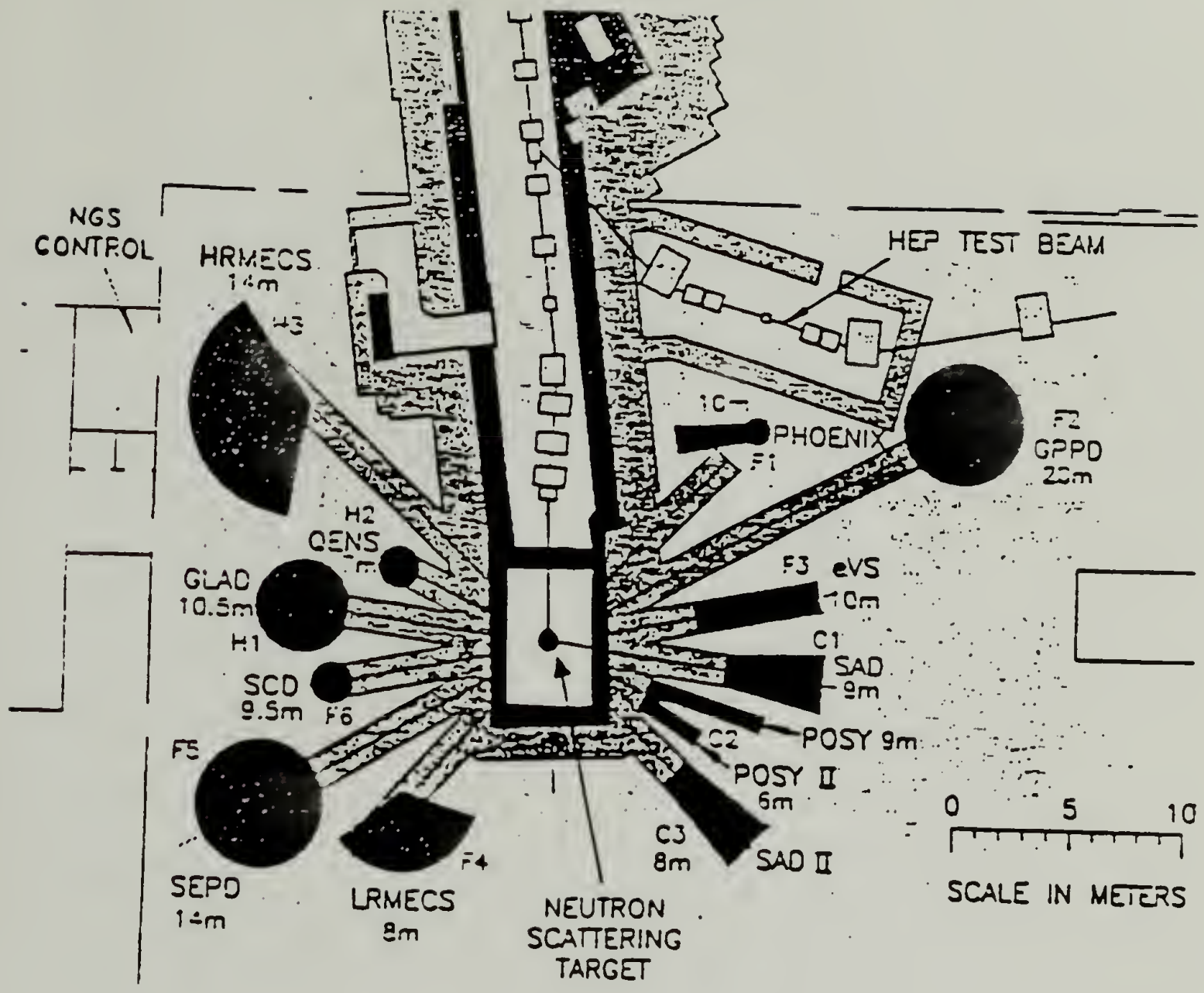

Figure 3.3 IPNS small angle diffractometer.

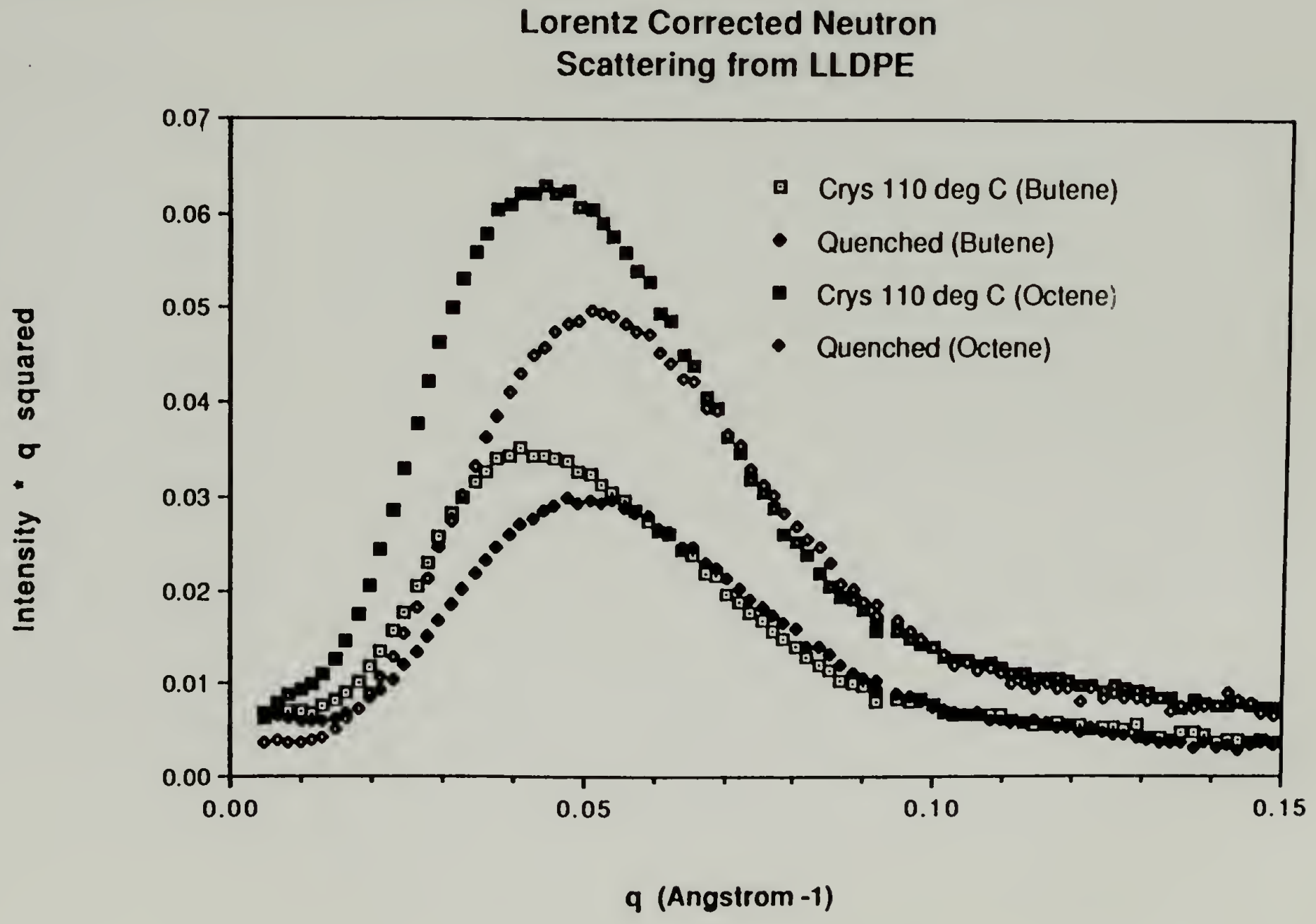

Figure 3.4 Lorentz corrected neutron scattering profiles for selectively deuterated LLDPEs.

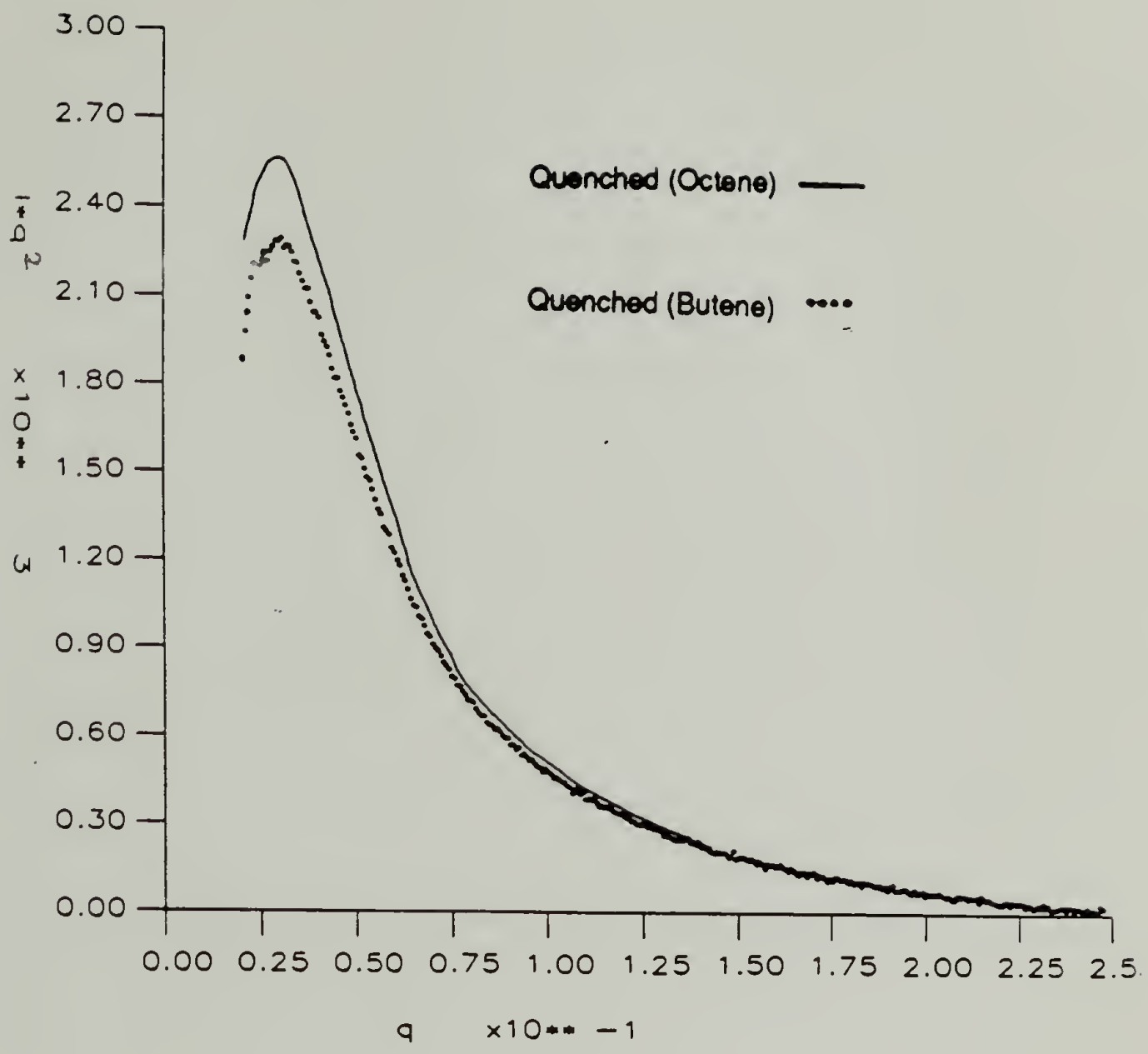

Figure 3.5 Lorentz corrected SAXS for selectively deuterated LLDPEs.

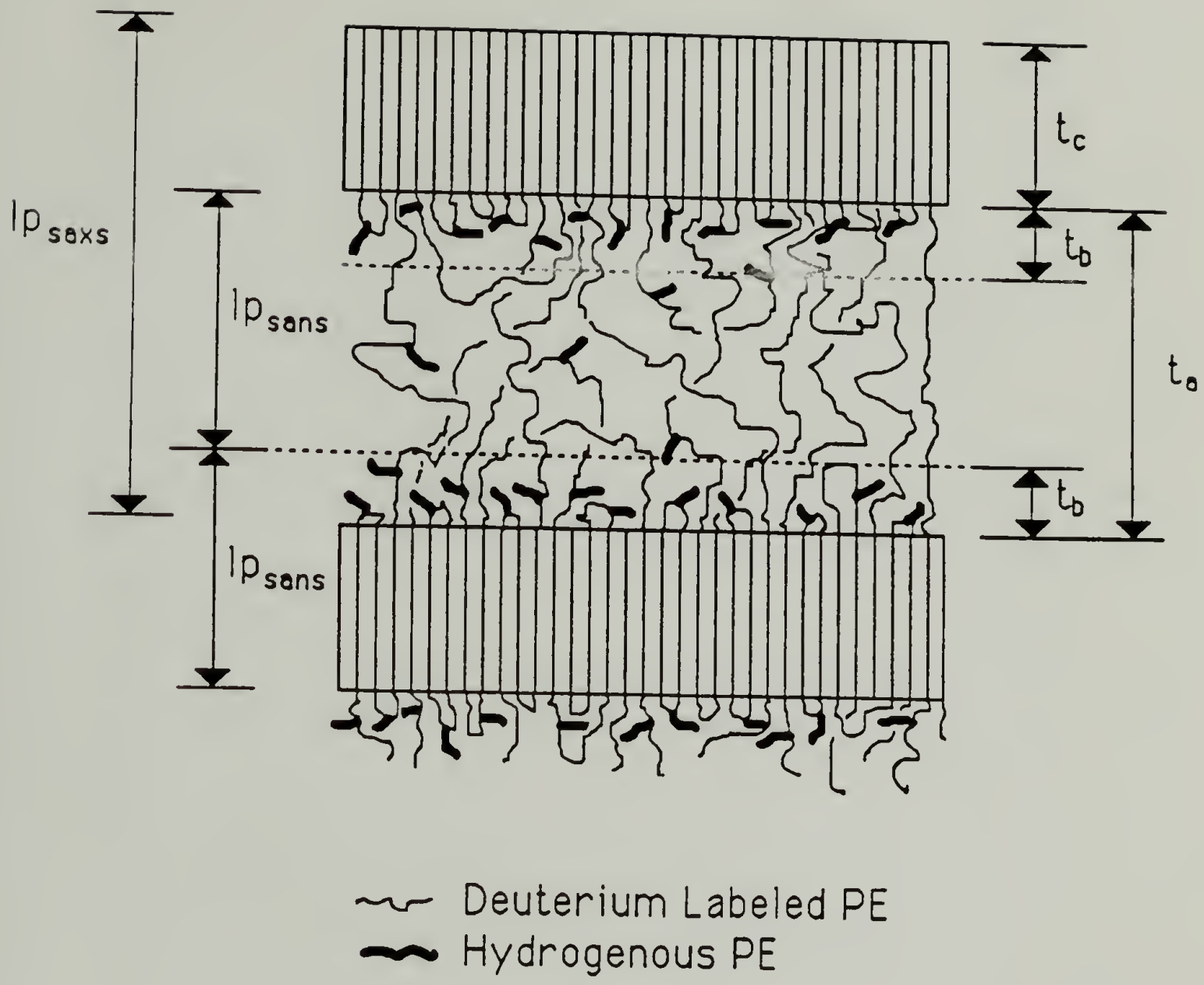

Figure 3.6 Possible concentration enhancement of short chain branches at the crystalline-amorphous boundary.

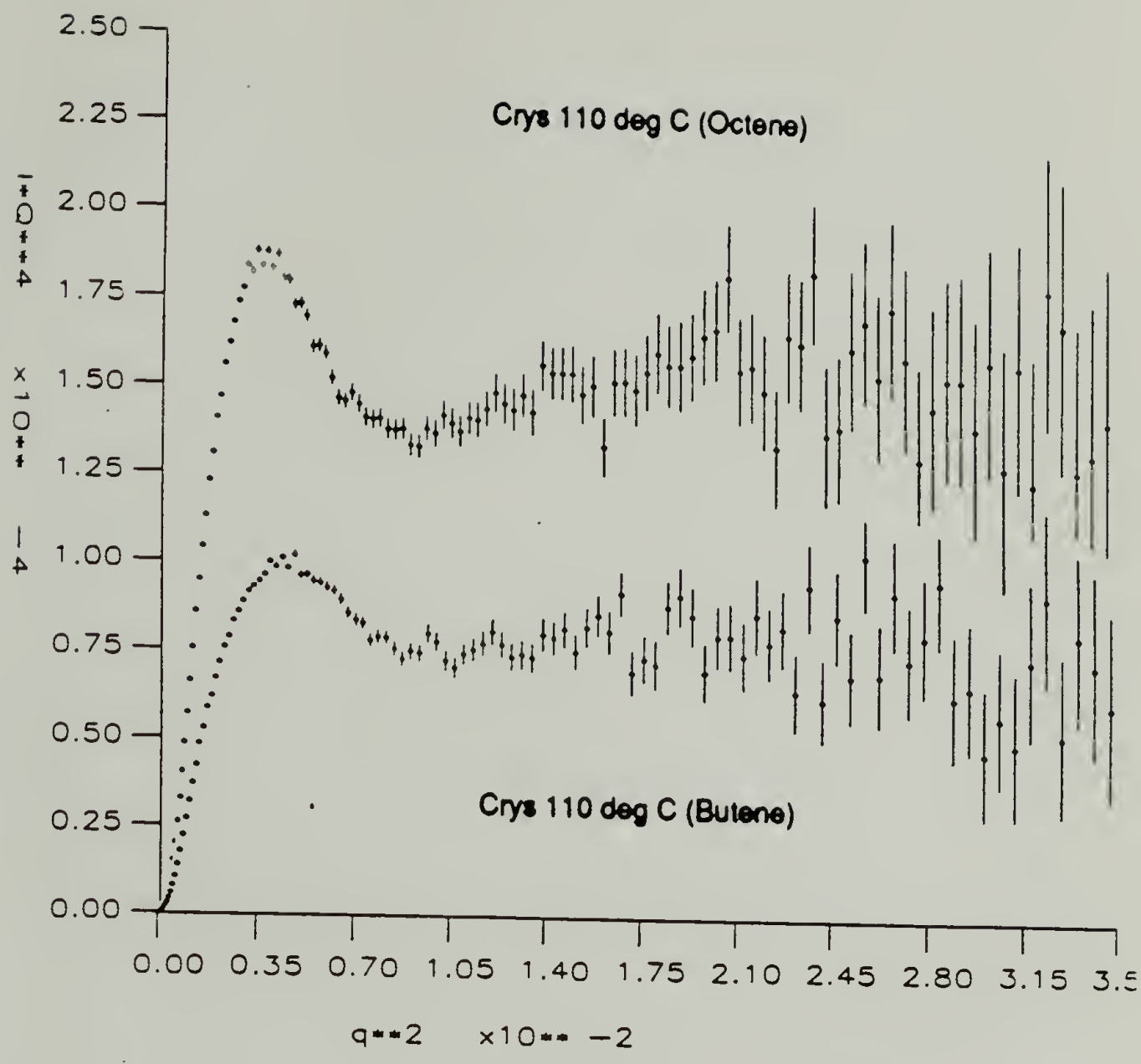

Figure 3.7 Porod plots for SANS.

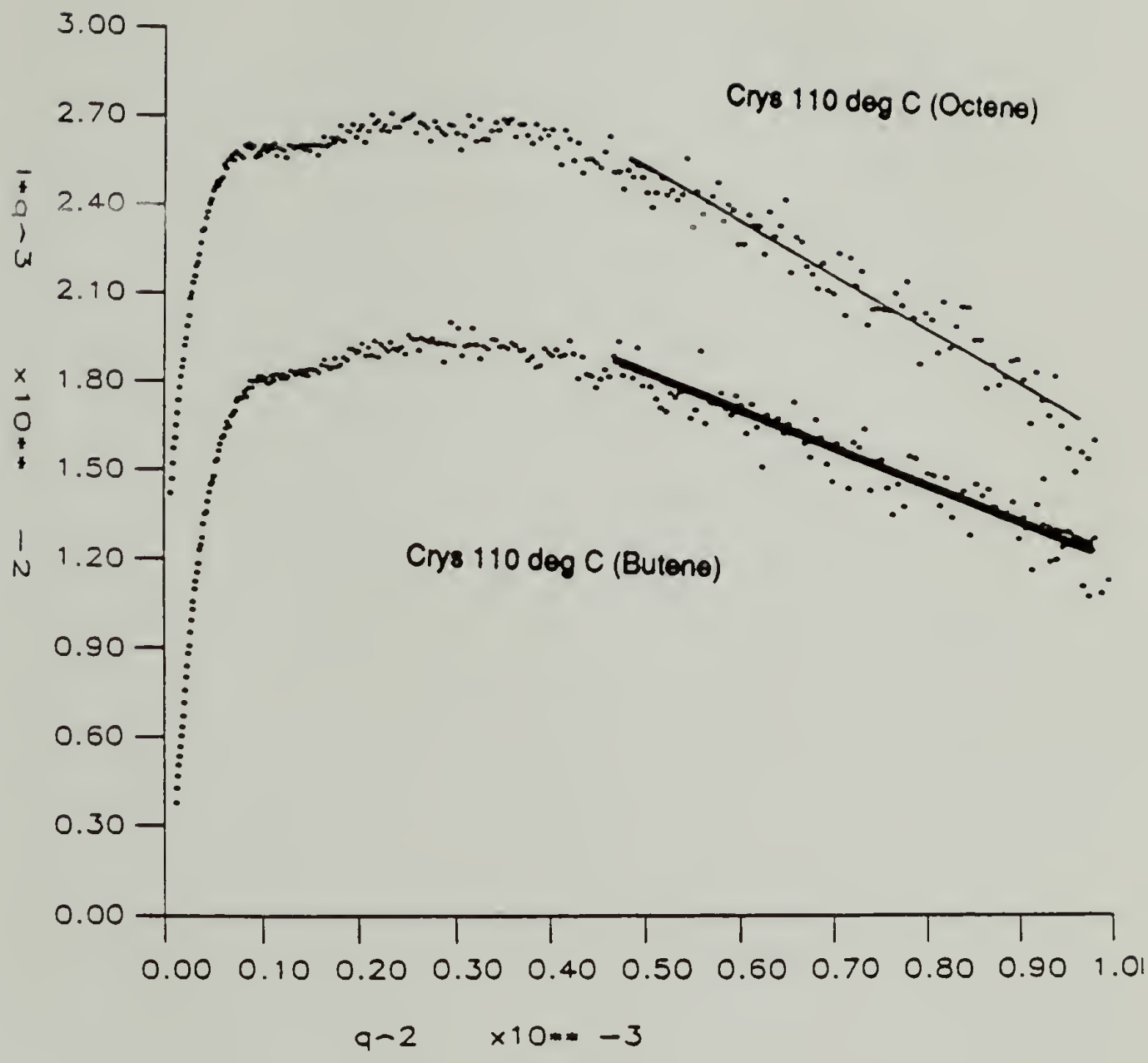

Figure 3.8 Porod plots for SAXS.

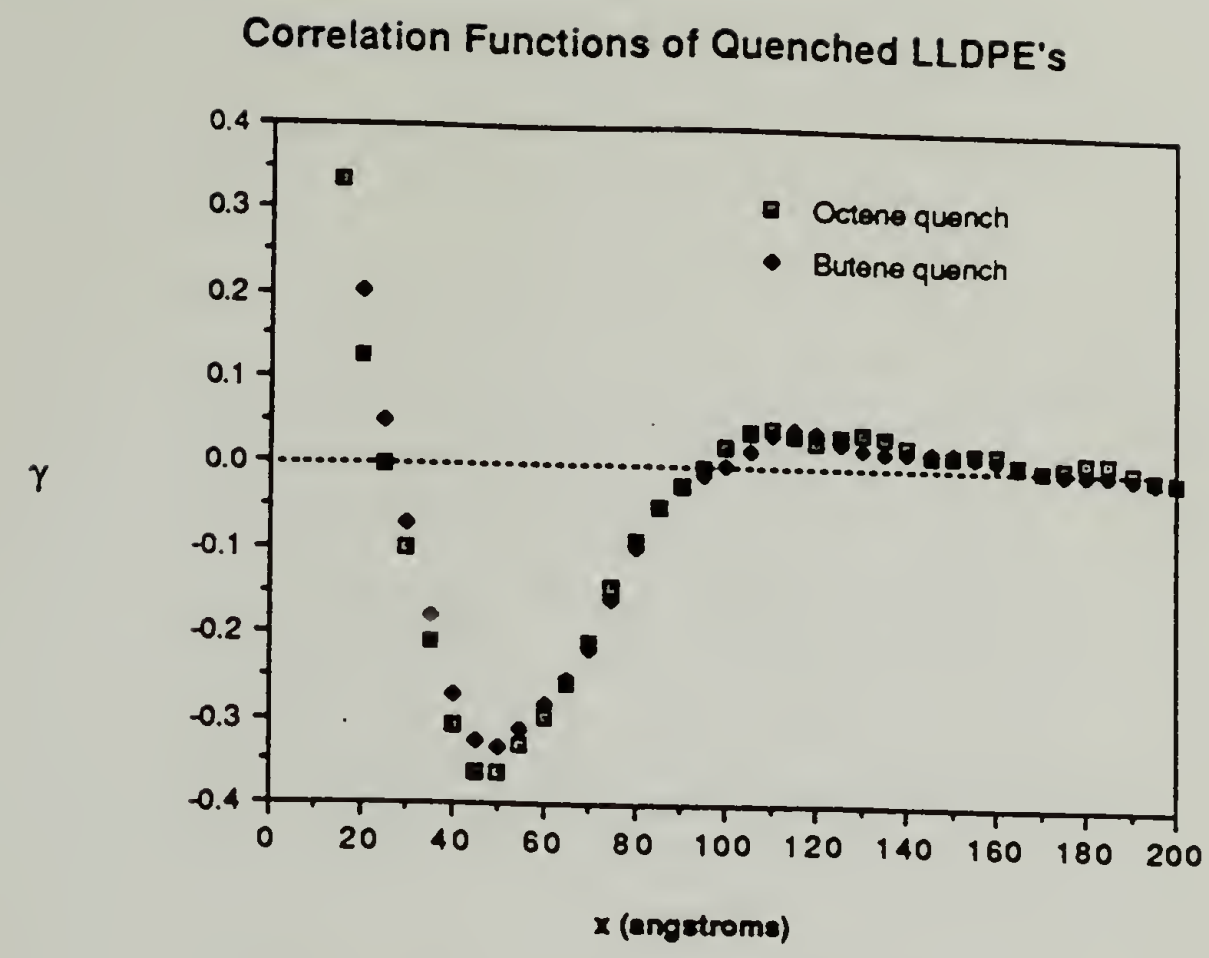

Figure 3.9 Correlation functions from neutron scattering.

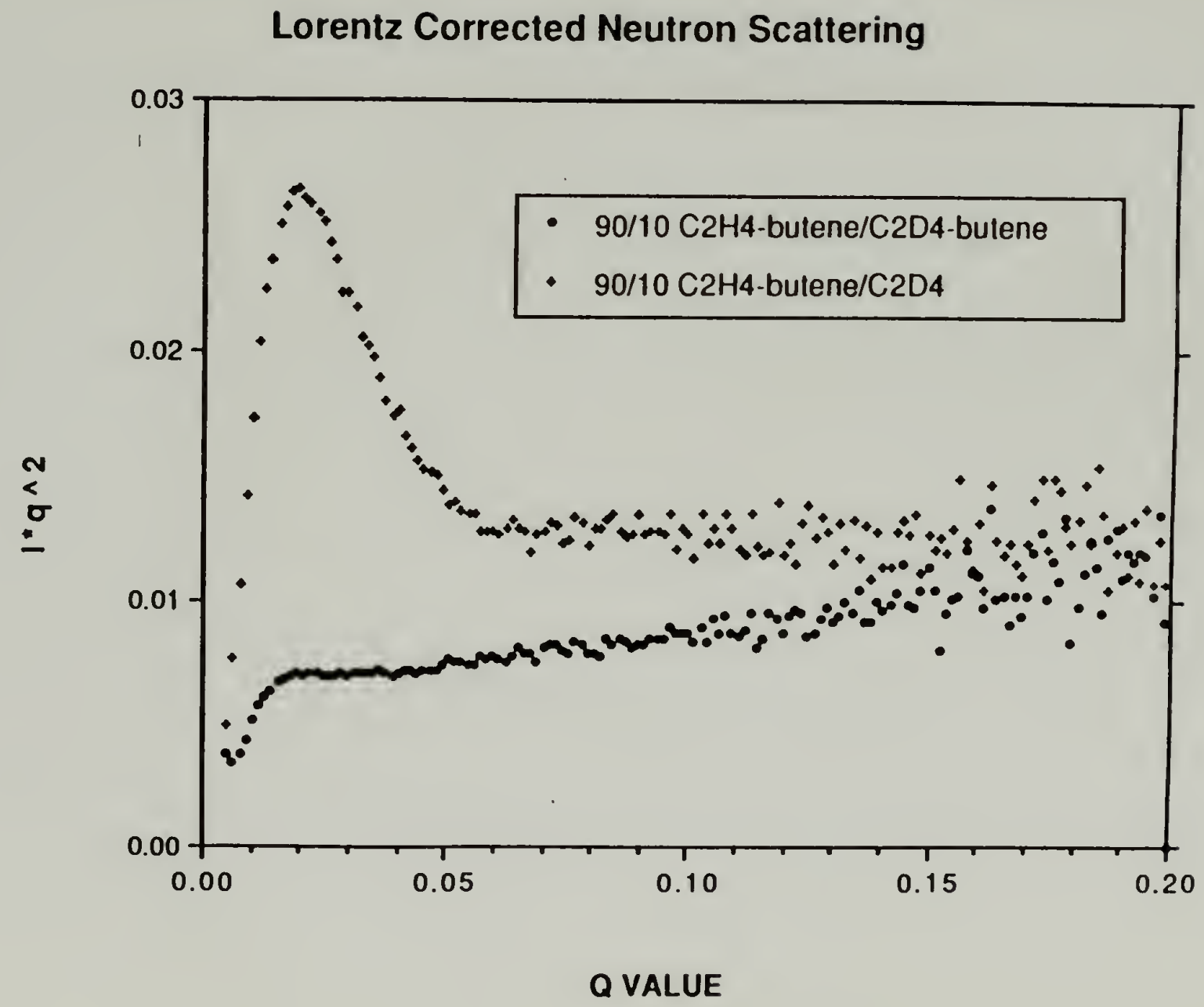

Figure 3.10 SANS profiles for 10/90 d-butene LLDPE/ butene LLDPE and 10/90 d-HDPE / butene LLDPE blends.

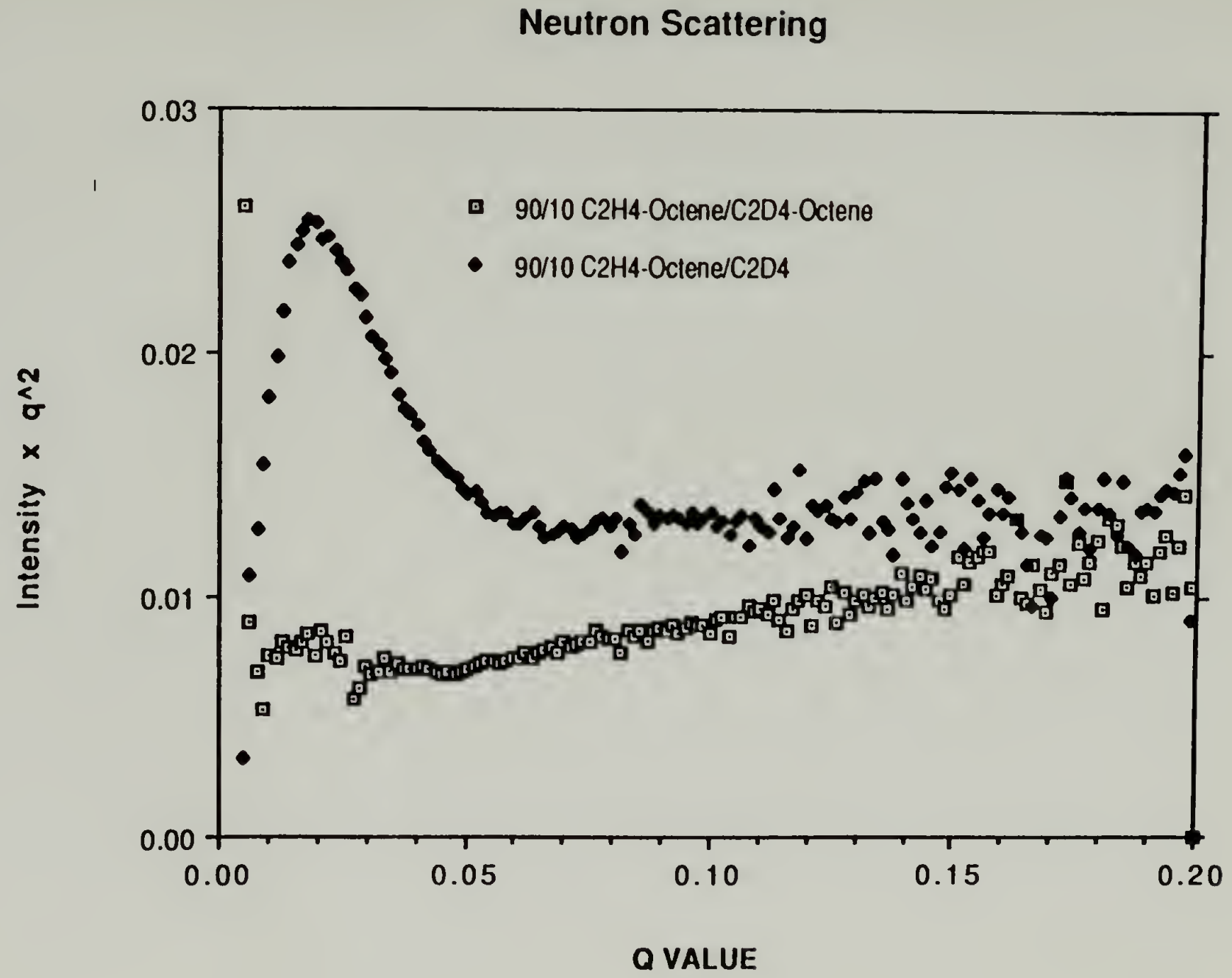

Figure 3.11 SANS profiles for 10/90 d-octene LLDPE/ octene LLDPE and 10/90 d-HDPE / octene LLDPE blends.

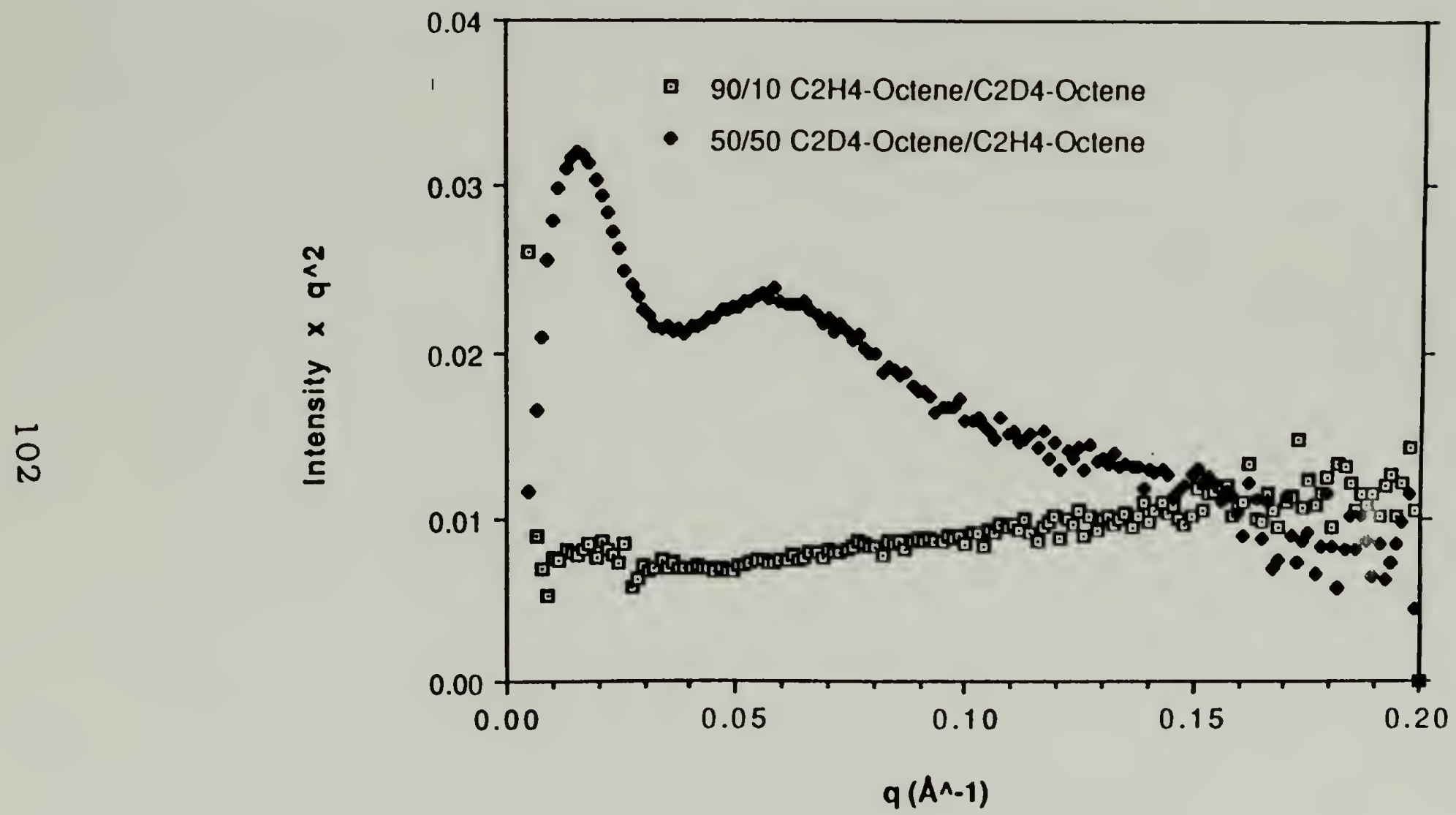

Figure 3.12 SANS profiles of d-octene LLDPE/ octene LLDPE blends of different concentrations (10/90 and 50/50).

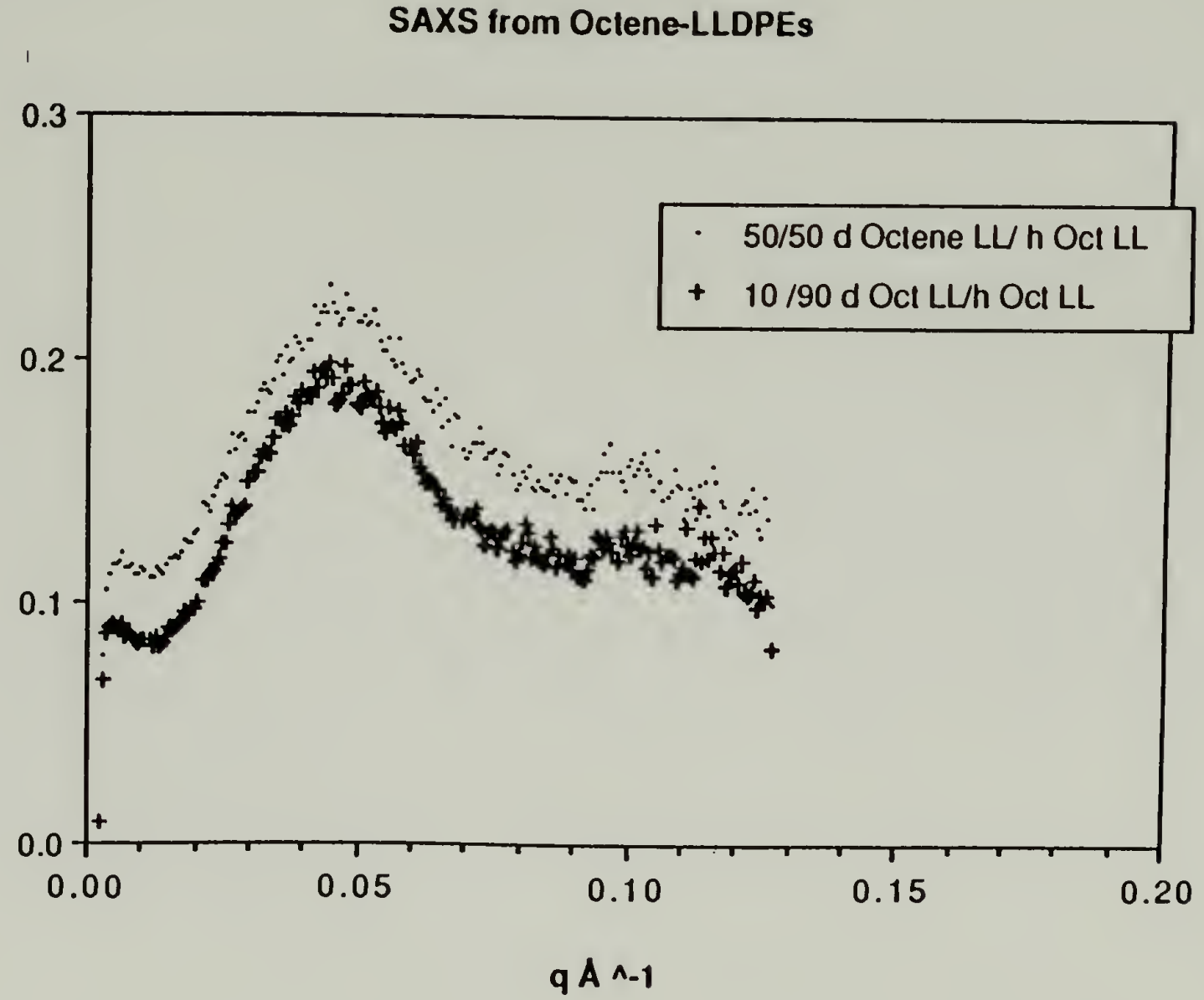

Figure 3.13 SAXS profiles of d-octene LLDPE/ octene LLDPE blends of different concentrations (10/90 and 50/50).

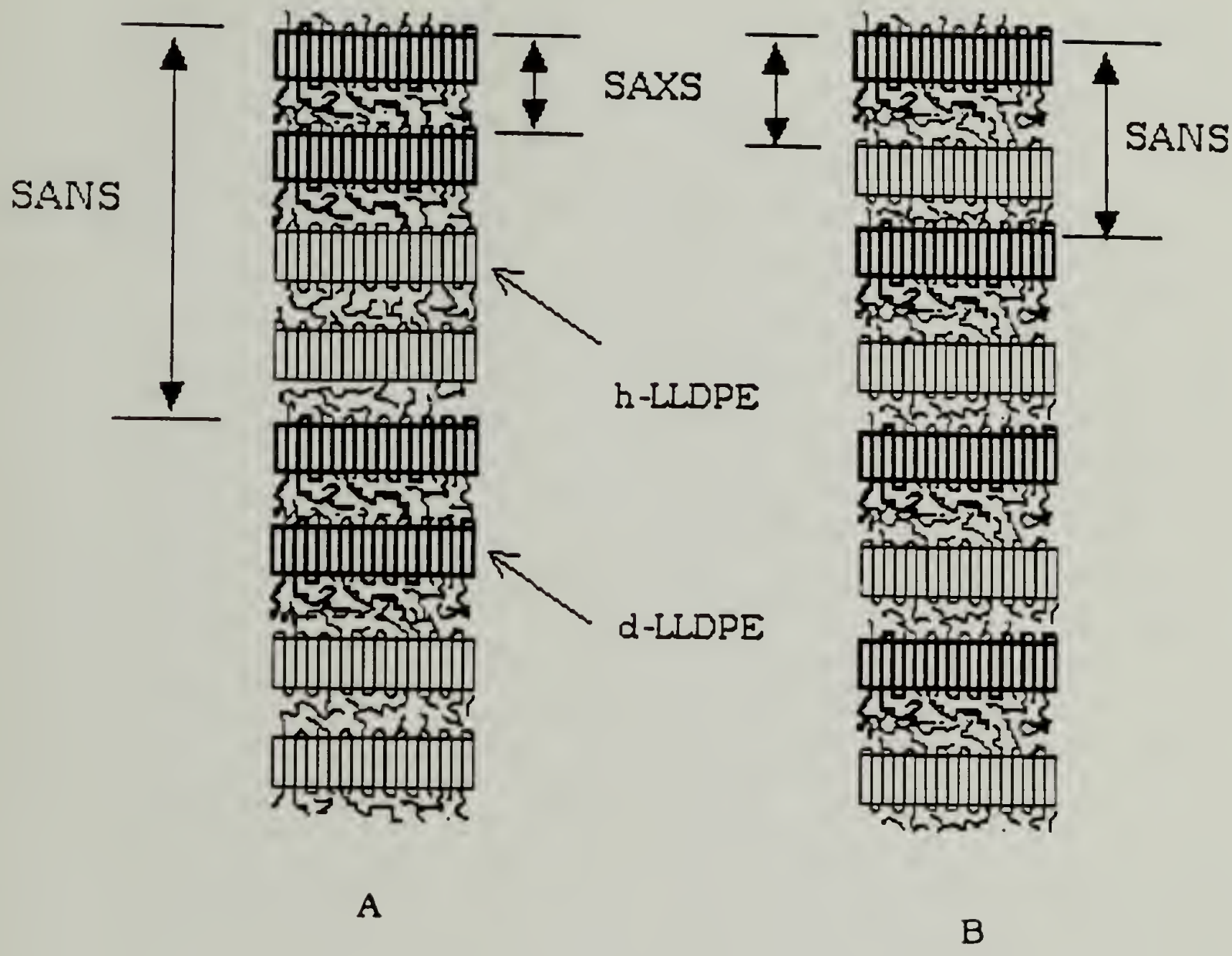

Figure 3.14 Lamellar Segregation Schemes A) Two Lamellae in Bundle B) Alternating.

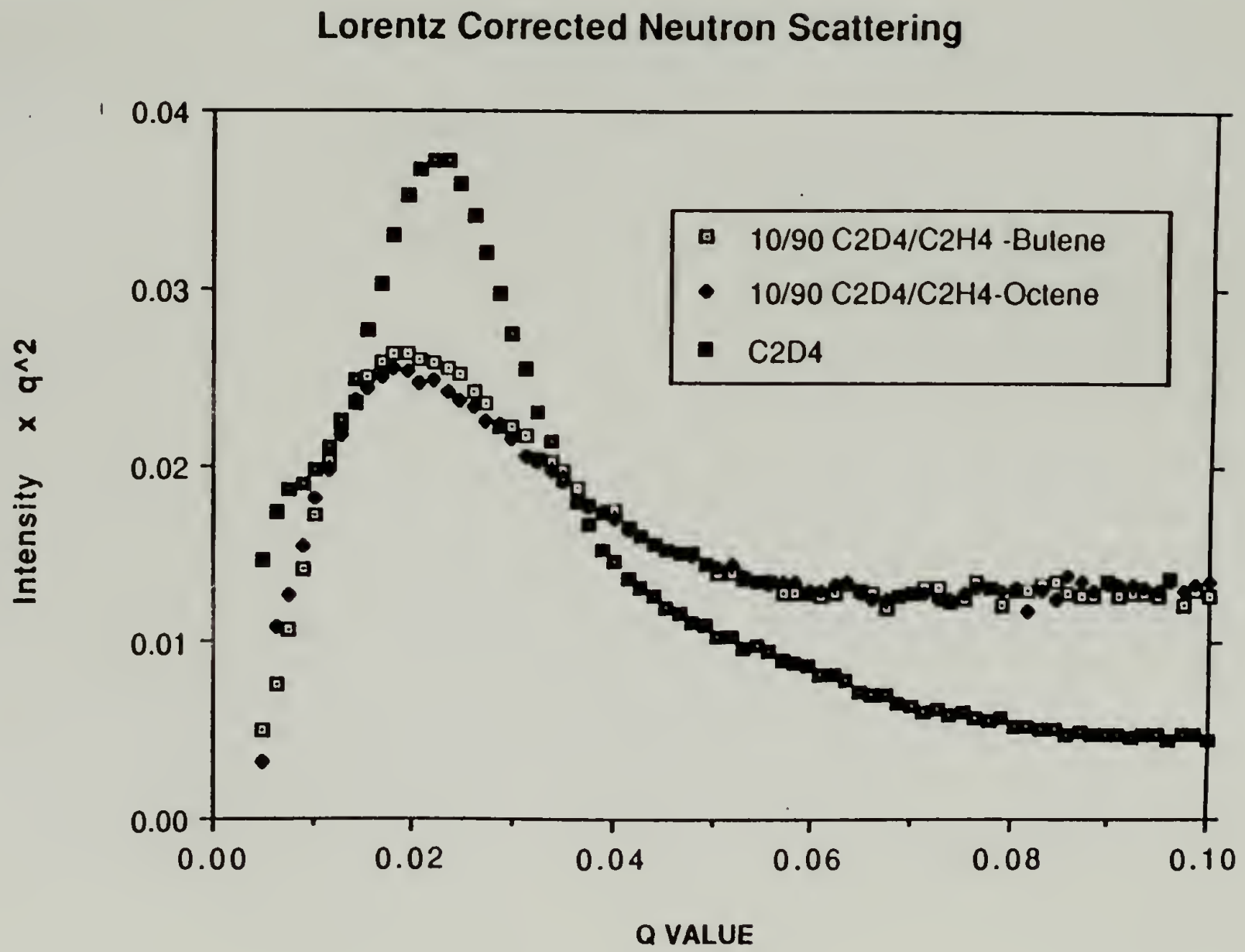

Figure 3.15 SANS profiles of d-HDPE / LLDPE blends and pure d-HDPE.

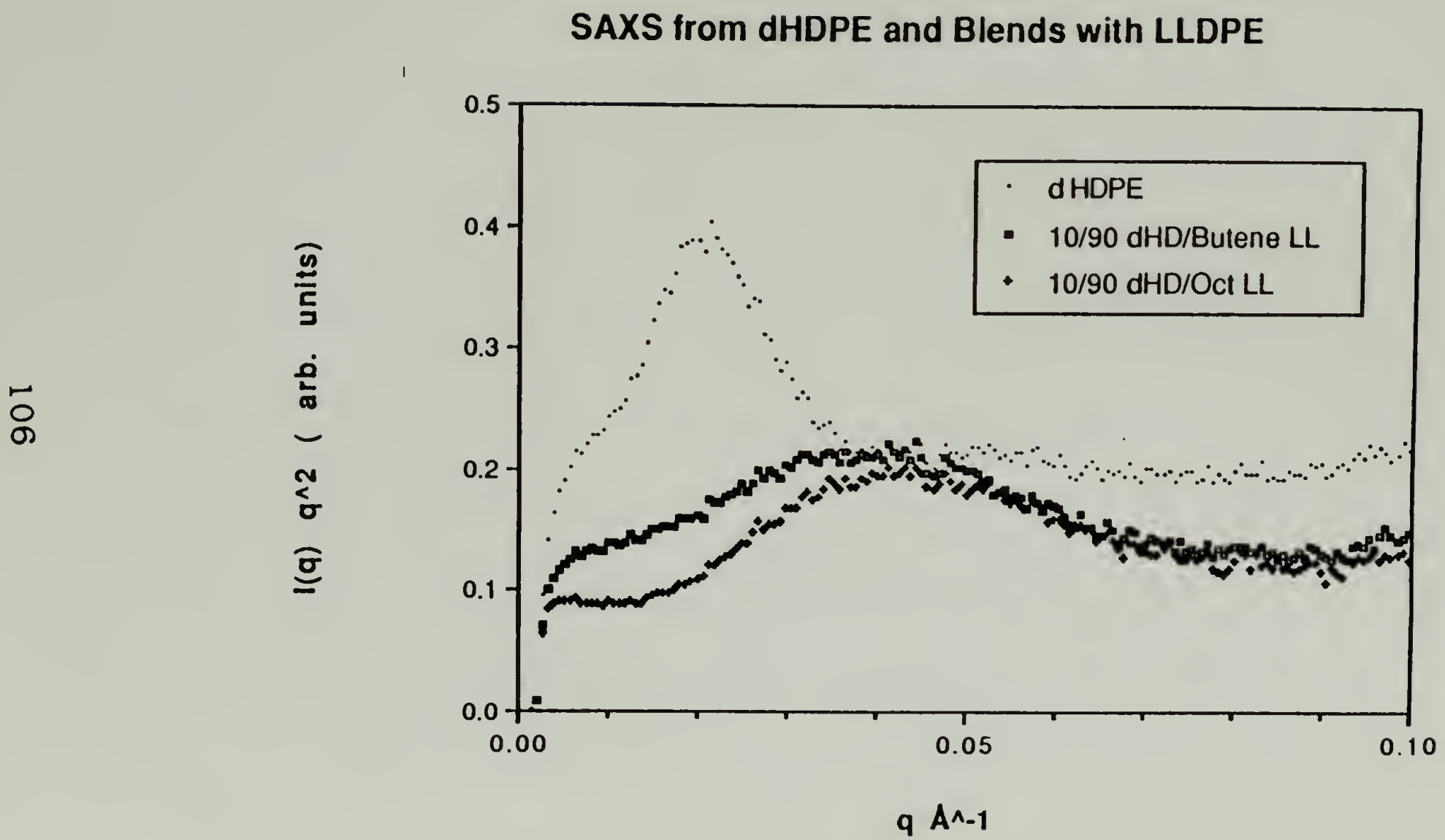

Figure 3.16 SAXS profiles of d-HDPE /LLDPE blends and pure d-HDPE.

CHAPTER 4

NEUTRON SCATTERING FROM HIGHLY DRAWN ULTRAHIGH MOLECULAR WEIGHT POLYETHYLENE

4.1 Introduction

Ultradrawn polyethylenes are good examples of materials in which the polymer chains are almost completely extended. These materials exhibit remarkable mechanical properties in the drawing direction. The maximum attainable modulus for these types of materials is as much as 200-300 GPa.[1-6] Conventional techniques such as x-ray scattering and infrared dichroism are insensitive for measuring chain orientation in these samples. For example, the orientation function, fc, ($fc=(3 < \cos^2\phi > -1)/2$), of the c axis of the PE crystallites which describes how the angle ϕ between the c axis and the draw direction changes, is essentially equal to one (perfect alignment) for extension ratios greater than five (see Figure 4.1)[7] Although there is little change in crystallite orientation after draw ratios of 5, physical properties such as Young's modulus continue to increase drastically (see figure 4.2) Small angle neutron scattering (SANS) is capable of measuring the single chain dimensions perpendicular and parallel to the stretching direction. This enables one to examine the single chain dimension and orientation in these extended specimens.

Previous studies of oriented polymers using neutron scattering have shown that for amorphous polystyrene samples, the deformation is affine for draw ratios up to ten.[8,9] For semi-crystalline polymers,

such as polyethylene, the deformation is non-affine for draw ratios greater than four.[10,11] This earlier work concentrated on moderate deformations (less than 15X) on high density polyethylene. The radius of gyration in the parallel direction, $Rg_{\parallel}$, increased from 250 angstroms undeformed to 1034 Angstroms at draw ratios of 12. The radius of gyration perpendicular to the draw, $Rg_{\perp}$, decreased from 250 to 125 in the same range. Much higher extension ratios can be achieved with ultra high molecular weight polyethylene (UHMWPE). Prepared by the gelation - crystallization process, these polymers can be drawn up to 200 times their original length. In this process, the polymer is dissolved in a solvent at concentrations slightly greater than the overlap concentration. This produces a gel that is subsequently dried, producing a polymeric solid that has relatively few entanglements. The absence of extensive entanglement accounts for the remarkable drawability of these films[12,13] In general, these polymers are highly crystalline. The dried gel mats usually are 80% crystalline before drawing After draw ratios of 12 the crystallinity rapidly increases to about 95%. The molecule might then be thought of as nearly completely extended except for folds or kinks randomly distributed about the chain.

4.2 Experimental

UHMWPE samples were supplied to us by Professor Lemstra at University of Groningen (The Netherlands). All samples were prepared by gelation/crystallization from semi-dilute decalin solutions at 150°C and contained 10/90 mixture of deuterated and hydrogenous UHMW PE. The specimens were tensile drawn at 120° C.

Preliminary measurements were carried out at Oak Ridge National Laboratory, using the 10 meter camera at the ORR (Oak Ridge Research Reactor). Additional measurements were conducted at the Small Angle Diffractometer at the Intense Pulsed Neutron Source, Argonne National Laboratory

The radius of gyration , R_g , is determined from the Guinier approximation of the scattered Intensity, I(**q**).[14]

$$I(\mathbf{q}) = I(0) \exp -(R_g^2 q^2 / 3) \qquad (1)$$

Here $q = 4\pi/\lambda \sin(\theta/2)$, θ being the scattering angle. The pattern is analyzed by taking slices of the scattering pattern perpendicular and parallel to the draw direction (see figure 4.3). An alternative way of determining R_g is through the modified Zimm equation.[15-17]

$$I^{-1}(q) = \frac{1}{CM_w}\left[1 - \frac{R_g^2 q^2}{3} \right] \qquad (2)$$

M_w is the molecular weight, and C is a constant. The advantage with this analysis is that molecular weight can be used as a check for segregation.

4.3 Results and Discussion

Samples with extension ratios 25, 40 and 50 were studied at ORR. Shown in Figure 4.4 is the isointensity contours of the 25X sample. At these extensions, the scattering from the long axis of the molecule is completely within the beam stop. Any scattering that appears to be present in the parallel direction is a consequence of smearing due to instrument geometry. The geometry of the scattering instrument can effect the pattern by smearing the intensity. Smearing is most evident when the collimation sizes are large, the intensity is measured at small angles, and the sample to detector distance is short. The intensity scattered at an particular momentum transfer vector, **q**, ($q= (4\pi/\lambda) \sin(\theta/2)$ has an uncertainty in the direction the incident beam because the collimation size is so large. Therefore the scattering is spread out or smeared over a range of scattering angles. For an ideal system consisting of pinhole collimation combined with a large sample to detector distance the effect of instrumental smearing is negligible. The present camera geometry at ORNL is suitable for obtaining smear free data for most normal applications. In the case of highly elongated samples, the anisotropy in the scattering pattern necessitates measuring intensities at the smallest angles possible, if measurements of $Rg_{\parallel}$ are to be made. Under these conditions, the assumption of ideal pinhole geometry breaks down. Consequently, data obtained is subjected to smearing, and must be corrected. While the theory for desmearing isotropic systems is well developed, no known procedure exists for desmearing scattering from anisotropic systems. At present it is only possible to smear theoretical patterns. The

geometry of ORR 10 meter device (and the similiar SAD-1 at IPNS) has a limit of about a Rg > 800 Å. before smearing becomes severe. Lo's work demonstrated the practical limit of smearing theoretical profiles matched to data curves to be about $Rg_{\parallel}$ =1500Å. For UHMW PE ,the extensions are so long that measuring $Rg_{\parallel}$ is impossible. Consequently, only $Rg_{\perp}$ was obtained. Despite the low flux at this device, values of $Rg_{\perp}$ of about 30-50 Angstroms were determined. For Rg's in this range no smearing corrections need to be applied.

Samples were in the form of thin tapes. Because of the highly oriented nature of these molecules, a misalignment of the tapes of less than a degree can cause the measured value of $Rg_{\perp}$ to be overstated by a significant amount. To circumvent this problem, the orientation can be randomized by stacking the films so that the vector representing the draw direction would assume all directions in the plane perpendicular to the beam. This is in effect a randomization in the plane of the film. Since the scattering due to the chain long axis occurs at such small angles as to be obscured by the beam stop; the scattering in the experimentally accessible region is due mostly to the transverse chain length.

Scattering from a model system consisting of long cylinders was calculated. Patterns were calculated from

$$I(q)=Kn^2\int_0^{\pi/2}\frac{\sin^2(qH\cos\theta)}{q^2H^2\cos^2\theta}\cdot\frac{4J_1^2(qR\sin\theta)}{q^2R^2\sin^2\theta}\cdot d\theta \qquad (3)$$

which is a modified form of the expression due to Fournet.[12] H is the height of the cylinders, while R is the width. φ is the angle the cylinder makes with a reference axis , and J_1 is a Bessel function of the first kind. The results of the calculation for cylinder with different aspect ratios are shown in figure 4.5. Two linear sections are evident. The first steep portion is due to the long axis of the cylinder. The second linear portion is scattering from the width of the cylinder. As long as the ratio of height to width is larger than ten, two linear regions can be distinguished.

A series of experiments using the randomizing technique was conducted at the SAD-1 IPNS.The samples studied are listed in table 4.1. Some samples were soaked in paraffin oil for 1 week under atm pressure in order to study the effect this would have on scattering from voids that may be in the samples. If scattering from voids were a major contributor to the scattering, it was expected that the paraffin soaked samples would scatter much differently than the unsoaked samples. Such was not the case. Soaked and unsoaked samples showed nearly identical scattering.

The radii of gyration in the perpendicular direction were determined from randomized Guinier plots (Figure 4.6). The scattering profiles are very similar to the calculated curves of figure 4.5. The rapidly rising inner portion of the curve is scattering from the longitudinal dimension of the chain, while the second linear region is mostly scattering from the chain width. For draw ratios greater than 12, $Rg_{\perp}$ remains roughly the same, about 20 Angstroms.

However , Ln-Ln plots show there is a change in the tails of the curve (figure 4.7). For a gaussian coil, $I(q) \sim q^{-2}$, while for a rod $I(q) \sim q^{-1}$. Experimental values of q^{-n} show $1 < n < 2$. (Table 4.2.)

This changing power law for I(q) suggests that the molecule is becoming more "rodlike" while still maintaining a 20 Angstrom perpendicular radius of gyration. This can occur if folds and other defects are removed as the draw ratio is increased. This causes longer linear segments in the molecule, but enough defects still remain to allow a 20 Angstrom $Rg_{\perp}$. This is illustrated in figure 4.8. This situation is very different from the case of non gel crystallized systems such as those studied by R. Lo. In Lo's work, the samples were HDPE (M.W. 220,000) prepared by solid state coextrution. These samples showed considerably larger $Rg_{\perp}$ than that seen in the present work near similiar draw ratios (12). The smaller $Rg_{\perp}$ observed here is obviously a consequence of the reduced number of entanglements in the pre-drawn gel-crystallized polymer.

4.4 Conclusions

It appears that circularly averaging SANS data can used to eliminate the effect of misalignment in the samples. Data profiles closely resembled those obtained from model scattering from simple rods. The profiles could not be fitted to these calculations because they do not reflect the true geometry of the molecule. Calculating the theoretical patterns from models such as shown in figure 4.8 is a non-trival problem because of the exact scheme to use for the averaging of

the chains is complicated. One would have to average various types of defects as well as their position on the chain..

The transverse dimension for all drawn samples with extension ratios between 12 and 60 was found to be 20Å 8Å. It is clear that $Rg_{\perp}$ changes little in this extension range; certainly neutron scattering is not sensitive enough to determine smaller changes than this. The limiting behavior of the scattered intensity at large angles does change for these same extensions , however. The decrease in the exponent of $I(q) \sim q^{-n}$ indicates that the molecule is undergoing a change in geometry toward a more rod-like structure. The insensitivity of $Rg_{\perp}$ between draw ratios of 12 and 60, and the change in the exponent of the limiting scattered intensity suggests that the transverse dimension of the molecule is nearly fixed at low extension ratios and then defects such as chain folds and kinks are subsequently pulled out with increasing draw ratio.

Table 4.1

UHMW Samples

Draw Ratio	Preparation Conditions
5	paraffin soaked
12	
25	paraffin soaked
50	paraffin soaked
60	

Table 4.2.

Values of Power n for Intensity ~ q^{-n} Drop-Off.

Draw Ratio	Power n
12	1.56
25	1.30
50	1.25
60	1.20

References

1. C. Sawatari, M. Matsuo, *Colloid Polym. Sci.* **263**,783 (1985).
2. T. Kanamoto,A. Tsuruta, K. Tanaka, M. Takeda, R.S. Porter, *Polymer J. (Tokyo)* **15**, 327 (1983).
3. S.K. Roy, T. Kyu, R. St. John Manley, *Macromolecules*, **21**, 1741 (1988).
4. A. Peterlin, *Colloid & Polym. Sci.*, **265**, 357 (1987).
5. J. De Boer, A. J. Pennings, *Polym Bull.*, **7**, 317 (1981).
6. R. Hikmet, P.J. Lemstra, and A. Keller, Colloid & Polym. Sci., **265**, 185 (1987).
7. K. Anadakumaran, S. Roy, R. St. J. Manley, *Macromolecules*, **21**, 1746 (1988).
8. A. Hill, R.S. Stein, A. Windle, *Macromolecules* ,**20**, 1720 (1987).
9. G. Hadziioannou, L. Wang, R.S. Stein, R.S. Porter, *Macromolecules*, **15**, 880 (1982).
10. R. Lo, Ph. D. Thesis, University of Massachusetts 1986.
11. R. Lo, A. Hill, R.S. Stein, *J Polym. Sci.* (to be published).
12. P.J. Lemstra, N. van Aerle, C.W. Bastiaansen, *Polymer J.* ,**19**, 85 (1987)
13. P. Smith, P. Lemstra, *J. Collid Polym. Sci.* ,**258**, 7, (1980).
14. A. Guinier , A. Fournet, *Small Angle X-ray Scattering*, Wiley, New York 1955.
15. R.G. Kriste, W.A. Kruse, and K. Ibel, *Polymer*, **16**,120 (1975).

16. D.G. Ballard, A. N. Burgess, P. Chesire, E.W. Janke, A. Nevin, J. Schelten, *Polymer*, **22**, 1353 (1981)

17. G.D, Wignal, D.H. Ballard and J. Schelten, *Eur. Polym. J.* , **10**, 861 (1974).

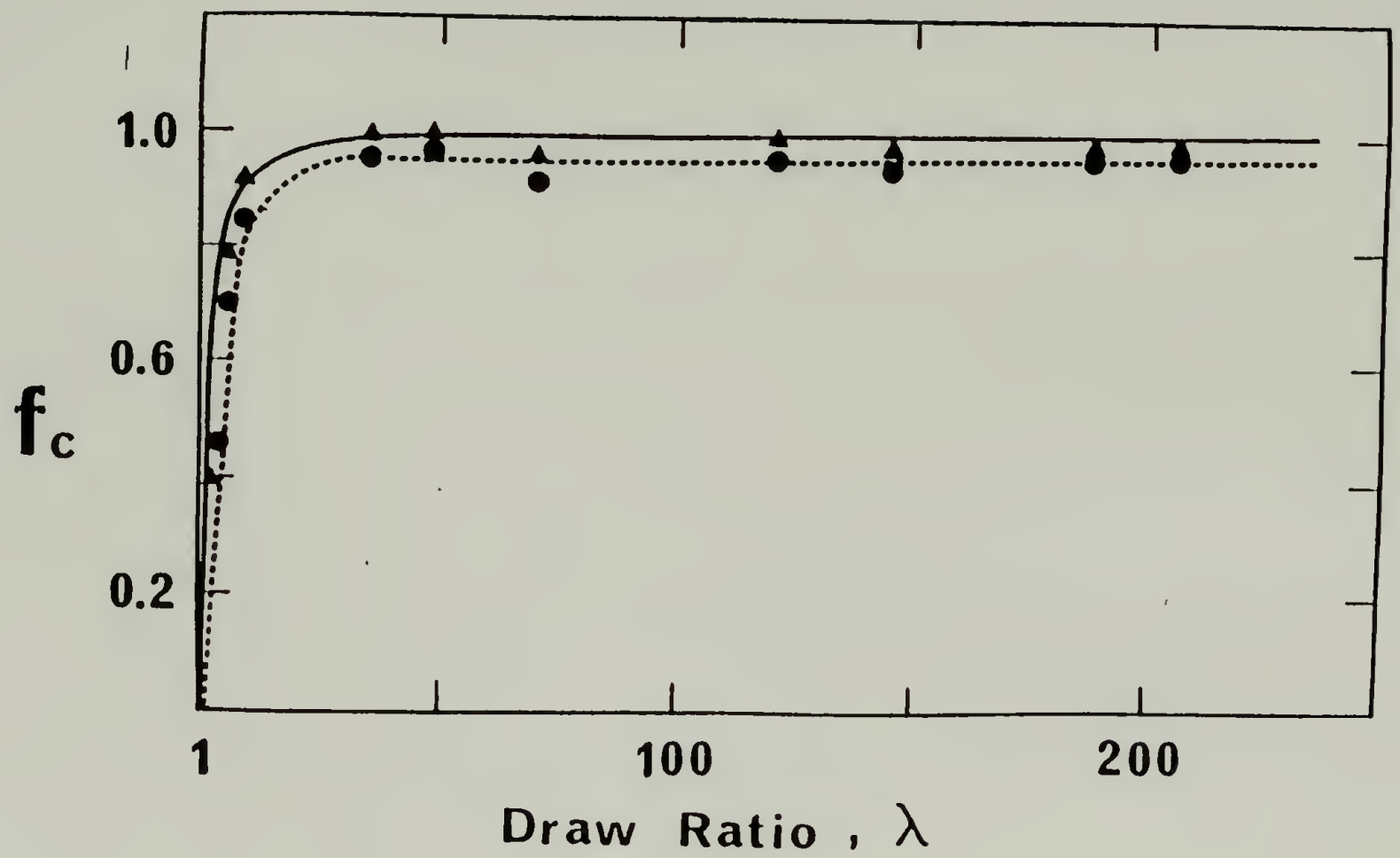

Figure 4.1 Crystal c axis orientation function as function of draw ratio for UHMW PE. From reference 7.

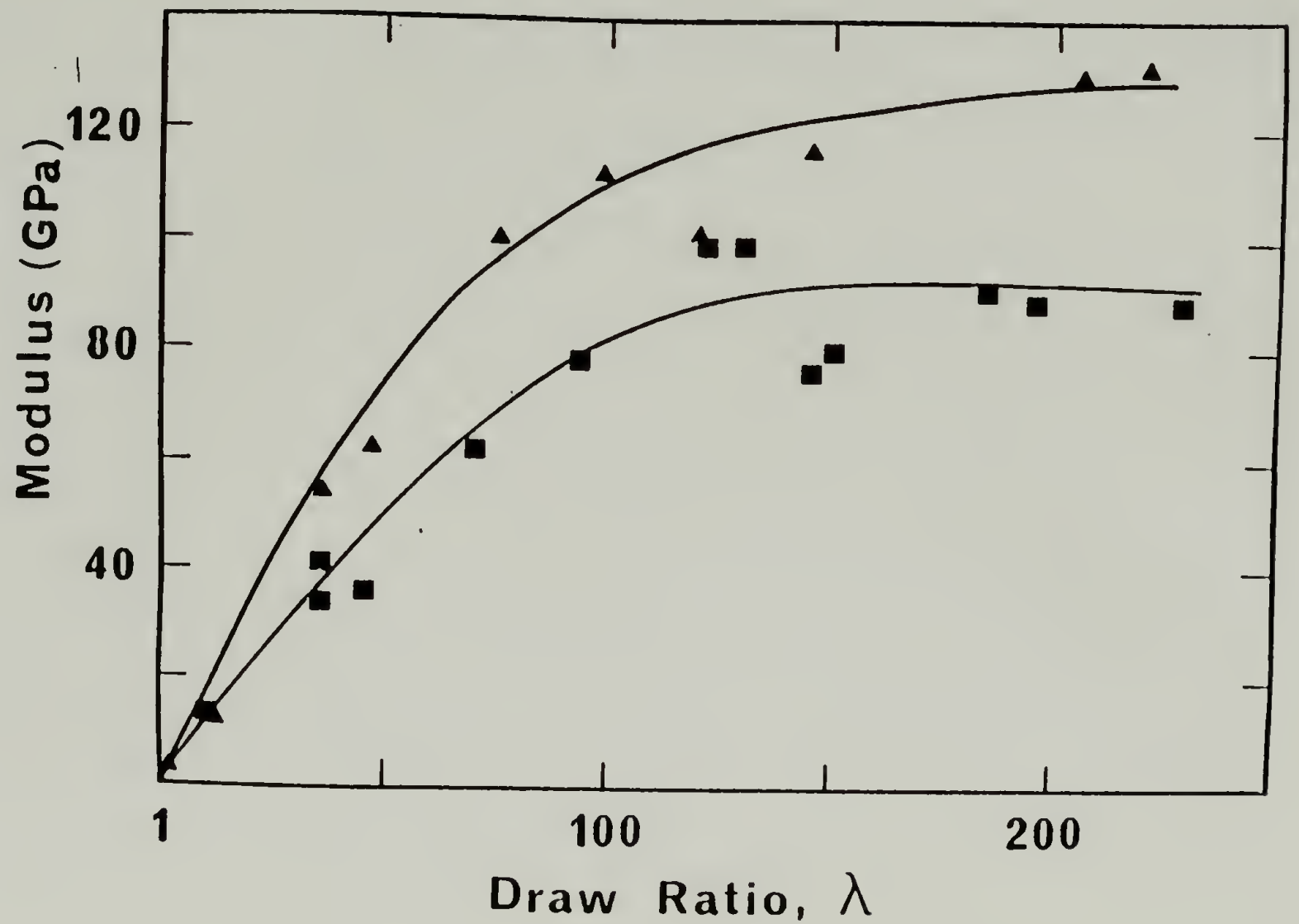

Figure 4.2 Young's modulus as a function of draw ratio for UHMW PE from reference 7.

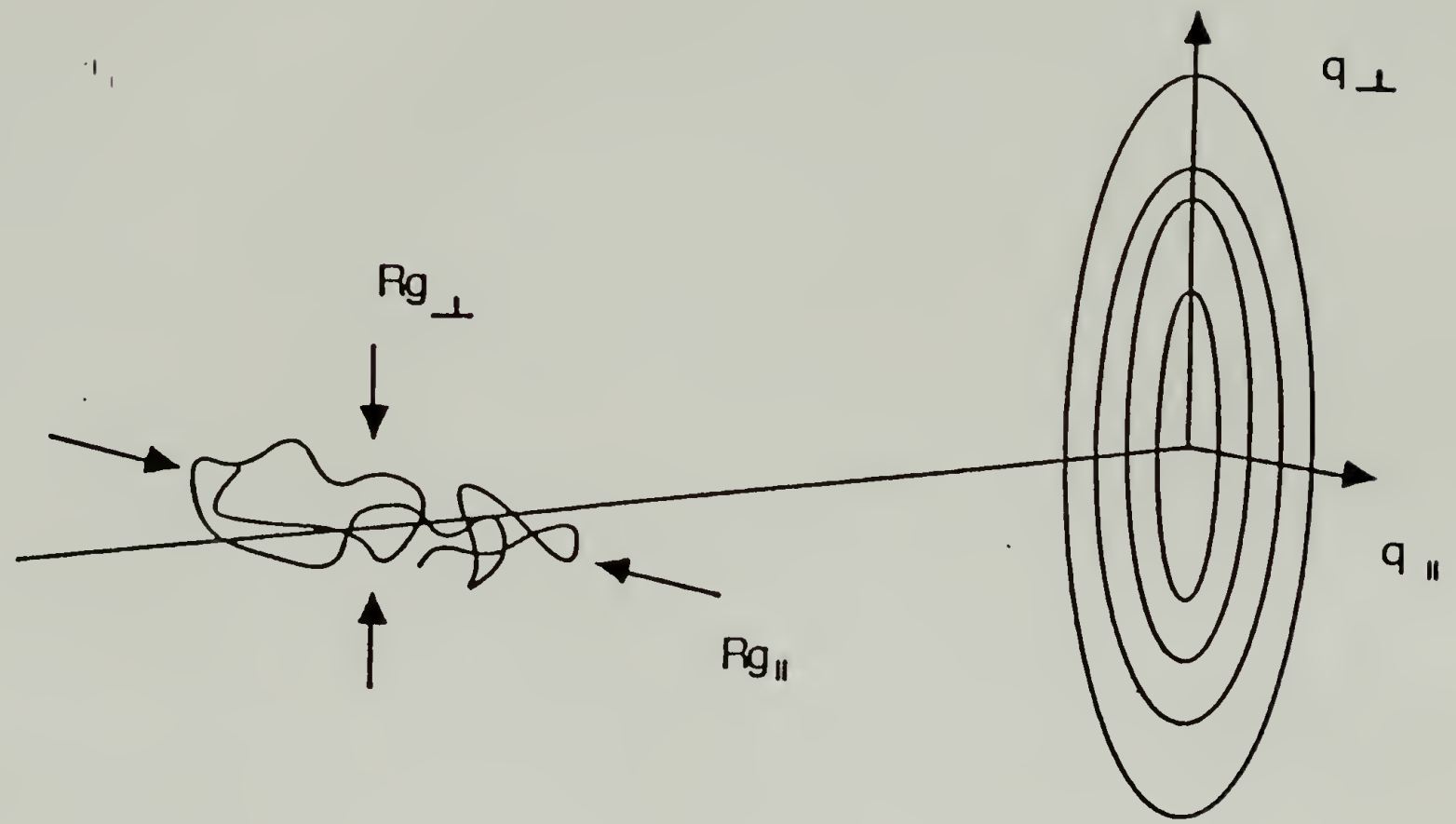

Figure 4.3 Relationship between q and draw direction .

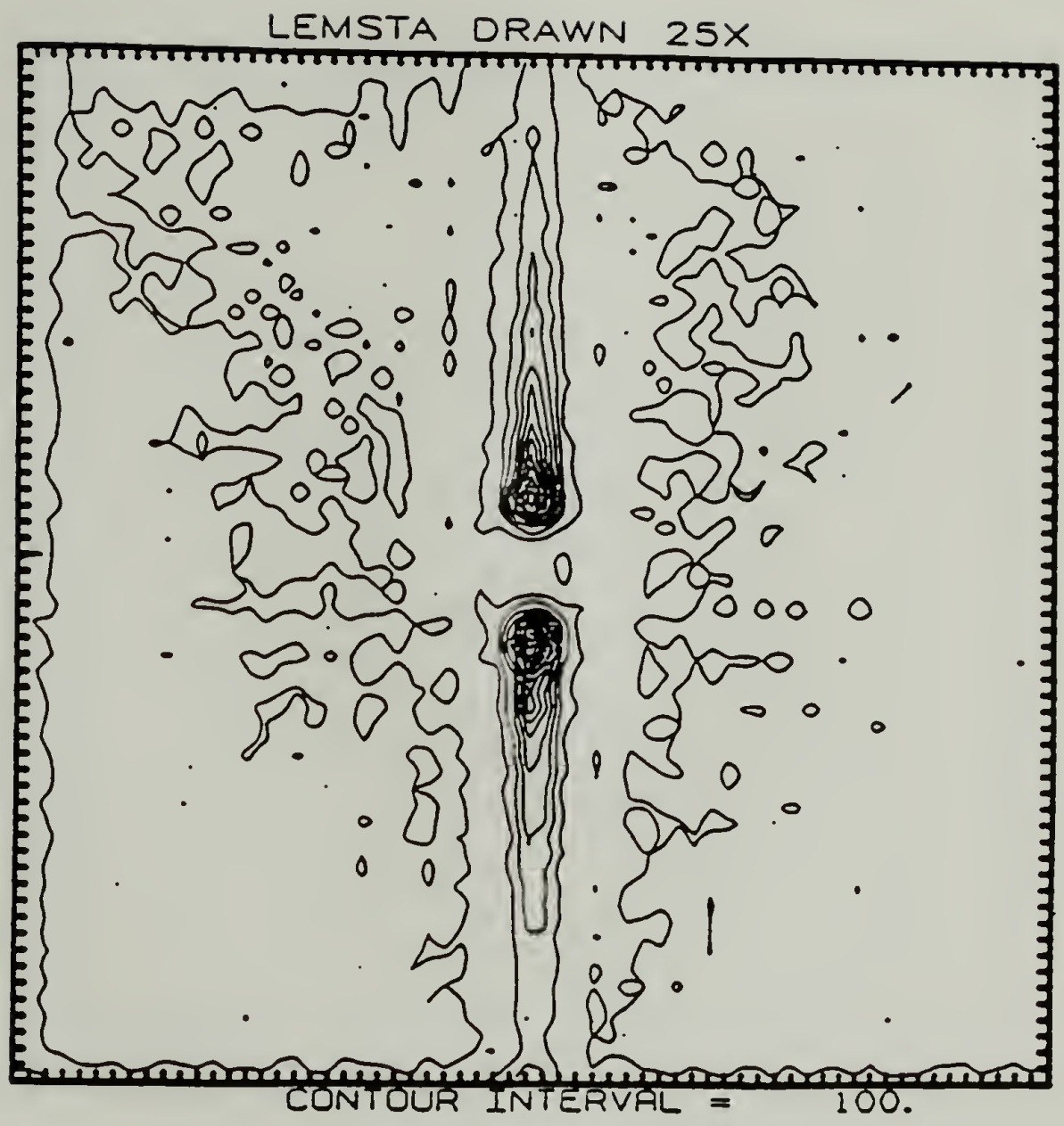

Figure 4.4 Isointensity SANS contours for 25X drawn UHMWPE.

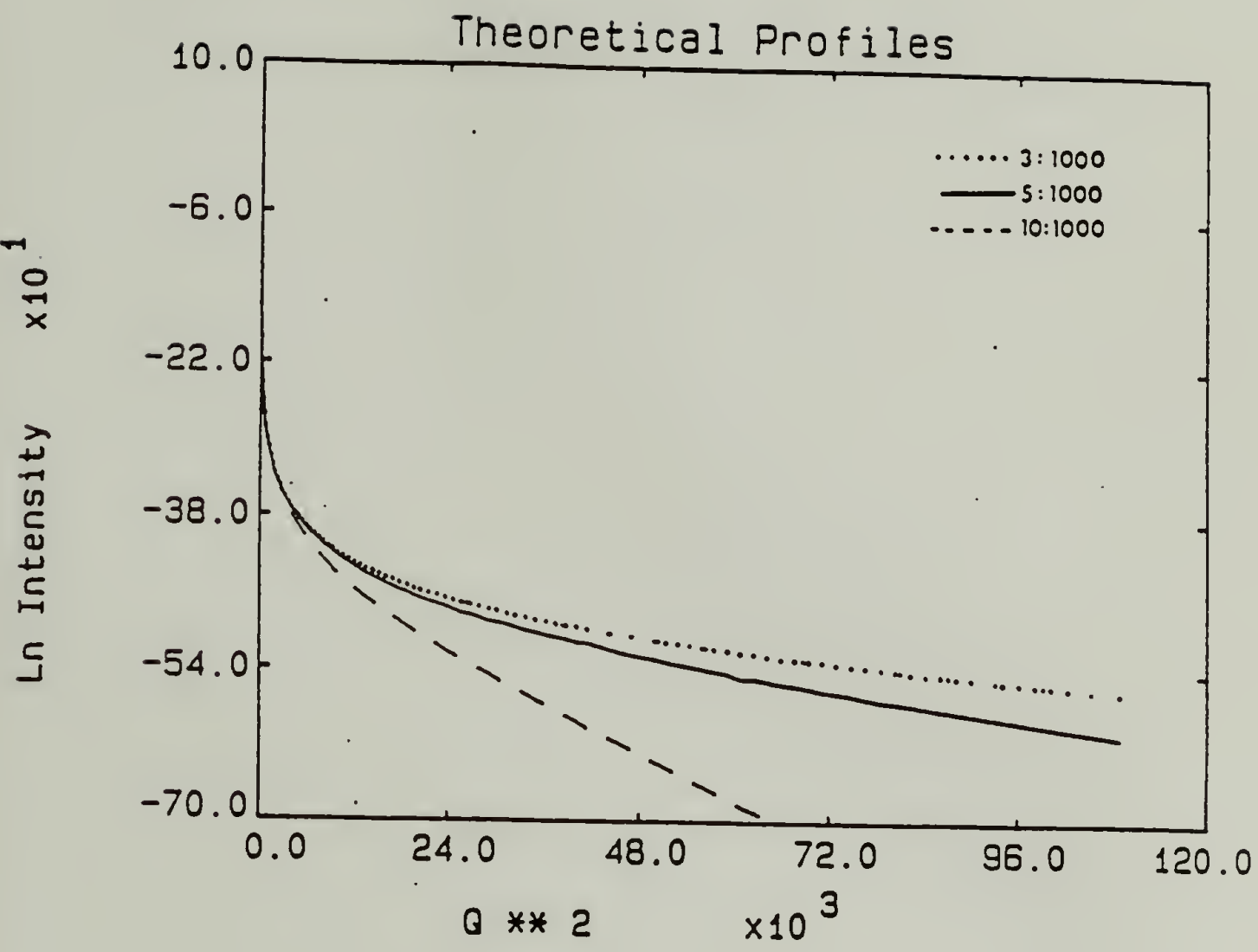

Figure 4.5 Calculated Guinier plots for rotationally averaged cylinders of different aspect ratios.

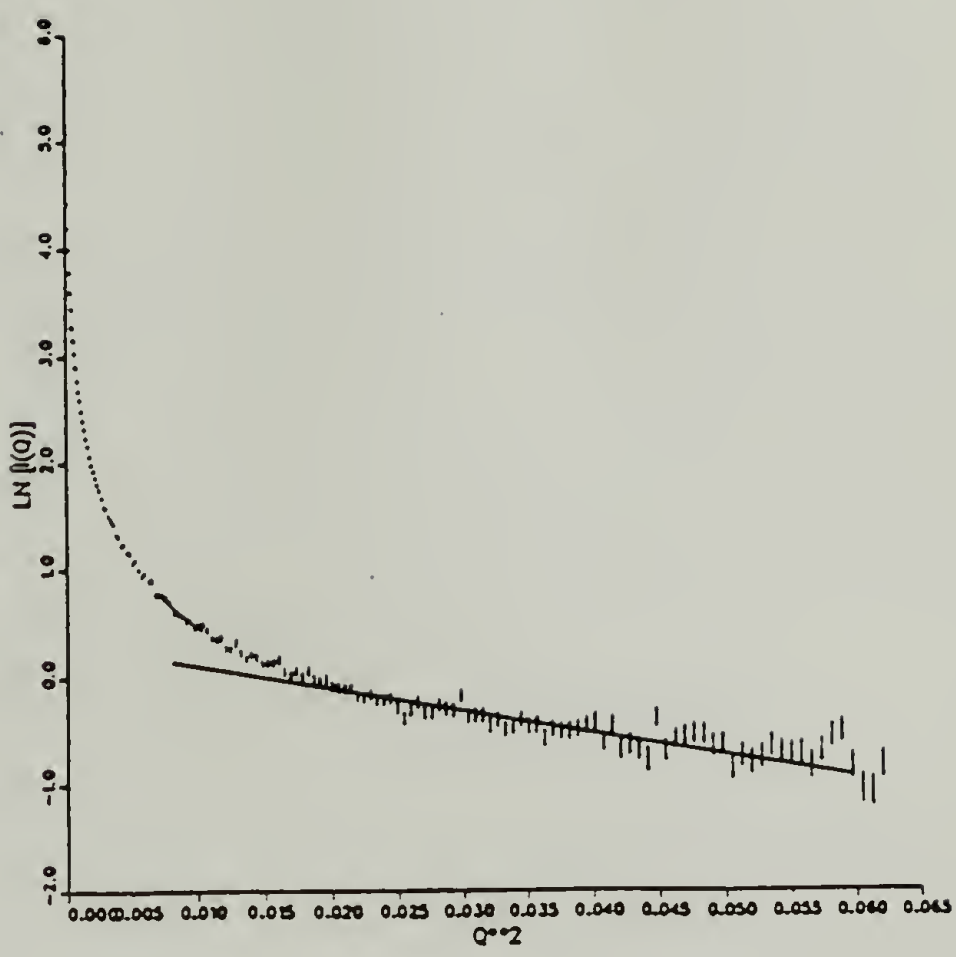

Figure 4.6 Experimental Guinier plot rotationally averaged for 25X drawn UHMW PE

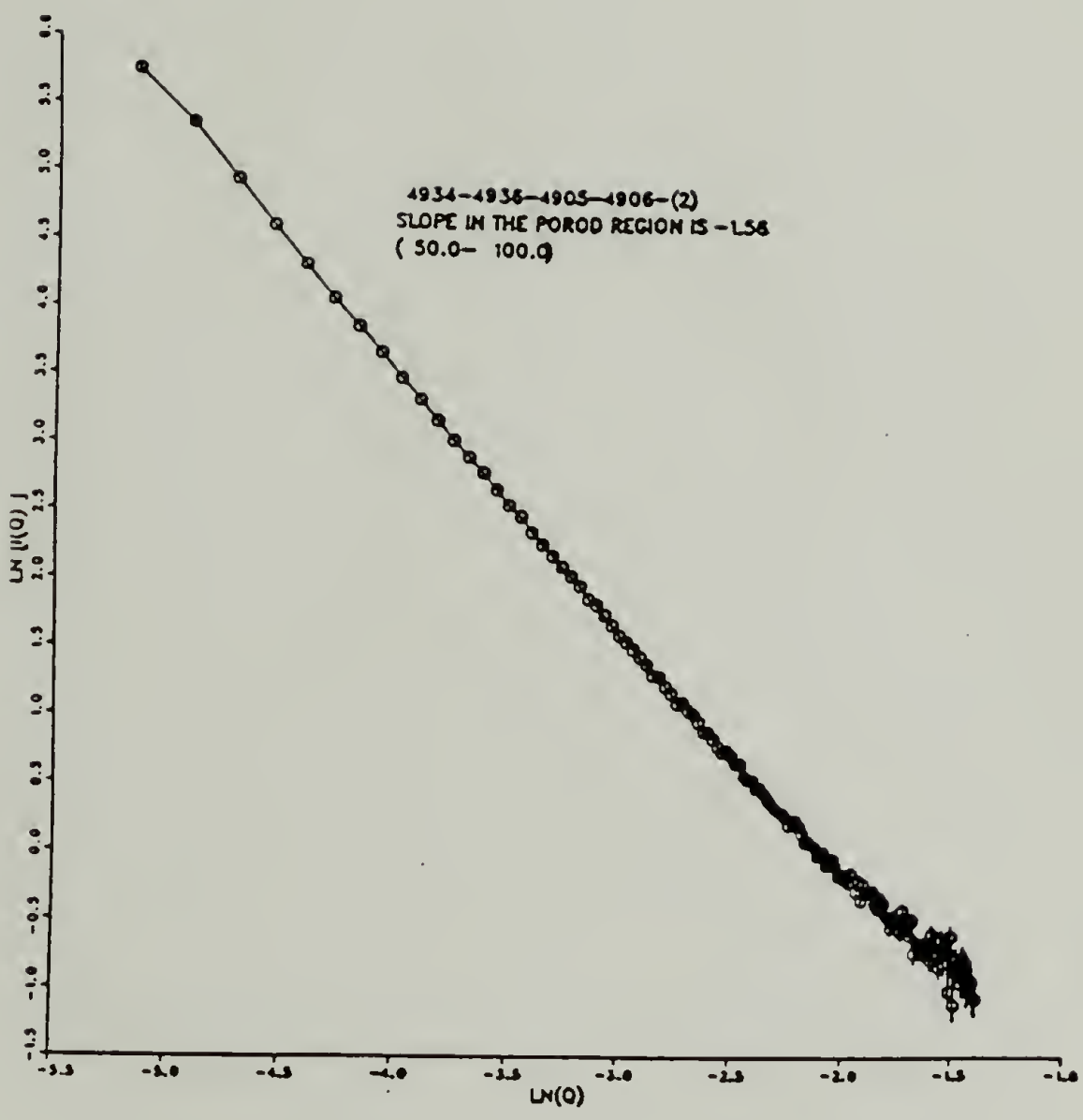

Figure 4.7 Ln -ln plots of rotationally averaged 25X drawn UHMW PE

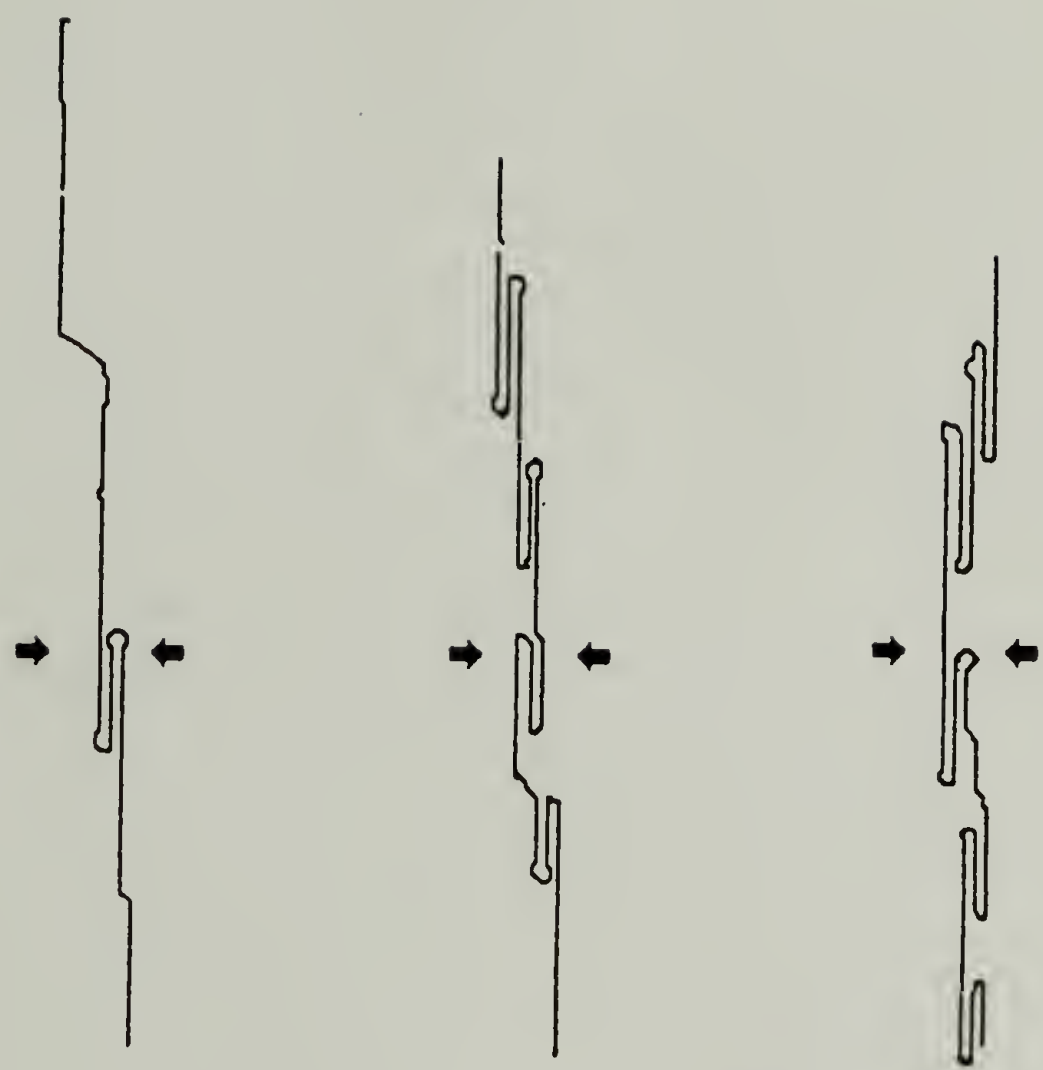

Figure 4.8 Schematic figure of extension of PE showing how the molecule becomes more rod-like without changing its $Rg_{\perp}$ significantly.

Chapter 5

GENERAL CONCLUSIONS AND FUTURE WORK

The results from chapter two have proved the usefulness of real time x-ray studies. The degree of lamellae segregation was determined for both LLDPE/LDPE and HDPE/LDPE blends. These studies should be extended in two major directions first, studies on PE blends that show extensive cocrystallization such as ultra high molecular weight PE and HDPE should be examined. It would be interesting to compare the results with blend systems such as HDPE/LDPE which show produced segregation upon crystallization. A second step in continuing these studies would be to augment the x-ray data with neutron scattering on the same systems. In chapter three we have seen how the combination of SAXS and SANS yielded definitive results in the segregation of dHDPE/LLDPE and d-LLDPE/ h-LLDPE blends. The same sort of work should be carried out with d-HDPE/h-LDPE blends. This would provide a quantitative measurement on the segregation scale of the HDPE.

The possibility of selectively deuterating specific sites on a molecule such as LLDPE, has shown great promise in elucidating the role in which various parts of the molecule play in the morphology. In this case, the segregation of the short chain branches near the crystalline-amorphous boundary was suggested by the differences between the SANS and SAXS. For the continuation of the work on selectively deuterated LLDPE, the key experiment is the measurement of the neutron scattering of the reverse deuterated LLDPE. These are

samples where the branches are deuterated and the main chain is hydrogenated. These are currently being prepared by Stehling. The samples are better for the study of branch segregation, since the contribution of the crystalline-amorphous density difference to the neutron scattering is much lower. A calculation based on contributions to the invariant from the different phases shows that for some crystallinities the total amount of scattering from the crystal-amorphous density difference can be as high as 30% of the total scattering. With deuterated branches , this contribution is limited to less than 1%. This is because of the magnitude of (a_c-a_a) in equation 3.9a is greatly reduced compared to terms described by equations 3.9b and 3.9c, since the scattering length of CH_2 is nearly zero. This type of experiment will be plagued by a high incoherent scattering, due to the presence of more hydrogen atoms. The incoherent scattering , however is more easily correctable than adjustments for crystalline-amorphous scattering. In general it is a very slowly varying function of angle. At the time of this writing, Mattice has been refining his cruder cubic lattice model of the amorphous zone in crystallizing branched polymers to a tetrahedral lattice. Other improvements such as varying branch length and chain tilt might bring the model to point where realistic predictions of the neutron scattering may be possible.

The work on orientation of ultradrawn films is at a point where some realistic model of the scattering needs to be calculated in order to justify more neutron scattering. The extremely small radii of gyration change in the perpendicular direction to the draw after 12x , indicates that the major structural rearrangement of the molecule

takes place at relatively small draw ratios. The rearrangement of the geometry after 12X, however is of practical interest because after these extensions is where the modulus is increases the most. The change in the limiting value of scattered intensity indicates some change in the structure to a more rod like molecule during extensions in this range, but just how much is difficult to ascertain. One suggestion has been to calculate the scattering brute force from various defects in the chain using molecular coordinates. This approach however, is a monumental task when one considers the number of defects to be considered. For just a simple fold alone one must consider the different possibilities for fold planes {(100), (110), (220) ,etc. } and their combination in a single fold, the tightness of the fold, and its length. In the end calculations for all the different defects will probably just smear out to some indistinguishable, nonunique average.

The only practical alternative to this approach is probably a Monte Carlo type of simulation where a near-linear chain is generated, the scattering calculated, and then averaged over a few hundred thousand or so chains. A possible model would have a predetermined average number of linear segments, a number of "defects" (in the sense of a group of non linear chain segments) and a parameter describing the elongation of the molecule. In this scheme, a linear chain is generated in the +x direction; a random defect is then introduced. The chain wanders randomly for a few steps, then continues in the linear +x or -x direction depending on the elongation parameter. The number of linear segments is related to the

crystallinity, the number of defects might be determined by WAXS line broadening, and the elongation parameter could be related to the extension ratio. This approach offers more hope than the brute force calculations of being able to correlate with physical property observations.

BIBLIOGRAPHY

Acierno, D. , Curto, F. P. , LaMantia, P. and Valenza, A., *Polym. Eng. Sci.*, **26**, 28 (1986).

Alexander, L. E., *X-Ray Diffraction Methods in Polymer Science*, Robert E. Kreiger Publishing Company, New York, 1979.

Anadakumaran, K., Roy, S. and St. J. Manley, R., *Macromolecules*, **21**,1746 (1988).

Baker, C. H., Mandelkern, L.,*Polymer*, **7**, 71 (1966).

Ballard, D. G., Burgess, A. N. , Chesire, P., Janke, E. W., Nevin, A., and Schelten, J.,*Polymer*, **22**, 1353 (1981).

Chu, B. , Wu, D. Q. , Wu, C., *Rev. Sci. Instrum.*, **58**, 1158 (1987).

Coven A. W. , *Phys Rev.*, **41**,422 (1932).

Datta, N., and Birley, A., *Plas. Rub. Pro. Appl.*, **2**, 237 (1982).

De Boer, J., and Pennings, J., *Polym Bull.*, **7**, 317 (1981).

Debye, P., *Ann. Physik*, **46**, 809 (1915).

Foster, G., from *Polymer Reaction Engineering, an Intensive Short Course on Production Technology of Polyolefins*, McMaster Univesity, 1989.

Groeninckx, G., and Reynaers, H., *Macromolecules* **22**, 237 (1989).

Guinier, A. , and Fournet, A. *Small Angle X-ray Scattering*, Wiley, New York 1955.

Guttman, C., Hoffman, J. D. , Dimarzio, E., *Diss. Faraday Soc.* (1979).

Guttman, C., Hoffman, J.D. , Dimarzio, E., *Polymer*, **22**, 1466 (1981).

Hadziioannou, G., Wang, L., Stein, R. S. , and Porter, R., *Macromolecules*, **15**, 880 (1982).

Herman, W., Ph.D Dissertation, Univ. Massachusetts, Amherst,1987.

Hikmet, R. , Lemstra, P.J., and Keller, A., *Colloid & Polym. Sci.*, **265**, 185 (1987).

Hill, A., Stein, R. S., Windle, A, *Macromolecules* ,**20**, 1720 (1987).

Holdsworth, P. J., Keller, A., *Makromol. Chem.*, **125**, 82 (1969).

Holmes, E. A., *J. Polym. Sci.*, **46**, 245 (1960).

Hoseman, R. , Bachhi, S. , *Direct Analysis of Diffraction by Matter*, Interscience Publishers, New York, 1962.

Hu, S., Kyu, T., Stein, R. S., *J. Polym Sci Polym* **25**, 7 (1987).

Jauncey, G. E. M. and Pennell, F., *Phys. Rev.*, **43**, 585 (1932).

Kakudo, M. and Kasai, N., *X-Ray Diffraction by Polymers* ,Elsevier Publishing Company, New York, 1972.

Kanamoto, T. ,A. Tsuruta, K. Tanaka, M. Takeda, R.S. Porter, *Polymer J. (Tokyo)* **15**, 327 (1983).

Kessler, T. O. J., *Polyethylene*, Reinhold Publishing Corporation, New York, 1958.

Kortleve, G., C. Vonk, *Kollid. Z.* , **220**, 19 (1967).

Kortleve, G., C. Vonk, *Kollid. Z.* , **225**, 124 (1968).

Kriste, R. G. , W.A. Kruse, and K. Ibel, *Polymer*, **16**,120 (1975).

Kyu, T. , Hu, S. R., and Stein, R. S., *J. Polym Sci. Polym. : Phys. Ed.*, **25**, 89 (1987).

LaMantia, F.P. and Acierno, D., *Eur. Polym. J.*, **21**, 811 (1985).

Lemstra, P. J., van Aerle, N., Bastiaansen, C.W., *Polymer J.* ,**19**, 85 (1987)

Lin, J. S., Hendricks, R.W., Shultz, J., and McCready, M. J., *J. Polym. Sci. Polym. : Phys. Ed.*, **20**, 1365 (1982).

Lo, R. , Hill, A. , Stein, R. S., *J Polym. Sci.* (to be published).

Lo, R. , Ph. D Thesis, University of Massachusetts, Amherst 1987.

Magill, J. H., Schultz, J. M., and Lin, J. S., *Colloid &Polymer Sci.* **265**, 193 (1987).

Mandelkern, L., *Crystallization of Polymers*, McGraw Hill, New York, 1964.

Mathur, S., Mattice, W., *Macromolecules*, **21**, 1354 (1988).

Mathur, S., Mattice, W., personal communication.

McGuire, S. , Esnault, P., Satkowski, M., Stein, R.S., (Manuscript Submitted *Macromolecules*)

McGuire, S., Masters Thesis University of Mass. , Amherst (1989).

Minkova, L., Mihailov, M., *Colloid & Polymer Sci.*, **265**, 1 (1987).

Mirabella, F. , and Ford, E., *J. Polym Sci: Part B: Polymer Physics*, **25**, 777 (1987).

Peterlin, A., *Colloid & Polym. Sci.*, **265**, 357 (1987).

Porod G. , *Kolloid-Z.*, **124**, 83 (1951).

Porod, G. , *Kolloid-Z.*, **125**, 51 (1952).

Porod, G., *Kolloid-Z.* **124**, 83 (1951).

Preedy, J. E. , *Br. Polym. J.* **5**, 13 (1973).

Reckinger, C. , Larbi, F. C. , Rault, J., *J. Macrol. Sci.*, **B23**, 511 (1985).

Ree, M. , Ph.D. Thesis, Univ. of Massacusetts, Amherst 1987.

Ree, M. and Stein, R. S., *Macromolecules* (Submitted)

Ree, M., Kyu, T., and Stein, R. S., *J. Polym Sci. Polym. : Phys. Ed.*, **25**, 105 (1987).

Rego Lopez, J. M., and Gedde, U. W. , *Polymer* , **30**, 22 (1989).

Roe, R. J., *J. Chem Phys.*, **53**, 3026 (1973).

Roy, S. K., Kyu, T., St. John Manley, R., *Macromolecules*, **21**, 1741(1988).

Ruland, W. , *Polymer*, **5**, 89 (1964).

Ruland, W., *Acta Cryst.* **14**, 1180 (1961).

Ruland, W., *J. Appl. Cryst.* **4**,70 (1971).

Russel, T. P., Stein, R. S., *J. Polym. Sci. Phys.*, **20**, 1593 (1982).

Sawatari, C., Matsuo, M., *Colloid Polym. Sci.* **263**,783 (1985).

Schouterdern, P., Vandermarliere, M., Rickel, C., Koch, M. K., and Schmatz, W., *Polymer*,**17**,751 (1976).

Shishesaz, M.R. and Donatelli, A. A., *Polym Eng. Sci.*, **21**, 869 (1981).

Shultz, J. M. , J.S. Lin, and R.W. Hendricks, *J. Appl. Crystallogr.* **11**,551 (1978).

Shultz, J. M., .*J. Polym. Sci.*, **14**, 2291 (1976).

Smith, P., Lemstra, P., *J. Collid Polym. Sci.* ,**258**, 7, (1980).

Snell, T.P. in *Modern Plastics Encyclopedia*, J. Agranoff, ed., Vol. 59, McGraw Hill, New York, 1982.

Song, H. H. , Wu, D. Q., Chu, B., Satkowski, M. , Ree, M., Stein, R.S. and Phillips, J.C., *Macromolecules* (in press).

Speed, C.S. *Plastic Eng.*, July, **29** (1982).

Swan, P.R., *J.Polym. Sci.* **56**, 409 (1962).

Thayer, A. M. *Chem. Eng. News*, **67**, 7 (January 30, 1989).

Vile, J., Hendra, J., Willis, H. A., Cudby, M. E. A., and Bunn, A., *Polymer*, **25**, 1173 (1984).

Voight-Martin, I.G., Alamo, R., and Mandelkern, L., *J. Polym. Sci. Phys. Ed.*, **24**, 1283 (1986).

Vonk, C. G., and Pijpers, A. J., *J. Polym. Sci.* **23**, 2517 (1985).

Vonk, C., in *Small Angle Scattering*, H. Brumberger, ed., John Wiley, 1977.

Wignal, G. D., Crist, B., Russel, T.P., and Thomas, E. L., ed. *Scattering, Deformation and Fracture in Polymers*, Materials Research Society Symposia Proceedings, Pittsburgh, 1987

Wignal, G. D., Ballard, D.H., and Schelten, J., *Eur. Polym. J.* , **10**, 861 (1974).

Yoon, D., P.J. Flory *J. Appl. Cryst.*, **11**, 531 (1978).

Yoon, D., and Flory, P.J., *Polymer*, **16**, 645 (1975).

Yoon, D., and Flory, P.J., *Macromolecules*, **9**, 294 (1976).